INVESTIGATION OF YTTERBIUM DOPED FIBER LASER

By

USHA CHAKRAVARTY

PHYS 03201104006

Raja Ramanna Centre for Advanced Technology, Indore

A thesis submitted to the

Board of Studies in Physical Sciences

In partial fulfillment of requirements

for the Degree of

DOCTOR OF PHILOSOPHY

of

HOMI BHABHA NATIONAL INSTITUTE

August, 2018

Homi Bhabha National Institute

Recommendations of the Viva Voce Committee

As members of the Viva Voce Committee, we certify that we have read the dissertation prepared by Usha Chakravarty entitled "Investigation of Ytterbium doped fiber laser" and recommend that it may be accepted as fulfilling the thesis requirement for the award of Degree of Doctor of Philosophy.

Chairperson – Prof. S. R. Mishra	SR Mishra	**Date:**	4.10.2019
Guide / Convener – Prof. K. S. Bindra	KeulSil	**Date:**	04-10.2019.
Examiner- Prof. M. R. Shenoy	MRShenoy	**Date:**	04/10/2019
Member 1- Prof. S. K. Majumder	S.Majumder	**Date:**	4/10/19
Member 2- Prof. A. Moorti	Anand Moorti	**Date:**	4/10/2019.
Member 3- Prof. P. K. Mukhopadhyay	Pranab K Mukhopadhyay	**Date:**	4/10/2019
Member 4- Prof. C. Mukherjee	C. Mukherjee	**Date:**	04/10/19
Member 5- Prof. Vasdev	Vasdev	**Date:**	04/10/19
Technical Advisor - Prof. B.N. Upadhyaya	BNUpadhyaya	**Date:**	04/10/19

Final approval and acceptance of this thesis is contingent upon the candidate's submission of the final copies of the thesis to HBNI.

I hereby certify that I have read this thesis prepared under my direction and recommend that it may be accepted as fulfilling the thesis requirement.

Date: 04/10/2019.

Place: RRCAT, Indore

KeulSil

K. S. Bindra

STATEMENT BY AUTHOR

This dissertation has been submitted in partial fulfillment of requirements for an advanced degree at Homi Bhabha National Institute (HBNI) and is deposited in the Library to be made available to borrowers under rules of the HBNI.

Brief quotations from this dissertation are allowable without special permission, provided that accurate acknowledgement of source is made. Requests for permission for extended quotation from or reproduction of this manuscript in whole or in part may be granted by the Competent Authority of HBNI when in his or her judgment the proposed use of the material is in the interests of scholarship. In all other instances, however, permission must be obtained from the author.

Usha

Usha Chakravarty

DECLARATION

I, hereby declare that the investigation presented in the thesis has been carried out by me. The work is original and has not been submitted earlier as a whole or in part for a degree / diploma at this or any other Institution / University.

Usha

Usha Chakravarty

List of Publications arising from the thesis

Journal

1. "Study on self-pulsing dynamics in Yb-doped photonic crystal fiber laser", **Usha Chakravarty**, A. Kuruvilla, H. Harikrishnan, B. N. Upadhyaya, K. S. Bindra and S. M. Oak , *Optics & Laser Technology*,**2013,** *Vol. 51*, 82-89.
2. "Linearly polarized intracavity passive Q-switched Yb-doped photonic crystal fibre laser", **Usha Chakravarty**, A. Kuruvilla, Rajpal Singh, B. N. Upadhyaya, K. S. Bindra and S. M. Oak, *Pramana-Journal of physics*, **2014**, *Vol. 82*, 379-383.
3. "Narrow-linewidth broadly tunable Yb-doped Q-switched fiber laser using multimode interference filter", **Usha Chakravarty**, P. K. Mukhopadhyay, A. Kuruvilla, B. N. Upadhyaya, and K. S. Bindra, *Applied Optics*, **2017**, *Vol. 56*, 3783-3788.
4. "Generation of more than 40 W of average output power from a passively Q-switched Yb-doped fiber laser", **Usha Chakravarty**, Antony Kuruvilla, Ravindra Singh, B. N. Upadhyaya, K. S. Bindra, S. M. Oak, *Applied Optics*, **2016,** *Vol. 55*, 288-296.
5. "Short pulse generation in active Q-switched Yb-doped all fiber laser and its amplification", **Usha Chakravarty,** Srikanth Gurrama, Antony Kuruvillaa, B.N. Upadhyaya, K.S. Bindra, *Optics & Laser Technology*, **2019,** *Vol. 109*, 186-192.

Conferences

1. **Usha Chakravarty**, Srikanth Gurram, A. Kuruvilla, Rajpal Singh, B.N.Upadhyaya, K.S. Bindra, "Amplification of Q-switched pulses to more than 25 W average power in single mode Yb-doped dual stage all fiber amplifier", 26th DAE-BRNS National Laser Symposium (NLS-26), BARC, Mumbai, 2017.
2. **Usha Chakravarty**, Antony Kuruvilla, G. Srikanth, Rajpal Singh, B. N. Upadhyaya, and K. S. Bindra, "Study of multi-wavelength generation in Yb-doped photonic crystal fiber laser", 25th DAE-BRNS National Laser Symposium (NLS-25), KIIT, Bhubaneswar, 2016.
3. **Usha Chakravarty**, Antony Kuruvilla, Rajpal Singh, B.N. Upadhyay, K. S. Bindra and S. M. Oak, "Study and generation of 17 W average power passively Q-switched Yb-doped fiber laser", Proceedings of National Laser Symposium, Tirupati, 3-6 Dec, 2014.
4. G. Srikanth, **Usha Chakravarty**, A Kuruvilla, B.N. Upadhyaya, K.S. Bindra, S.M. Oak, "Studies on effect of output coupling on output characteristics of Yb-doped fiber ring laser", 21st DAE-BRNS National Laser Symposium (NLS-21), BARC, Mumbai, 6-9 Feb., 2013.
5. **Usha Chakravarty**, G. Srikanth, Antony Kuruvilla, Hari Krishnan, B.N.Upadhyay, K. S. Bindra and S. M. Oak "Mode-locked Yb-doped fiber laser oscillator in all-normal-dispersion regime of operation without use of intra-cavity spectral filter and polarization controller elements", 21st DAE-BRNS National Laser Symposium (NLS-21), BARC, Mumbai, 6-9 Feb., 2013.
6. **Usha Chakravarty**, G. Srikanth, B. N. Upadhyaya, K. S. Bindra, S.M.Oak, "Study of CW and pulsed amplification in Yb-doped fiber amplifier", Eleventh International

conference on Fiber Optics and Photonics, Photonics-2012, IITM, Chennai, India, Dec 09-12, 2012.

7. P. K. Mukhopadhyay, S. K. Sharma, P. K. Gupta, B. N. Upadhyay, **Usha Chakravarty**, A. J. Singh, Jogy George, K. S. Bindra and S. M. Oak, "Mode-locked Yb-doped fiber oscillator in all-normal-dispersion regime with long gain element: studies on Spectral and temporal profiles", 20th National Laser Symposium (NLS-20), Chennai, 09-12 January, 2012.

Usha

Usha Chakravarty

DEDICATION

This thesis is the manifestation of motivation, support and reliance of my beloved parents. I dedicate this thesis to my mother, late Smt. Deomani Chaturvedi and my father Shri Chandra Shekhar Chaturvedi. The determination of "Amma" made me a responsible person; she is my role model as from her I learnt to execute my duties through concrete action and not mere preaching. She transformed me from a wandering, obstinate child to a motivated person. My father's patience and wisdom, in handling my childhood's unconventional queries gave me the freedom of thinking and taking decisions. His faith and encouragement as a father, as well as a companion has helped me to take debacles with composure and success with calmness and dignity.

ACKNOWLEDGEMENTS

I am extremely thankful to my mentor and thesis guide Dr. K.S. Bindra, for his continuous guidance, encouragement and motivation in carrying out the experiments, discussions and finding solution to physics aspects of the observations.

I am thankful to the Committee members for their valuable feedback during the course of the work.

I am highly thankful to Dr. B.N. Upadhyaya for his valuable suggestions, constant support and encouragement, throughout the course of this work.

I am grateful to Dr. P.K. Mukhopadyay for the discussions about the work and the research problem. I will always be indebted to him for being instrumental in my progression from the darkness of ignorance to the light of understanding.

Also, it is my utmost pleasure to express my sincere thanks to Shri Srikanth Gurram for motivation, support and encouragement for carrying out the experiments in a cordial way and their analysis. The present research work could not have been completed without the help of my exceptionally motivated colleague Shri Antony Kuruvilla for carrying out the experiments throughout this journey of research.

I thank Shri Ravindra Singh, Shri Vijay Kumar Bharadwaj and Shri Avadhesh for their support. I thank Shri Rajpal, Shri Basant, Shri Ekka, Shri Mahendra, and Shri Bhaskar for the support in completion of the work. I whole heartedly thank Ms. Jagriti, Ms. Smita and Ms. Shryner for their continuous support in the whole process. I thank all the LDIAD members for their support.

I am short of words to express my gratitude to Ms. Asmita and Ms. Sunita for their enjoyable company and support during thick and thin of the process.

A special thanks to my family, for their endless support in carrying out this research. I also thank my dearest sister Ms. Deepa for her eternal support during this work.

I am highly thankful to my friend and life partner, Uday for providing me inspiration in carrying out this work from his childlike inquisitiveness towards his dedication for science and research. His sense of humor, innocence, songs and selfless love has always made my world.

I feel blessed to have two sweet children Aalo and Avi .They are like teacher of my life. I have learnt patience from them and gained strength to handle every situation with a warm heart and unconditional smile.

CONTENTS

Chapter 1

Introduction

One of the most significant invention of this century is the invention of lasers [1], which has led to the investigation of plenty of phenomena in physical, chemical, and biological sciences [2,3], apart from its uncountable applications in material processing, defense, medicine, entertainment, etc. In all types of lasers, it is the stimulated emission phenomenon through which generation and amplification of light takes place in an active gain medium, additionally an optical cavity provides feedback and a pump source supply energy to the active medium [4]. The first fiber laser was demonstrated [5, 6] soon after the demonstration of the first Ruby laser. Exploration of fiber laser has intensified the use of lasers in various application areas in industries, research, and medicine. Fiber lasers offer numerous advantages like high efficiency, high reliability, low thermal problems, excellent beam quality, and flexible fiber delivery together with small footprint [7]. However, rapid growth in fiber laser technology has taken place mainly with the introduction of cladding pumping [8], which has enabled the rise in output power of fiber lasers to kW level [9-11]. Power scaling capability of fiber lasers is also attributed to the development of high power laser diodes and various fiber optic components such as low loss active and passive fibers, pump combiners, fiber Bragg gratings (FBG's), isolators, fiber optic couplers, and fiber end caps.

During the initial years of development of lasers, neodymium was the dopant of interest due to availability of high quality and large size Nd-doped crystalline and bulk glass sources. Both high power and high energy solid state Neodymium based bulk lasers have been developed for research and industrial uses. Initial success of Nd-doped fiber lasers and development of simple rare-earth doping procedures in low-loss silica fibers led to further investigation of other rare-earth doped fibers like Ytterbium, Thulium, and Holmium [12- 14]. For high power fiber lasers, Nd-doped fibers are not suitable, due to the low solubility of Nd ions in silica which leads to longer length of the fiber and favours the deleterious nonlinear effects. Nd- doped fibers also have large quantum defect which causes thermal effects in high power fiber lasers. Ytterbium-doped fibers have a number of advantages over their counterparts due to their simple electronic structure, absence of any excited state absorption, and low quantum defect, which favors their exploitation in high power laser systems [12].

Generation of high CW output power in ytterbium doped fiber lasers have achieved a state-of-the-art technology, still there is a research interest in such fiber lasers. Various aspects in CW and pulsed operation in Yb-doped fiber lasers have been addressed in this thesis. The presence of self-pulsing phenomena is encountered while working with such lasers. The generation of random pulses even during the CW pumping scheme, is termed as self-pulsing. These random pulses have sufficient intensity to damage the intracavity components. To mitigate the problem of self-pulsing, in this thesis we have presented an experimental and analytical study of self-pulsing dynamics in Yb-doped PCF fiber laser. In the self-pulsing study, it is observed that the intensity of the self-pulses are significant in the single end pumping configuration as compared to the double end pumping configuration. In both the cases, it was noted that when the pump power was sufficiently high, the amplitude and the occurrence of the self-pulses were reduced. The reduction in the amplitude of the self-pulses was much more appreciable in the double end pumping case. The rate equation analysis showed the significant non-uniform single pass distribution of upper level population along the length of the fiber which could enhance the re-absorption losses causing saturable absorption action that can be one of the major causes for the self-pulsing inside the fiber. In the single end pumping, single pass distribution of upper level population is more non-uniform as compared to the double end pumping, so the intensity and the frequency of occurrence of the pulses are higher in single end pumping as compared to the double end pumping configuration.

High-peak-power short-pulse Q-switched fiber lasers are highly promising in the field of industrial processing, range finding, remote sensing, and medicine owing to their higher efficiency, good beam quality, and compactness. Passive Q-switching is favored over active Q-switching due to its simple experimental configuration, compactness, and ease of operation. Saturable absorbers such as Cr^{4+}:YAG crystal, Sm-doped fiber, graphene etc. has been used for passive Q-switching of Yb-doped fiber lasers. The high average power from these system is limited to ~20 W due to damage to optical components at high power. The studies in passive Q-switching operation of Yb-doped fiber laser in a special T-type double-end pumping configuration has been performed to enhance output power. In this configuration, average output power of 41.6 W has been achieved, which is the maximum average output power in PQS Yb-doped fiber laser oscillator reported so far in the literature. It was possible to achieve such a high value of average output power by means of low-loss end caps spliced at both the ends of the doped fiber. The effect of saturable absorber on random self-pulsing dynamics and on the spectral behavior of the output signal near the threshold for Q-switching has also been investigated. Studies on output pulse characteristics with different linear transmission of saturable absorbers has also been performed. Our results show that with lower values of the initial transmission of the passive Q-switch crystal, output pulse energy increases and pulse-to-pulse stability also improves. Detailed studies were also performed to observe the spectral evolution of PQS Yb-doped fiber laser as a function of pump power as well as the dependence of output spectral characteristics on the length of the gain medium.

The spectral width in active and passive Q-switched fiber lasers are quiet large and inhomogeneous due to broad fluorescence linewidth, however pulsed fiber lasers with narrow linewidth and tunable output are useful in nonlinear frequency conversion applications, spectroscopic detection, remote sensing, wavelength division multiplexing, and Lidar systems. Various methods have been employed to generate Q-switched pulses with narrow linewidth and tunable output. One of the preferred method to tune the Q-switched output is via bulk grating, but this is not compatible with all fiber configuration. Fiber Bragg gratings have been used as Q-switching element to generate Q-switch pulses with narrow linewidth, but whole process of Q-switching is cumbersome and wavelength tunability is limited to few nm range. We have worked on the narrow-linewidth generation and broadly tunable output from a Yb-doped Q-switched fiber laser using an acousto-optic modulator (AOM) and multimode interference filter in Yb-doped fiber laser in all fiber configuration. Due to the all-fiber nature, the ring cavity resonator with a narrow line-width and tunable operation can be potentially used as an oscillator for further amplification of output power in the master oscillator power amplifier configuration.

Although acousto-optic (AO) Q-switched fiber lasers are preferable for the generation of high energy pulses, but the pulse duration achieved is typically 100's of nanoseconds. Stimulated Brillouin scattering (SBS) Q-switching generates pulses of duration of 10's of nanosecond but the pulses are highly random in nature. Further, it is difficult to achieve pulse width shorter than cavity round-trip time in conventional Q-switching process. We have generated sub-cavity round-trip time pulses by controlling the modulation window ON time of AOM (anomalous pulses). The experimental results show that the anomalous pulses actually are generated at the falling edge of modulation off time of AOM. The pulse duration of anomalous pulses are in the range of 50-55 ns. The anomalous pulses are more than ~24 times shorter than the normal pulses obtained with conventional Q-switching at the same value of the pump power. These anomalous pulses are highly stable and have been amplified to achieve ~19 W of average output power.

Yb-doped fibers have very broad emission bandwidth, which favours broadband amplified spontaneous emission (ASE) generation and hence these are useful as superfluorescent sources for many applications. We have carried out preliminary experiments to study the effect of pumping configuration, fiber length, fiber core diameter on ASE generation in Yb-doped fibers which is paramount for generating stable, high power and broadband signal output. It has been observed in Yb-doped fibers that generated ASE spectrum depends on the length of the fiber. Further, to enhance ASE power, an amplifier configuration using single mode double clad Yb-doped fibers with different spectral characteristics in the seed part and in the amplifier part were used. We also carried out our studies with large mode area fibers. These studies will help in designing low cost broadband ASE source that is useful in biological optical coherence tomography measurements.

To cover all the aspects mentioned above the thesis is organized as following.

Chapter 1 begins with the basics of fiber laser, discussion on energy level diagram of Yb-doped fiber laser and limitations in achieving high power output in CW and pulsed mode of operation. The chapter provides the overview of Yb-doped CW and pulsed fiber lasers. Nonlinear effects like stimulated Raman scattering (SRS) and SBS, fiber fuse effect are also addressed. Chapter 2 describes the study of self-pulsing dynamics in Yb-doped photonic crystal fiber laser in single-end and double-end pumping configurations. Further, multi-wavelength and narrow linewidth polarized operation of Yb-doped photonic crystal fiber (Yb-PCF) laser by using dichroic mirror and fiber Bragg grating (FBG) mirror has been presented. This chapter also describes the thermal effects in high-power Yb-doped double-clad fiber laser. In chapter 3, passive Q-switching (PQS) operation of Yb-doped fiber laser using Cr^{4+}: YAG crystal as a saturable absorber (SA) in a special T-type double-end pumping configuration has been studied. The effect of the SA on the random self-pulsing dynamics and the spectral behavior of the output signal near the threshold for Q-switching has also been investigated. Chapter 4 describes the narrow linewidth generation and broadly tunable output from Yb-doped Q-switched fiber laser using acousto-optic modulator (AOM) and multimode interference filter in the linear bulk cavity and all-fiber ring cavity configurations. Chapter 5 describes generation of sub-cavity round-trip time pulses (anomalous pulses) in all-fiber AO Q-switched fiber laser. These anomalous pulses were amplified in the pre-amplifier and power amplifier stage. Amplification of conventional AO Q-switched pulses in MOPA configuration has also been done in two stage configuration. Chapter 6 describes broad linewidth ASE generation studies in Yb-doped fibers in single-end pumping, double-end pumping, single mode fiber, large mode area fibers. The amplification of seed ASE signal from single mode fiber was carried out in MOPA configuration using single mode YDF in both seed and amplifier stages to increase the signal power and ASE bandwidth.

1.1 Basics of fiber laser

In this section, a brief description of optical fibers and different fiber laser components has been provided.

1.1.1 Structure of optical fiber

The most important element of fiber lasers are doped fibers, which act as the gain medium. Fibers are made of low loss silica core having higher refractive index (n_1) and an outer cladding with lower refractive index (n_2) for total internal reflection [15]. Double clad fibers have two cladding layers, one for guidance of signal and other for guidance of pump beam. Figure 1.1(a) shows optical fiber structure with total internal reflection and Fig. 1.1(b) shows typical refractive index profile of double-clad fibers [15]. Propagation of light in the core takes place by the process of total internal reflection. If the angle of incidence $i < i_m$, total internal reflection takes place and light rays are guided. Numerical aperture (NA) of the fiber defines the light gathering power of the fiber and is given by [15]

$$NA = \sin(i_m) \qquad (1.1)$$

where, i_m is the maximum angle of incidence for total internal reflection. The concept of rays, as shown in figure 1.1(a) is valid for multimode fibers, where the core radius '*a*' is large enough (≈25μm or more), whereas for single mode fibers mode concept is utilized for study of beam propagation. In the following section, different types of fibers used in the experimental work has been discussed.

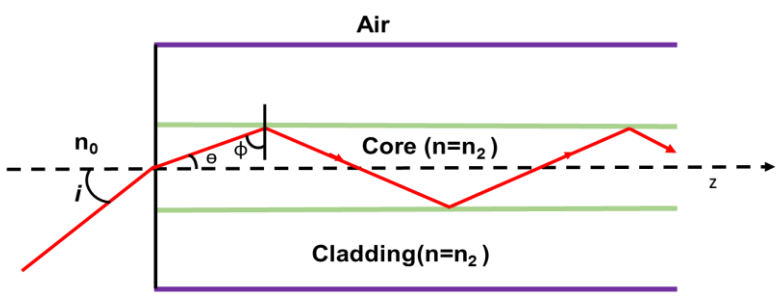

(a)

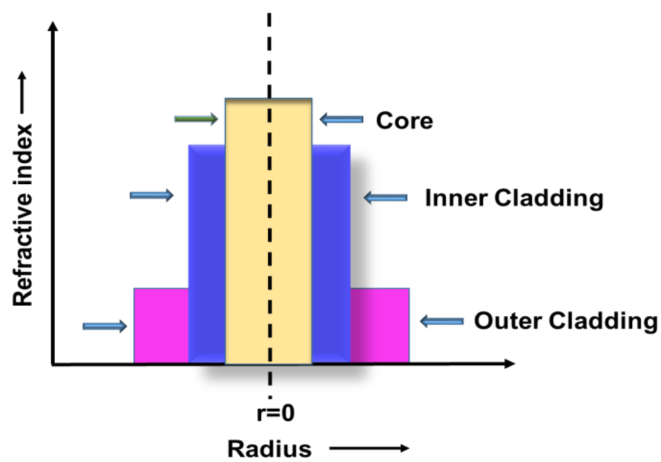

(b)

Fig. 1.1: *(a) Structure of optical fiber showing total internal reflection. Incident angle is represented by 'i' and 'ɵ' represents the refracted angle, (b) Refractive index profile of double-clad fiber.*

1.1.2 Different types of fiber

a) <u>Multimode and single mode fibers:</u> Mode of an optical fiber is defined as an electric field distribution in the transverse direction that propagates along the length of the fiber without any change in its field distribution except for a change in phase. Mathematically, field is written as [15]

$$\Psi(x,y,z,t)=\psi(x,y) \quad e^{\,i(\omega t-\beta z)} \tag{1.2}$$

where, $\psi(x,y)$ represents the field profile in the transverse direction and β is the propagation constant of a wave moving in the z-direction. Effective index of a mode having a propagation constant β is given by

$$n_{eff} = \frac{\beta}{\omega/c} \tag{1.3}$$

The modes of the fiber are linearly polarized modes in weakly guiding approximation and are represented as LP_{lm}, where indices l and m correspond to number of zeros in azimuthal and radial directions. The waveguide parameter V is an important quantity characterizing an optical fiber and is given by

$$V=\frac{2\pi}{\lambda_0}a\sqrt{n_1^2-n_2^2} \tag{1.4}$$

For a step-index fibers, if V < 2.4045, fiber supports only lowest order mode LP_{01} having a Gaussian like field distribution. For a given fiber, the wavelength for which V = 2.4045 is known as the cut-off wavelength and is denoted by λ_{cutoff}. However, if V >2.4045, the fiber is said to be multi-moded fiber.

b) <u>Active and passive fibers:</u> In fiber lasers, fiber acts as the gain medium in which the core of the fiber is doped with the active ions like Yb, Nd, Er, Tm etc. In passive fibers, no active ions are present in the core. Passive fibers are used for the transmission of laser beam, and they are backbone for fabrication the passive components in fiber lasers, like fiber Bragg gratings, couplers, isolators, pump combiners, etc.

c) <u>Single-clad and double-clad fibers</u>: In single-clad fibers, as the name suggests, there is only one cladding outside the core. Outer polymer cover acts as the protective cover. In this case, pumping can be done directly in the core, so the pump light and signal light both propagate inside the core. As the size of the core of the active fiber for single mode output is about 5-10 µm in diameter, so for efficient pumping of fiber lasers using single clad fibers, fiber coupled diode lasers pigtailed with single mode fiber having 5-10 µm diameter is required, which are not available at power levels of more than 1 W level and hence output from single mode single-clad fiber laser is limited to less than 1 W level. Therefore, double-clad fibers were designed such that the core supports a large-area fundamental mode for efficient absorption of the pump and inner cladding is made to have a larger diameter and high numerical aperture for efficient coupling from multimode diode bars. Cladding pumped fiber lasers do not require single-mode pump sources, but can still produce a single-mode laser output. Figure 1.2 shows a schematic of double-clad fiber (DCF), which has a primary waveguide (the core) for guidance of the signal surrounded by a lower-index inner cladding, and these are made from glass. The inner cladding acts as a secondary waveguide that guides the pump light. The inner cladding is surrounded by an outer cladding of lower refractive index polymer or glass to facilitate wave guiding. In either case, the fiber may have a further layer of polymer for protection. Typically, the fiber is rare-earth doped throughout the core, while the inner-cladding is un-doped. Since the core is located within the inner cladding and forms a part of the pump waveguide, pump light propagating in the pump waveguide passes through the core and excites the active rare-earth ions in the core.

d) <u>Large mode area fibers:</u> In order to enhance threshold for nonlinear effects in optical fibers, core area is increased and to still maintain single mode or few mode operation, NA of the core is accordingly reduced. These fibers are referred as large mode area fibers. By coiling them in small diameter spools these fibers provide single transverse mode output even at large output powers in the range of hundreds of watts.

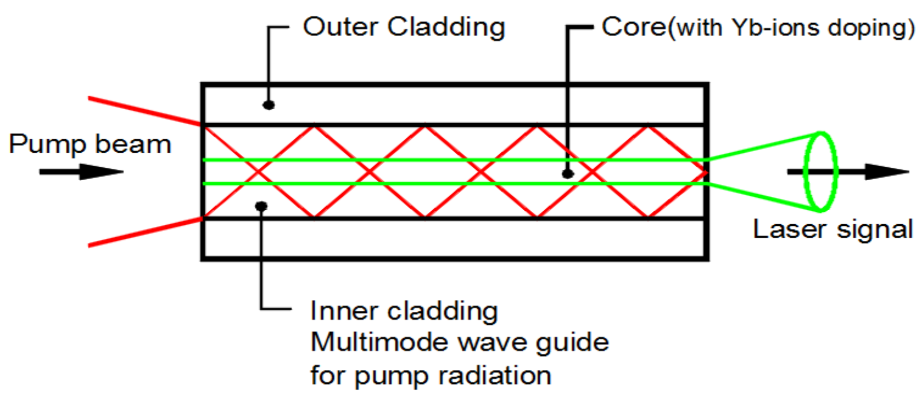

Fig. 1.2: *Schematic of double-clad fiber showing core, inner cladding and outer cladding; core is doped with active ions and laser signal is emitted from the core; inner cladding guides the pump beam as refractive index of outer cladding is made smaller than that of inner cladding.*

e) <u>Photonic crystal fibers:</u> In the recent year's, a new class of fibers referred as photonic crystal fibers (PCF) have been introduced which are special fibers that consist of a regular micro-structured array of holes, where core is made of a solid- or air-filled defect and the light guidance takes place due to the microstructures present in the fiber [16,17]. Due to the presence of air-clad in PCF, high value of numerical aperture (NA) of the order of ~0.8 can be achieved. The advantage of such a fiber is that the diameter of the inner cladding can be reduced while retaining its numerical aperture. Due to the increased ratio of active core area to inner cladding area, pump light absorption is improved and smaller fiber length can be used for efficient absorption of pump beam. As a result of single-mode guidance in large core area together with the significantly reduced absorption length, nonlinear interactions, which are in general the reason for performance limitation in high peak power ultrafast fiber laser and amplifier systems, are significantly reduced in such fibers. The first PCF laser was reported in the year 2000 and there are now several reports in the field of Yb-doped PCF lasers [18].

1.2 Passive fiber optic components used in the fiber laser system

Fig 1.3 shows the schematic of all fiber CW fiber laser system. The setup consists of YDF as the gain medium. Fiber Bragg gratings, FBG1 and FBG2 act as mirrors and they form the resonator in which FBG1 is highly reflecting mirror with more than 99% reflectivity and FBG2 acts as the output coupler with reflectivity varying between 5% to 10 %. Gain medium is pumped by fiber coupled laser diodes (LD) through pump to signal combiner (PSC). Isolator is spliced at the output of the cavity to avoid any feedback from the ends of the fiber. These passive components which are shown in the figure and have been used for our work in various fiber laser configurations are described in details in the present section.

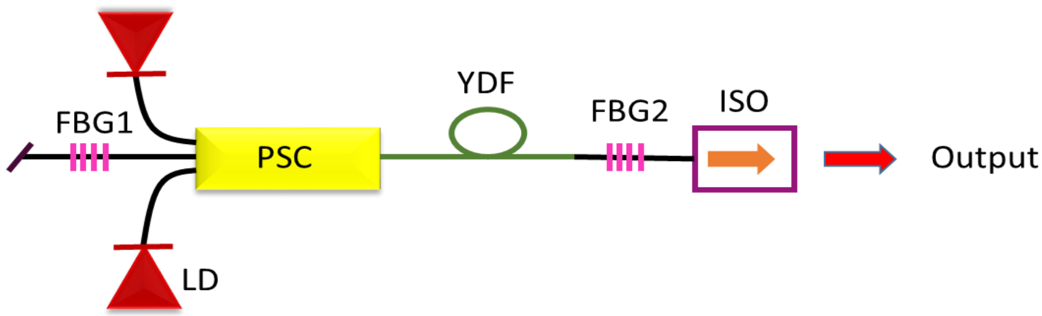

Fig. 1.3: *Schematic of CW all fiber, fiber laser system showing fiber Bragg grating (FBG1 and FBG2), pump to signal combiner (PSC), laser diode (LD), ytterbium doped fiber (YDF) and isolator (ISO).*

1.2.1 Fiber Bragg Grating

Fiber Bragg grating is a fiber optic device in which there is a periodic modulation of refractive index along the length of the fiber and acts as a wavelength specific mirror. It reflects particular wavelength depending upon the period of the grating and transmits all other wavelengths which are incident upon it. There are two main techniques for fabrication of FBG i.e., by phase masking and by interference pattern of Fresnel Biprism. In both the techniques, core of the fiber is exposed to intense periodic spatial pattern of ultraviolet light. UV rays result in increase in the refractive index of core in a periodic manner. This grating is permanent in nature. Fiber Bragg grating works on the principle of Bragg condition in which all the reflected signals from the refractive index modulation interfere constructively at one particular wavelength referred as Bragg wavelength and the condition is called Bragg condition. All other wavelengths other than Bragg wavelength interfere destructively in the reflection direction and are transmitted through the grating [15].

1.2.2 Fiber optic pump and signal combiners

Fiber optic multimode pump combiners and pump to signal combiners are used to convert the bulk setup of coupling the pump beam to the gain fiber using optical lenses into all-fiber setup

[15]. This is also helpful in combining the power of many pump diodes into a single output. This is one component which has revolutionized the high power laser development. In fiber-optic pump combiners, as the cladding diameters and multimode fibers are involved, simple splicing of all the required fibers together serve the purpose. There is direct coupling of the pump beam from the pump ports to the output port. The signal port provides the two way operation of the pump combiners. In the master oscillator power amplifier configuration, pump combiners with the signal port is used to inject the seed signal for further amplification. The combiners have very high coupling efficiency, low insertion loss and back reflection, high optical power handling and no misalignment problem. Thermal packaging of pump combiners is carried out carefully to handle high pump powers.

1.2.3 Fiber optic isolators

A fiber optic isolator is a passive device which allows the propagation of optical signal in only one direction and prevents reflections in the backward direction. This is very useful in optical amplifiers in which backward reflections are highly deleterious and may damage amplifier stages. Magneto-optic devices are generally used to function as isolators. Optical isolators work by rotating the plane of polarization of incoming light ray [15].

1.3 Ytterbium-doped Silica Fiber

Ytterbium is one of the most versatile laser ions in a silica-based host. It offers several attractive features, in particular, an unusually broad absorption band that stretches from below 850 nm to above 1070 nm associated with $^2F_{7/2} \rightarrow {}^2F_{5/2}$ transition. The absorption and emission spectrum of

Yb-doped fiber is illustrated in figure 1.4 [19]. The energy level structure of the Yb^{3+}-ion is simple as compared to other rare-earth ions consisting of only two relevant manifolds: the ground state $2F_{7/2}$ (with 4 Stark levels) and a metastable state $^2F_{5/2}$ (with three Stark levels) spaced by approximately 10000 cm^{-1}. The radiative lifetime of the $^2F_{5/2}$ state is typically in the range 700-1400 μs depending on the host. The transitions between sublevels are not fully resolved for Yb^{3+}-ions in a glass at room temperature due to strong homogenous broadening although weaker inhomogeneous broadening is also observed as the emission spectra varies to some extent with pump wavelength. It is important to note that the detailed absorption and emission spectrum depends to some extent on the host glass composition. The cross-sections of Yb-doped germanosilicate fibers as shown in figure 1.4(b) vary up to about 30% depending on the different content of germanium, aluminum and boron. The measured fluorescence decay time is typically around 0.8 ms also varies by about 30%. Yb^{3+} in pure silicate glass has a lifetime of around 1 ms, a higher content of germanium tends to decrease the lifetime of the excited state. Flourescence lifetime is important in the case of kHz repetition rate master oscillator power amplifier (MOPA) configuration of pulsed laser as it directly influences the amount of ASE produced.

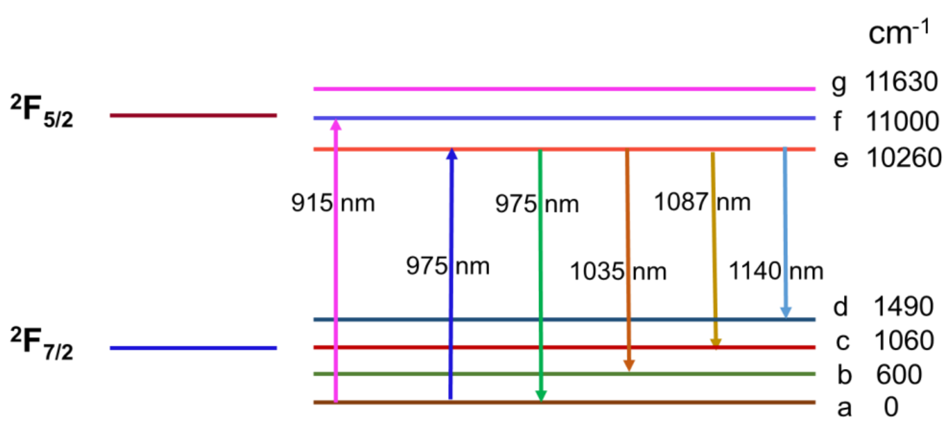

(a)

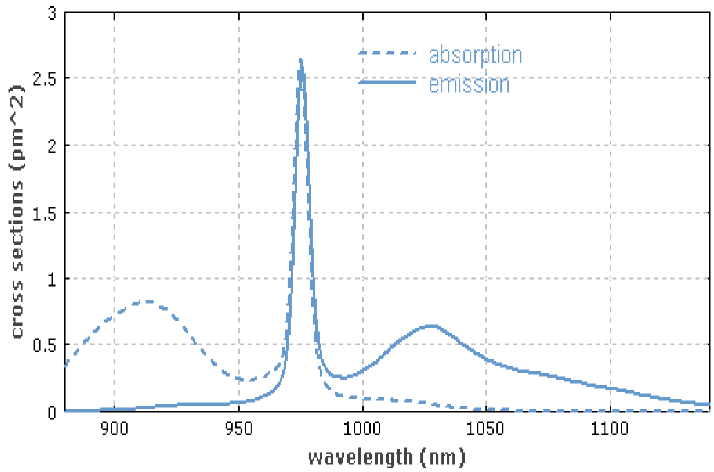

(b)

Fig. 1.4: *(a) Energy level diagram of Yb^{3+} ions in silica [19]. (b) Emission and absorption cross section of Yb^{3+}ions in silica.*

Yb-doped silica fibers are excellent media for high power lasers and amplifiers. The absence of higher energy levels greatly reduces the effect of multi-phonon relaxation and excited state absorption (ESA). Yb^{3+}-ions in silica has much higher absorption and emission cross-sections than multi-component. Furthermore, cooperative up-conversion, a process in which two near neighbouring Yb^{3+}-ions combine their excitation energy to emit a single photon in the green region of the spectrum is very small even in strongly doped fibers. This combination of advantages allows very high pump absorption and very short length fiber lasers.

The other advantage of Yb-doped fiber laser is the small quantum defect (percentage of Quantum defect). Due to the emission wavelength near ~1060 nm and pump wavelength in the 915 to 975 nm range, Yb-doped fiber lasers offer excellent optical-to-optical efficiency and results in reduced heat generation in the gain medium. In addition, the long and thin optical fiber (typically on the order of 10 m long and 125 µm in diameter) has a high surface area-to-volume ratio, which allows the fiber to expel heat rapidly. If one would like to scale a laser to high average power, this is a wonderful combination, because the Yb-doped fiber laser generates relatively little heat, and the heat it generates is quickly dissipated. Due to the small quantum defect and large upper state life time, Yb-doped fiber lasers are suitable for the development of high power CW and pulsed fiber lasers.

1.1 Ytterbium doped CW fiber lasers

Yb-doped fiber lasers superior power-scaling properties stem from an exceptionally low quantum defect for laser diode pumping at 915 nm or 975 nm and thus a low thermal load as well as high permissible dopant concentrations and thus high pump absorption per unit length. Both of these are important factors for power scaling of fiber lasers with thermal management greatly further simplified by the fiber geometry. Nonlinearities and damage are equally important factors. These are easiest to avoid in CW operation and consequently the record-breaking CW fiber lasers of high power have been developed. Thus, by means of rather simple and robust configurations one achieves a large enhancement of the fiber laser's beam brightness compared to that of the pump. Cladding-pumped YDFLs allow for up to six orders of magnitude brightness enhancement theoretically, and close to five orders have been demonstrated experimentally. Jeong et al. demonstrated a highly-efficient cladding-pumped YDFL generating 1.36 kW of continuous-wave output power at 1.1 μm with 83% slope efficiency and near diffraction-limited beam quality [9].

A novel approach to overcome the primary obstacles in power scaling of broadband single-mode fiber lasers involves use of fiber lasers to resonantly pump final stage high power amplifier rather than using pump diodes [10]. This scheme is known as tandem pumping. In tandem-pumping, one or several fiber lasers pump another one, which offers several advantages for power scaling. In particular, it makes it possible to pump close to the emission wavelength so that the quantum defect heating can be low resulting in a reduced thermal load. IPG's 10 kW fiber laser was pumped by Yb-doped fiber lasers at 1018 nm and emitted at 1070 nm, for a quantum defect of less than 5%, which is roughly half of that of a directly diode-pumped Yb-doped fiber laser [10]. The high pump brightness possible with tandem-pumping also allows for a reduction in the dimension of the inner cladding required to reach high power levels. Although it is possible to launch sufficient diode power into a thick but realistic Yb-doped fiber to reach 10 kW output power level given the brightness of current state-of-the-art pump diodes, however it is quite challenging. YDFLs are also capable of generating pulses with high energy and peak power. Different Q-switching techniques to generate nano-second pulses have been discussed in the following section.

1.2 Pulsed fiber lasers

High-peak-power short-pulse Yb-doped fiber lasers are very promising in the field of industrial processing, range finding, remote sensing, and medicine owing to their higher efficiency, good beam quality, and compactness [19, 20, and 21]. One of the technique to produce short pulses in the nanosecond range with high pulse energy is by Q-switching. In Q-switching, energy is stored in the amplifying medium by keeping Q-value of the cavity low, by precluding laser oscillation. Due to optical pumping, the energy stored in the medium is high, but losses are also high in the cavity and hence, lasing doesn't take place. In this case, energy is stored in the form of high value of population inversion, which is directly dependent upon the upper state life time of the gain medium. When Q-value of the cavity is made high, the stored energy is released in a very short time in the form of a short pulse with high energy and peak power. There are two basic techniques of Q-switching, passive Q-switching and active Q-switching. For active Q-switching we have used

Acousto-optic modulator (AOM), and for passive Q-switching Cr^{4+}: YAG crystal has been used in Yb-doped fiber laser.

1.5.1. Active Q-switching

In active Q-switching, Q-of the cavity is controlled externally by means of an external control signal. The Q-switch can be mechanical device like shutter or chopper wheel, it can be a modulator, such as acousto-optic modulator or an electro-optic device like pockel cell. Due to the external control, repetition rate of pulses can be controlled externally, but the active Q-switching devices are more expensive. In our work we have used, acousto-optic modulator (AOM) as a Q-switch for the generation of pulses. Working of AO Q-switch has been discussed in the following section.

Working of an acousto-optic Q-switch

When an acoustic wave propagates in a Q-switch cell having quartz medium, a periodic refractive index variation in the medium is created due to the compression and rarefaction by the acoustic waves, via photo-elastic effect and this leads to the formation of a refractive index grating in the medium. The grating has a period equal to the acoustic wavelength and an amplitude proportional to the acoustic wave intensity. When the incident light beam interacts with such a refractive index grating, it produces either single-order diffraction or multiple-order diffraction depending on the length of interaction. Multiple order diffraction is referred as Raman-Nath diffraction and single order diffraction is referred as Bragg diffraction. In Bragg regime, the grating acts as a thick phase grating. Acousto-optic Q-switches work on the principle of Bragg diffraction, where periodic refractive index is created in an acousto-optic cell by the application of radio frequency (RF) waves to a transducer, which is attached to a transparent medium on one end. At the other end of the acousto-optic cell, an acoustic absorber is placed to avoid reflected acoustic waves. Frequency of the RF waves are in tens of megahertz range, which falls in the ultrasonic frequency range, and the beam interaction length is of the order of a few centimeters. When a laser beam of frequency ω is allowed to pass through such an acousto-optic cell at Bragg angle (acoustic wave of frequency Ω), diffraction of the beam takes place. The laser beam is diffracted to a single order if the beam is incident at an angle equal to the Bragg angle, which is given by [22]

$$\sin\Theta = \frac{\lambda_0}{2n_0\Lambda} \tag{1.5}$$

where, n_0 is the refractive index of the medium, λ_0 is the free space optical wavelength and Λ is the acoustic wavelength.

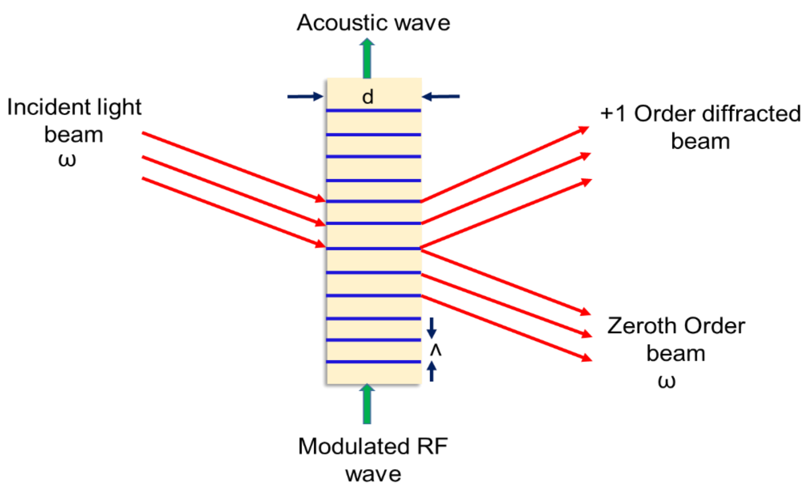

Fig. 1.5: *Schematic of Bragg diffraction by acousto-optic Q-switch cell.*

Diffracted beam in the +1 order will have a frequency ω+Ω and the diffraction efficiency will depend on acoustic intensity, interaction length and figure of merit of acousto-optic material. Figure 1.5 shows a schematic of single order Bragg diffraction from an acousto-optic cell. In the process of Q-switching, when RF signal is applied to the AO-Q switch, it diffracts the laser radiation in the first order. In fiber laser, for Q-switching, cavity is aligned in the first order. Since the cavity is aligned in the first order, losses are created when no RF signal is applied to the Q-switch cell. In this duration population inversion build-up takes place inside the gain medium. When RF signal is applied, the beam is diffracted and the feedback from the mirrors are resumed and a giant pulse with high peak power and low pulse duration of nanosecond order is generated.

1.5.2 Passive Q-switching

In passive Q-switching, saturable absorber acts as a Q-switching element. Saturable absorber is a material whose transmission is dependent on the intensity of light and it increases with increase in the intensity beyond a threshold level. For Yb-doped fiber laser, Cr^{4+}: YAG crystal can be used as a passive Q-switching element. Energy level diagram of a saturable absorber is shown in the Fig. 1.6. Level 1 is the ground level and required absorption occurs from level 1 to level 3 transition. It is assumed that transition from level 3 to level 2 and level 4 to level 2 are fast, and life time of upper state level 2 is large so that, there is a saturation of level 2 with increase of laser intensity [22]. Thus the transmission through the saturable absorber will increase with input intensity. Initially, when the intra-cavity intensity is low, the loss inside the cavity is high as saturable absorber absorbs the photons and a high population inversion is created in the gain medium. When the intra-cavity intensity increases, it saturates the absorber, i.e., rapidly reduces the resonator loss, so that output average power increases. In this condition, absorber is in the state of low loss and Q of the cavity is increased, so the stored energy comes out in the form of a laser pulse. After the emission of laser pulse, again the absorber resumes its high loss state and population inversion is created. In this way, the intra-cavity intensity controls the working of saturable absorber. In a passively Q-switched CW pumped laser, peak power and pulse width remains constant, but the repetition rate increases approximately linearly with input pump power [22]. In this case, direct control of the repetition rate can be achieved by using a pulsed pump source.

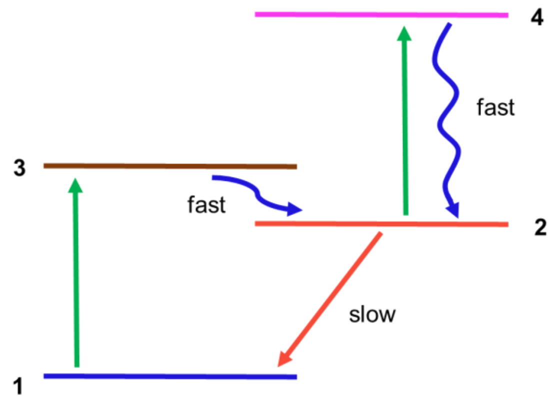

Fig. 1.6: *Energy levels of a saturable absorber.*

Although these Q-switching techniques can be applied in fiber lasers also, but there are certain limitations in the path of development of high power CW output, higher values of pulse energy and average power due to thermal effects, nonlinear effects, fiber fuse effect etc. These limitations are discussed in the following section.

1.6 Physical limitations for power scaling of fiber lasers

The typical approach for power scaling from a fiber laser oscillator or amplifier is to increase core diameter, since nonlinear and facet-damage thresholds increase with increase in core diameter. There is an optimum fiber length and a maximum output power that can be achieved with good beam quality from a single fiber laser oscillator or amplifier. In this section, critical limits relevant to the power scaling of fiber lasers has been discussed. These include limits imposed by thermal considerations, fiber non-linearities, facet damage and brightness of pump diode lasers. The combination of limits on rare earth doping concentration, finite brightness of the pump diode lasers and requirement for high efficiency places bounds on the relative ratio of the core and inner cladding diameters of active fiber [23].

1.6.1 Thermal limitations

Although fiber lasers are known to have lower thermal problems due to large surface to volume ratio, however in high power fiber lasers heat dissipation becomes considerable due to two main reasons; i.e., quantum defect and quantum efficiency. Quantum defect is the energy difference between pump and laser photons and is lost to the silica host in the form of non-radiative transitions. It is given by $\left(1-\frac{\lambda_{pump}}{\lambda_{laser}}\right)$, and is ~19% for pumping at 976 nm and lasing at 1064 nm. The quantum efficiency of the laser transition is less than $\frac{\lambda_{pump}}{\lambda_{laser}}$ in all practical applications, since the non-radiative decay rate from the lasing level is non-zero and a fraction of the pump power is directly dissipated as heat. The heat dissipated by gain fiber should be removed either by conduction cooling or forced convection cooling for effective heat transfer and reliable operation. Heat dissipated in the core having dopants is conducted through inner clad to outer clad and then to environment. Thus, in steady state, a temperature gradient ΔT is created between the central fiber core axis and external environment. This temperature gradient across fiber cross-section leads to thermal stress in the fiber and at very high pump powers, it may cross the fracture limit of the fiber, which in turn sets an upper limit for maximum amount of heat that can be dissipated in the gain fiber. As the refractive index of core and cladding also depend on temperature, a higher temperature gradient will change V-number of the fiber and will also degrade beam quality. Further, since outer cladding is made of soft flouro-acrylate polymer, operation of the outer clad at high temperature may lead to its chemical instability and its burning also. Thus, a high temperature rise of the outer clad should be prevented by applying appropriate effective heat transfer methods to the surrounding. Figure 1.7 shows geometry of the gain fiber with core radius 'a' and inner clad radius 'b', r is radial co-ordinate and φ is tangential angle. Flow of heat occurs from high temperature core region to inner and outer clad region of the active fiber.

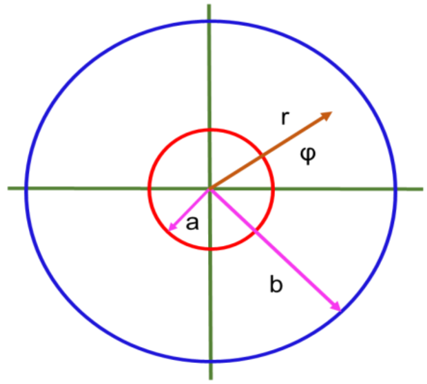

Fig.1.7: *Geometry of the fiber showing core and inner cladding radius for heat flow.*

Using basic heat equations as described in Chapter 2, temperature distribution in the core and cladding can be formulated and the maximum tolerable heat power P_{hf}^{M} per unit length without thermal fracture of the active fiber is given by [23,24]

$$\frac{P_{hf}^{M}}{L} = \frac{4\pi R_m}{1-\frac{a^2}{2b^2}} \tag{1.6}$$

where, L is the length of the active fiber, R_m is the rupture modulus of the glass (2460 W/m in silica [25]). If, η_h is the heat fraction of absorbed pump power, the maximum extractable power P_{exf}^{M} per unit length at fracture limit is given by [25].

$$\frac{P_{exf}^{M}}{L} = \frac{4\pi R_m}{1-\frac{a^2}{2b^2}} \frac{(1-\eta_h)}{\eta_h} \tag{1.7}$$

Thus, for a given fiber, maximum tolerable heat and extractable power without fracture can be evaluated using Eq. (1.6) & (1.7) and its pumping power limit can be decided for safe operation.

1.6.2 Limitations due to non-linear effects

While considering continuous wave (CW) high power fiber lasers and amplifiers, there is an interest in lasers that have broad bandwidth as well as lasers that operate with very narrow spectral width. The two systems have different, but functionally similar non-linear limitations. In the broadband case, the limit to output power is imposed by stimulated Raman scattering (SRS) and in narrow linewidth case, it is due to stimulated Brillouin scattering.

1.6.2.1 Stimulated Raman Scattering (SRS)

Raman scattering is an inelastic scattering that arises from the interaction of light with the vibrational modes of the constituent molecules in the scattering medium; equivalently this can be considered as the scattering of light from optical phonons. In spontaneous Raman scattering a small fraction ($\sim 10^{-6}$) of the incident optical beam at frequency ω_p is converted to an optical beam at down shifted frequency ω_s determined by vibrational state as shown in Fig. 1.8 (a) [26]. In fiber due to long interaction length stokes signal at the peak wavelength of the Raman gain (~13.2 THz in case of silica glass) becomes a significant fraction of the propagating power. As the signal power at ω_p increases, eventually the power length product in the fiber reaches a point where Raman gain is very high and lead to stimulated Raman scattering (SRS) phenomenon as shown in Fig 1.8 (b).

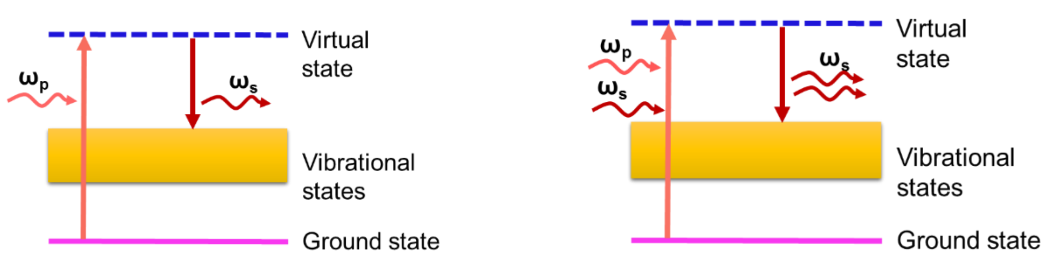

(a) (b)

Fig.1.8: *(a) Spontaneous Raman Scattering and (b) Stimulated Raman scattering processes.*

The threshold power for generation of SRS in fiber is given by [26]

$$P_{out}^{SRS} = \frac{16A_{eff}}{g_R L_{eff}} \tag{1.10}$$

where, g_R is the Raman gain coefficient (~10^{-13}m/W for silica), A_{eff} is the effective area of the mode and L_{eff} is the effective length of the fiber, which is dependent upon the fiber gain or loss. The signal power is then effectively limited and further increases in the pump power, results in conversion of signal power (ω_p) to progressively longer unwanted wavelengths (ω_s) [26, 27]. However, SRS is advantageous in development of Raman amplifiers.

1.6.2.2 Stimulated Brillouin Scattering (SBS)

Brillouin scattering arises from the interaction of light with propagating density waves or acoustic phonons. At high enough input powers, SBS will convert transmitted light in the fiber to a scattered, Stokes-shifted (downshifted) reflection well above typical Rayleigh scattering power levels. This phenomenon arises from the interaction between the optical field and acoustic phonons in the fiber, driven through an electrostrictive process where the medium becomes denser in regions of high optical density. For optical signals whose bandwidth is narrow compared to the Brillouin bandwidth (~50-100 MHz), the output amplifier power clamps when electrostriction creates an acoustic wave in the fiber, leading to back scattering of the signal power. The functional form of this limit is quite similar to the SRS limit [26, 28].

$$P_{out}^{SBS} = \frac{21A_{eff}}{g_B L_{eff}}\left[1+\frac{\Delta\upsilon_s}{\Delta\upsilon_B}\right] \qquad (1.11)$$

where, g_B is the Brillouin gain coefficient, which depends upon the laser signal linewidth, and its peak value is ~$5\text{X}10^{-11}$ m/W for silica optical fibers. $\Delta\upsilon_s$ and $\Delta\upsilon_B$ represents laser signal linewidth and Brillouin gain bandwidth.

1.6.3 Damage limitations

There is an extensive work on optical damage in both optical fibers and bulk silica glass, but even the relative magnitude of the damage threshold for optical fibers and bulk silica glass has not been established. Furthermore there are bulk optical damage mechanisms unique to fiber such as fiber fuse effect [29], which should also be considered. However, fiber damage is typically observed at the end facet. End-cap schemes that allow the fiber mode to expand in the bulk prior to striking an air-glass interface can increase the surface damage limit. All of these mechanisms put a limit on the allowed peak power density at the output end of the fiber. Thus, for a simple Gaussian-like fundamental mode, the maximum damage-limited output power of a fiber laser or amplifier is given by [25]

$$P_{out}^{damage} = \Gamma^2 I_{damage} \pi a^2 \tag{1.12}$$

where, I_{damage} is the upper limit of the intensity allowed in the fiber. Without end-caps, I_{damage} would be given by the surface damage limit of optical fibers, (~10 W/μm^2 for silica) [25]. With end caps, the bulk damage threshold is the damage limit.

1.6.4 Fiber Fuse Effect

Fiber fuse effect is a process in which there is a catastrophic damage of core of an optical fiber from the point of its creation towards the light source. It appears like a burning fuse and hence named as fiber fuse effect [29]. In this effect, damage occurs from the output end of the fiber. This effect was first reported in the year 1987 [29]. The threshold power density for the initiation of the fiber fuse effect was reported to be ~ 2-3 MW/cm^2 and it is independent of the core composition in the fiber [30]. It may be noted that the laser-induced-damage-threshold for fiber fuse is many orders of magnitude below intrinsic laser induced damage threshold for silica, which is ~10

GW/cm^2 for CW operation at 1064 nm [31]. There are various mechanisms proposed for the initiation of fiber fuse effect like thermal lensing of the light in the fiber, self-propelled self-focusing [29], and an exothermal chemical reaction involving the formation of Ge-defects [32]. But, the thermal mechanism are found to be responsible for the fiber fuse generation.

In the early studies, it was observed that at high temperatures beyond 1000°C, absorption of the silica-based core in the fiber rises abruptly. This is due to the formation of SiO gas and/or solid, which are produced in the silica glass and exhibit large absorption coefficient (α) values of the order of 10^4 m^{-1} at 2020°C [33]. Formation of SiO in the fiber core, triggered from the surface heating (the 1st step) due to the surface absorbing impurities, will result in the subsequent heating (the 2nd step) inside the core due to huge absorption of the guided laser light. This second step forms the fuse and the subsequent propagation of the fuse towards the light source [34].

Chapter 2

Study on self-pulsing dynamics, multi-wavelength generation and thermal effects in Yb-doped fiber laser

2.1 Introduction

In recent years, high power Yb-doped fiber lasers have become highly competitive options for the industrial and defense laser markets as high power fiber lasers offer numerous advantages like high efficiency, high reliability, low thermal problems, excellent beam quality, flexible fiber delivery, together with small footprint and volume. Along with the high power output, linearly polarized output is also preferred for a wide variety of applications, such as material processing and optical parametric processes [35, 36, and 37]. There are reports on the commercially available multi-kilowatt Yb-doped fiber lasers with up to 10 kW single mode output and about 50 kW multimode output power [10, 11]. However, the conventional large mode area fibers suffer from the limitations of nonlinear phenomena like stimulated Raman scattering (SRS), stimulated Brillouin scattering (SBS) and mode-quality degradation at high power levels. In recent years, a new class of fibers referred as photonic crystal fibers (PCF) have been introduced which are special fibers that consist of a regular micro-structured array of holes, where the core is formed by a solid- or air-filled defect and the light guidance takes place due to the microstructures present in the fiber [38]. Due to the presence of air clad in PCF, high value of numerical aperture (NA) of ~0.8 can be achieved. The advantage of such a fiber is that the diameter of the inner cladding can be reduced while retaining numerical aperture of the pump core. Due to the increased ratio of active core area to inner cladding area, the pump light absorption is improved and smaller fiber lengths are required for sufficient absorption. The first PCF laser was reported in the year 2000 [36]. Later on, 633 W of LP output with polarization extinction ratio greater than 16 dB by using Yb-doped large mode area (LMA) polarization maintaining (PM) fiber was demonstrated using external optics to maintain the polarization in PM fiber [37]. To remove the requirement of external polarizing optics, special PCF fibers referred as polarizing PCF were fabricated, which exploits the arrangement of air holes to generate polarized output [38]. There are various applications like spectroscopy, wavelength division multiplexing, and fiber optic sensors in which along with polarized signal, multi-wavelength output is also required [39,40]. Multi-wavelength operation has also been demonstrated in Yb-doped fiber lasers based on a few-mode fiber Bragg grating (FMFBG), multimode FBG and by controlling the birefringence inside the cavity [41, 42]. Dual wavelength operation in Yb-doped fiber laser has been reported by varying the length of the gain fiber and pump power [43]. Nonlinear effects such as stimulated Brillouin scattering (SBS) and four-wave mixing (FWM) in fibers also contribute to the multi-wavelength generation [44].

For generation of high CW output power, rare earth doped fiber lasers have achieved a state-of-the-art technology, still there is a continued research interest in such fiber lasers due to the presence of self-pulsing phenomena, which is encountered while working with such lasers. The random pulsed output of the fiber laser, generated even during the CW pumping scheme, is termed as self-pulsing and has been reported widely [45–54]. The various mechanisms which are attributed for self-pulsing in fiber lasers are: re-absorption by the unpumped part of the fiber which acts as a saturable absorber, external perturbations such as pump noise, thermal effects, SBS and interaction between the gain medium and the pump input [47, 48, and 49]. However, in spite of all the above mentioned works in this area, to the best of our knowledge, no detailed analysis of the self-pulsing dynamics in Yb-doped PCF lasers has been carried out. Similarly for multi-wavelength generation there are reports in which long length of the nonlinear fiber has been added to increase the effects like FWM to generate multi-wavelength, but the reports for multi-wavelength generation are limited to 1 W of output power range.

While working with high power fiber lasers, there is a prerequisite to understand thermal effects taking place in fiber laser components for efficient heat removal and thermal management. Mechanisms which are responsible for heat generation in the doped fiber are quantum defect, i.e. the energy difference between laser photons and pump photons and quantum efficiency which is always less than unity, so that a fraction of the excited atoms decay by non-radiative relaxation and generate heat [55, 56]. The generated heat creates a temperature gradient in the fiber along the radial as well as longitudinal direction. This pump-induced temperature gradient can cause a number of serious problems [57], such as formation of thermal cracks due to internal thermal stress and expansion, shortening of fiber lifetime due to damage of outer polymer jacket, even melting of the glass, degradation of laser beam quality due to thermal lensing, and decrease in laser quantum efficiency. Heating also affects the wave guiding and lasing properties of Yb-doped fibers due to variation of core temperature and population of the stark split energy sublevels. Yb-ions in silica possess simple atomic structure, with only two principal manifolds $^2F_{5/2}$ and $^2F_{7/2}$. It is the ideal rare earth element for the lasing as there is no excited state absorption. Weak multi-phonon decay is the only non-radiative channel that exists and it also results in heating. Population of these levels follows Boltzmann distribution.

In this chapter, we present the realization of 43 W of single transverse mode linearly polarized output using double-end pumping configuration, multi-wavelength and narrow linewidth polarized operation by using dichroic mirror and fiber Bragg grating mirror from a Yb-doped polarizing PCF with polarization extinction ratio of ~10.5 dB[58]. Polarization extinction ratio of 10.5 dB was achieved by proper alignment of the fiber birefringent axis and without using any polarizing optics. We also present self-pulsing dynamics of the Yb-doped polarizing PCF laser in single-end pumping configuration and double-end pumping configurations. It was observed that when the PCF laser was pumped in the single-end pumping configuration, self-pulsing was initiated due to the relaxation oscillations and was then sustained due to the saturable absorption in the weakly pumped portion of the PCF. When the pump power was increased sufficiently, intensity and frequency of occurrence of self-pulses were reduced in both the configurations. In the double-end pumping configuration, the intensity of the self- pulses were found to be less as compared to the single-end pumping at all values of absorbed pump powers. Rate equations have also been solved to comprehend the reason behind the occurrence of self-pulses in the low pump power regime and reduction in intensity of these pulses when the pump power was sufficiently increased [59]. Our analysis shows that the non-uniform single pass distribution of the upper level population in the gain medium is responsible for the occurrence of self-pulses. Due to the non-uniformity of single pass values of upper level population along the doped fiber, large population of atoms is present in the ground state resulting in re-absorption. The weakly pumped region of fiber acts as saturable absorber which leads to self-pulsing. Self-pulsing can be suppressed if uniform single pass distribution of upper laser level population along the length of the fiber is ensured. Estimated threshold power for SRS and SBS and the signal spectrum confirms that self-pulses are not generated due to the nonlinear interactions. Multi-wavelength operation in Yb-doped PCF laser has also been demonstrated by the addition of an extra length of passive fiber and FBG, which provides the output lasing wavelength operation in two wavelength ranges. We have also presented, study of thermal effects in high power Yb-doped double-clad fiber laser in single and double end pumping configuration by using thermal conductive equations and the steady-state rate equations.

2.2 Theoretical analysis

The steady-state rate equations for double-clad CW fiber lasers with Fabry–Perot cavity, the population of the upper level and the evolution of the pump and signal powers along the doped fiber are given by the following coupled equations [60, 61]

$$\frac{N2(z)}{N}=\frac{\dfrac{\left[P_p^+(z)+P_p^-(z)\right]\sigma_{ap}\Gamma_p}{h\nu_p A}+\dfrac{\Gamma_s}{hcA}\int\sigma_a(\lambda)\left[P_s^+(z,\lambda)+P_s^-(z,\lambda)\right]\lambda d\lambda}{\dfrac{\left[P_p^+(z)+P_p^-(z)\right]\left(\sigma_{ap}+\sigma_{ep}\right)\Gamma_p}{h\nu_p A}+\dfrac{1}{\tau}+\dfrac{\Gamma_s}{hcA}\int\left[\sigma_e(\lambda)+\sigma_a(\lambda)\right]\left[P_s^+(z,\lambda)+P_s^-(z,\lambda)\right]\lambda d\lambda} \tag{2.1}$$

$$\pm\frac{dP_p^{\pm}(z)}{dz}=-\Gamma_p\left[\sigma_{ap}N+\left\{\sigma_{24}-\left(\sigma_{ap}+\sigma_{ep}\right)\right\}N_2(z)\right]P_p^{\pm}(z)-\alpha\left(z,\lambda_p\right)P_p^{\pm}(z) \tag{2.2}$$

$$\pm\frac{dP_s^{\pm}(z)}{dz}=\Gamma_s\left[\left\{\sigma_e(\lambda)+\sigma_a(\lambda)\right\}N_2(z)-\sigma_a(\lambda)N\right]P_s^{\pm}(z,\lambda)+\Gamma_s\sigma_e(\lambda)N_2(z)P_0(\lambda)-\alpha(z,\lambda)P_s^{\pm}(z,\lambda) \tag{2.3}$$

where, $N=N_1+N_2$ represents the doping concentration of Yb^{3+} ions in the core, with N_1 and N_2 as the lower and upper level population densities; superscripts plus and minus represent propagation along positive and negative z-directions. σ_a and σ_e are the absorption and emission cross-sections with subscripts *p* and *s* for the pump and signal, respectively, and τ is the upper level lifetime. $\Gamma_p = A/A_{innerclad}$ *and* $\Gamma_s = P_{core}/(P_{core}+P_{clad})$ represent the power fill factor for pump and signal, respectively. α is the scattering loss coefficient and σ_{24} is the excited-state absorption cross-section. ν_p and ν_s are the pump and signal frequencies and *A* is the area of the fiber core. In Eq. (2.3), $P_0(\lambda)=2hc^2/\lambda^3$ is the power density per unit wavelength corresponding to the contribution of spontaneous emission into the propagating laser mode. $P_p^{\pm}(z)$ and $P_s^{\pm}(z)$ represent the pump and signal power, respectively. $P_s^{\pm}(z,\lambda)$ represents the signal power density per unit wavelength and is related to the signal power by

$P_s^{\pm}(z) = P_s^{\pm}(z,\lambda)\Delta\lambda_s$, where $\Delta\lambda_s$ is the signal bandwidth around the central lasing wavelength λ_s. As the signal is propagating in the forward as well as backward directions, the boundary conditions are given by,

$$P_s^{+}(0) = R_1 P_s^{-}(0) \tag{2.4}$$

$$P_s^{-}(L) = R_2 P_s^{+}(L) \tag{2.5}$$

where, R_1 and R_2 are the reflectivities of the rear and output coupler mirrors. L represents the fiber length. For strong pumping conditions, the contribution of spontaneous emission is negligible, and from Eq. (2.3), we have the following conservation condition

$$P_s^{+}(0)P_s^{-}(0) = P_s^{+}(L)P_s^{-}(L) = P_s^{+}(z)P_s^{-}(z) \tag{2.6}$$

The above equation implies that the product of forward and backward propagating signal power is constant along the fiber length, and is used to find the initial signal power that satisfies the boundary conditions. The output power obtained from the output coupler end is given by,

$$P_{out} = (1 - R_2)P_s^{-}(0) \tag{2.7}$$

The coupled equations 2.1, 2.2 and 2.3 were solved numerically by using fourth order Runge–Kutta method satisfying boundary and conservation conditions mentioned in the equations (2.4), (2.5) and (2.6) to evaluate the pump power and signal power distribution inside the fiber laser resonator. Evolution of instantaneous upper level population along the length of the fiber for single end and double end pumping was solved by assuming that there is no feedback in the cavity. The results of simulation have been discussed and compared with the experiments in the "Results and Discussions" part of this Chapter.

The pump light is absorbed by ytterbium ions in the core region. Thus, there is heat source in the core that does not exist in the cladding regions. Since the fiber length is much larger than the fiber cross-section, the capability of heat dissipation from the fiber end facet is a lot lower than that from the fiber side. Therefore the transverse and longitudinal temperature distributions in the Yb-doped double clad fiber at room temperature are governed by the following thermal conductive equations in the symmetric cylindrical co-ordinates [56]

$$\frac{1}{r}\frac{\partial}{\partial r}\left(r\frac{\partial \mathrm{T}_1(r,z)}{\partial r}\right)=-\frac{Q(r,z)}{\kappa_F} \qquad (0\le r\le r_1) \tag{2.8}$$

$$\frac{1}{r}\frac{\partial}{\partial r}\left(r\frac{\partial \mathrm{T}_2(r,z)}{\partial r}\right)=0 \qquad (r_1\le r\le r_2) \tag{2.9}$$

where, T_1 and T_2 are the temperature of the fiber core and fiber clad in the axial direction, respectively, r_1 and r_2 are the radius of the fiber core and inner-clad, k_F is the fiber thermal conductivity, $Q(r,z)$ is the heat dissipated in the unit volume of fiber. Temperature continuity at the inner boundaries and Newton's law of cooling are used as the two boundary conditions for determining the core temperature and they are given as,

$$T_1(r=r_1)=T_2(r=r_1), \quad \frac{\partial T_1(r=r_1)}{\partial r}=\frac{\partial T_2(r=r_1)}{\partial r} \tag{2.10}$$

$$\frac{\partial T_1(r=r_1)}{\partial r}=\frac{H}{k_F}[T_h-T_2(r=r_2)], \tag{2.11}$$

where, H is the convective heat transfer coefficient, which is temperature dependent, T_h is the temperature of the heat sink, which is taken as 298 K. Change in the refractive index due to temperature gradient is given by

$$\Delta n_{I,II}(r)=\beta(T_{I,II}(r)-T_h) \qquad \beta=\frac{dn}{dT} \tag{2.12}$$

Clad and core regions are represented by indices *I and II,* respectively. Parameters used in the simulation have been taken from references [55, 57].

With change in the temperature of the core of the fiber, population in the different levels of Yb-doped ions in the glass also changes, which is govern by the Boltzmann distribution equation given by,

$$\frac{N_b}{N_1} = e^{-\Delta E / k_b T} \tag{2.13}$$

where, N_b is the population of level "b" of Yb-doped ions(Fig 1.4(a)), N_1 is the population of the ground level, T is the temperature of the core, k_b is the Boltzmann constant and ΔE is the energy difference between ground level and level b. From the rate equation 2.1 and $N = N_1 + N_2$, N_b is calculated.

2.3 Experiment

2.3.1 Experimental setup for the study of self-pulsing dynamics

A schematic of the experimental setup for the study of self-pulsing dynamics in the single and double-end pumping configuration is shown in Fig. 2.1(a) and (b), respectively.

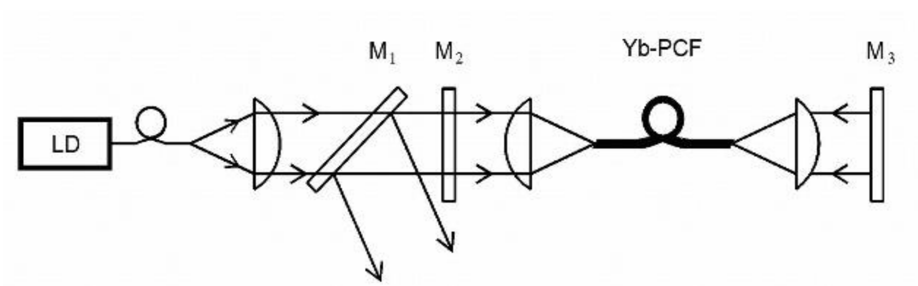

(a)

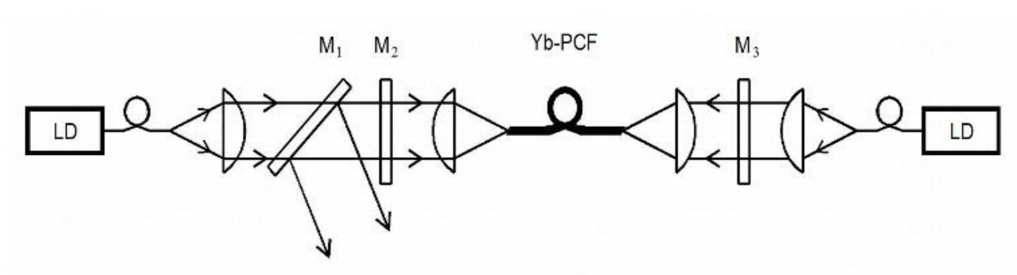

(b)

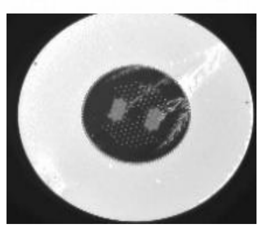

(c)

Fig. 2.1: *Experimental setup for the study of self-pulsing dynamics in a Yb-doped PCF fiber laser in (a) single end pumping configuration, (b) double end pumping configuration, and (c) end face*

Components	Parameters	Values
Yb-doped PCF	Absorption	10 dB/m
	Length	1.25 m (for self-pulsing study) and 1.5 m (for output power measurement)
	Core/cladding diameter	40/200 µm
	Birefringence	$1\text{x}10^{-4}$
Dichroic Mirrors	M_1	HR>99% @1035-1120 nm; angle of incidence (AOI)=25° ;HT >90% @960-980 nm
	M_2	R=4% @1035-1120 nm; AOI =0° ;HT >90% @960-980 nm
	M_3	HR>99% @1035-1120 nm; AOI= 0° ;HT >90% @960-980 nm
Coupling Lenses	Focal length	20 mm
	Diameter	15 mm
Pump laser diodes	Power	40 W@975 nm at 25°C at the highest value of input current
	Fiber pigtail Core diameter/NA	200 µm /0.22
Fiber Bragg grating	FBG	HR>99% @ 1090 nm

picture of Yb-doped PCF.

In each case, a Yb-doped polarizing PCF having a mode field diameter of 29.5 µm at 1060 nm with numerical aperture (NA) of 0.03, and an inner-clad diameter of 200 µm with an NA of 0.55 has been used. Large NA of inner clad relaxes the tolerances on coupling optics for coupling pump light into the inner clad of the PCF.

Table 2.1: *Experimental parameters of the components used in the experiment*

The clad-pump absorption of the doped fiber is 10 dB/m at 976 nm. Boron doped silicate rods in the micro-structured inner clad provide a birefringence of about $1\text{x}10^{-4}$. Fig. 2.1(c) shows the transverse cross-section of the PCF, with the core, pump clad and the second clad of the fiber. Both ends of the fiber are angle polished at 5º to prevent feedback from the end faces. Fiber-coupled laser diodes having 40 W CW power at the center wavelength of 975 nm at 25 ºC were used to pump 1.25 m length of the Yb-doped PCF either from one end or from both the ends. The coupling efficiency of incidence light in Yb-PCF is about 80%. It is estimated by measuring the leakage pump power from other end of the fiber and data of inner clad pump absorption provided by the supplier. The pump laser output, having a 200 μm core diameter fiber pigtail with 0.22 NA was collimated using a lens of 20 mm focal length and was then focused using another lens of 20 mm focal length to obtain a focused spot diameter of about 200 μm on the input end of the doped fiber. Two dichroic mirrors M_2 and M_3 formed the optical resonator; both mirrors have high transmission at 975 nm, while for the lasing wavelength mirror M_2 has 4% reflection at the normal incidence and mirror M_3 has high reflection in the broad range of 1035–1120 nm for normal incidence. Mirror M_1 is used to take laser beam out from the laser and has similar characteristics as M_3 for 25º angle of incidence. The experimental parameters of the components used in the experiment are given in Table 2.1.

2.3.2 Experimental setup for the study of multi-wavelength generation in Yb-doped PCF

Figures 2.2(a)-(d) show the schematic of the experimental setup of Yb-PCF laser in different configurations. Figures 2.2(a) and 2.2(c) show the experimental setups without and with passive fiber spliced to the Yb-PCF and dichroic mirror is used as the feedback mirror. Dichroic mirror

(DM) is used to take laser beam out from laser and is used to pass the pump beam and reflect the generated laser signal at an angle. Figures 2.2(b) and 2.2(d) show the corresponding experimental setups without and with passive fiber spliced to the Yb- PCF and FBG mirror is used for the feedback in the set up. FBG mirror has a high reflection of ~99.9% at 1090 nm with FWHM linewidth of 0.2 nm and is written in the core of double clad fiber with core/clad diameter of 20/400 µm. The output end of the FBG has been angle cleaved at 10° to prevent feedback from end faces. In each case Yb-doped PCF as described in Sec. 2.3.1 has been used as a gain medium with the length of 1.5 m which resulted in pump absorption of about 15 dB, or ~ 88% of pump power. Passive fiber used is a double-clad fiber, which is compatible with the fiber on which FBG mirror is written. Pump diode is same as described in the previous section.

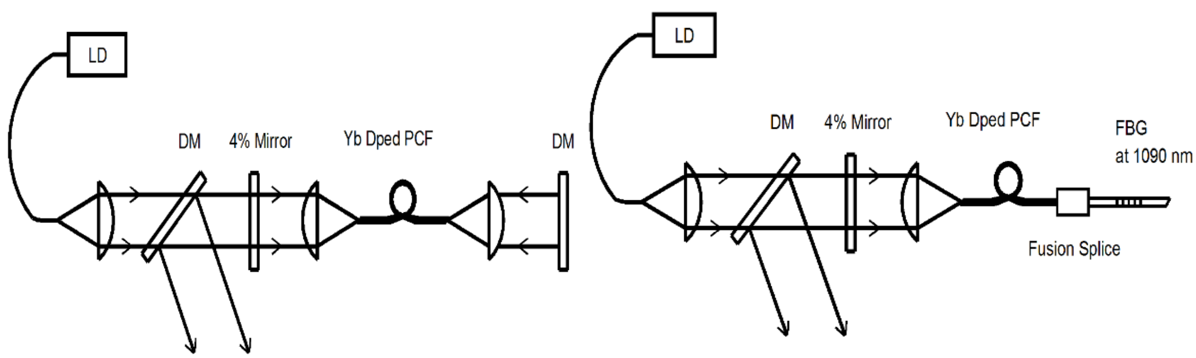

(a) **(b)**

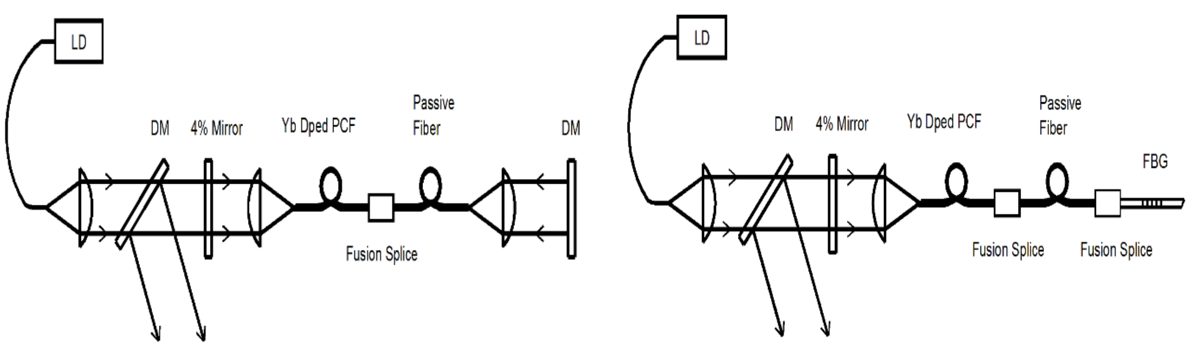

(c) **(d)**

Fig.2.2: *Schematic of the laser setup: (a) dichroic mirror (DM) is used as feedback mirror, (b) FBG is used as feedback mirror , (c) passive fiber is spliced with Yb-PCF and dichroic mirror is used as feedback mirror, (d) passive fiber is spliced between Yb-PCF and FBG.*

2.4 Results and Discussion

2.4.1 Self-pulsing dynamics in Yb-doped PCF laser

Figures 2.3(a) and (b) shows variation of the fiber laser output power as a function of the absorbed pump power for single end and double end pumping cases. To determine the absorbed pump power inside the gain fiber, leakage pump power at the other end of the fiber was measured.

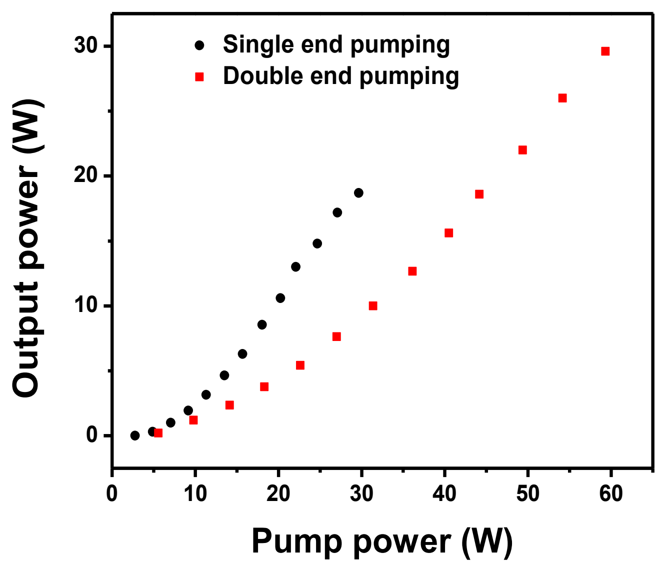

(a)

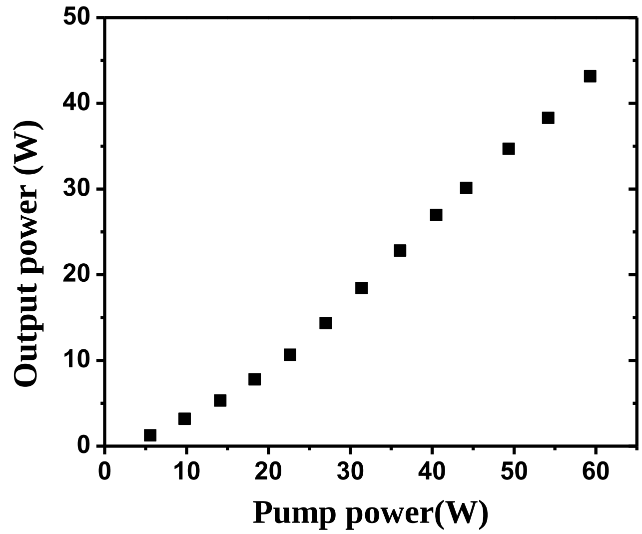

(b)

Fig. 2.3:*(a)Variation of laser output power as a function of pump power for single end (circle) and double-end pumping configuration (square) for 1.25 m length of the PCF. (b) Variation of laser output power as a function of pump power for double-end pumping configuration for 1.5 m length of the PCF.*

In the case of the single end pumping configuration, maximum output power of 18.7 W was achieved at an input pump power of 29.65 W with a slope efficiency of 75.3%. In the double end pumping configuration, maximum output power of 29.6 W was obtained at a combined input pump power of 59.3 W with a slope efficiency of 55.7% (Fig.2.3 (a)). It is observed that the slope efficiency in the double end pumping case is less compared to the single end pumping case. This may be due to the poor coupling efficiency from the other end of the diode laser. The laser output varies linearly with input pump power in each case, which shows that output is limited by the available pump power from the laser diode. The output power was linearly polarized with Polarization Extinction Ratio (PER) of 10.5 dB in the double end pumping configuration and was achieved by proper alignment of the fiber birefringent axis and without using any intra-cavity external optics. With a similar fiber, with a length of 1.5 m, we have achieved 43 W of output power in the double end pumping configuration at an input pump power of 59.3 W with a slope efficiency of 80.9% and PER of 10.5 dB (Fig. 2.3(b)) [58]. It may be compared with the results of Schrieiber et al. [63], who had reported 25 W of signal output power with a slope efficiency of 75% and a PER of 15.5 dB in the single end pumping case by using non-commercial polarizing PCF of comparable length (1.2 m), but with a higher inner-clad pump absorption of 14 dB/m at 976 nm [63].

Figure 2.4(a–f) shows recorded self-pulsing at various values of absorbed pump powers in the range from 4.89 W to 29.65 W for the single end pumping configuration. It was observed that self-pulses start from the onset of lasing action. Figure 2.4(a) shows the random pulses with approximate frequency range of about 50–100 kHz. This corresponds to the relaxation oscillations which occur due to the long upper state life time of Yb^{3+} ions in silica which is about 830 μs in the PCF, used in our experiments. The frequency of the relaxation oscillations is determined by the cavity photon life time, threshold pump power, and the intensity of the laser signal inside the fiber [22]. In fiber laser, the damping of the relaxation oscillations may be prevented by the fiber vibrations, temperature fluctuations or any in- homogeneities present inside the fiber. As the pump power was increased from 4.89 W to higher values of 24.68 W, the frequency of the pulses also increases from 50–100 kHz range to 550– 600 kHz range and the peak intensity of self-pulse increases from ~1 to ~250 in the amplitude scale. The magnitude of peak intensity is recorded by photodiode and oscilloscope.

Fig. 2.4 a-f: *Self-pulses in the case of an Yb-doped double-clad PC fiber in the single end pumping configuration at pump powers of (a) 4.89 W, (b) 8 W, (c) 13.5 W, (d) 19.14 W, (e) 24.68 W and (f) 29.65 W.*

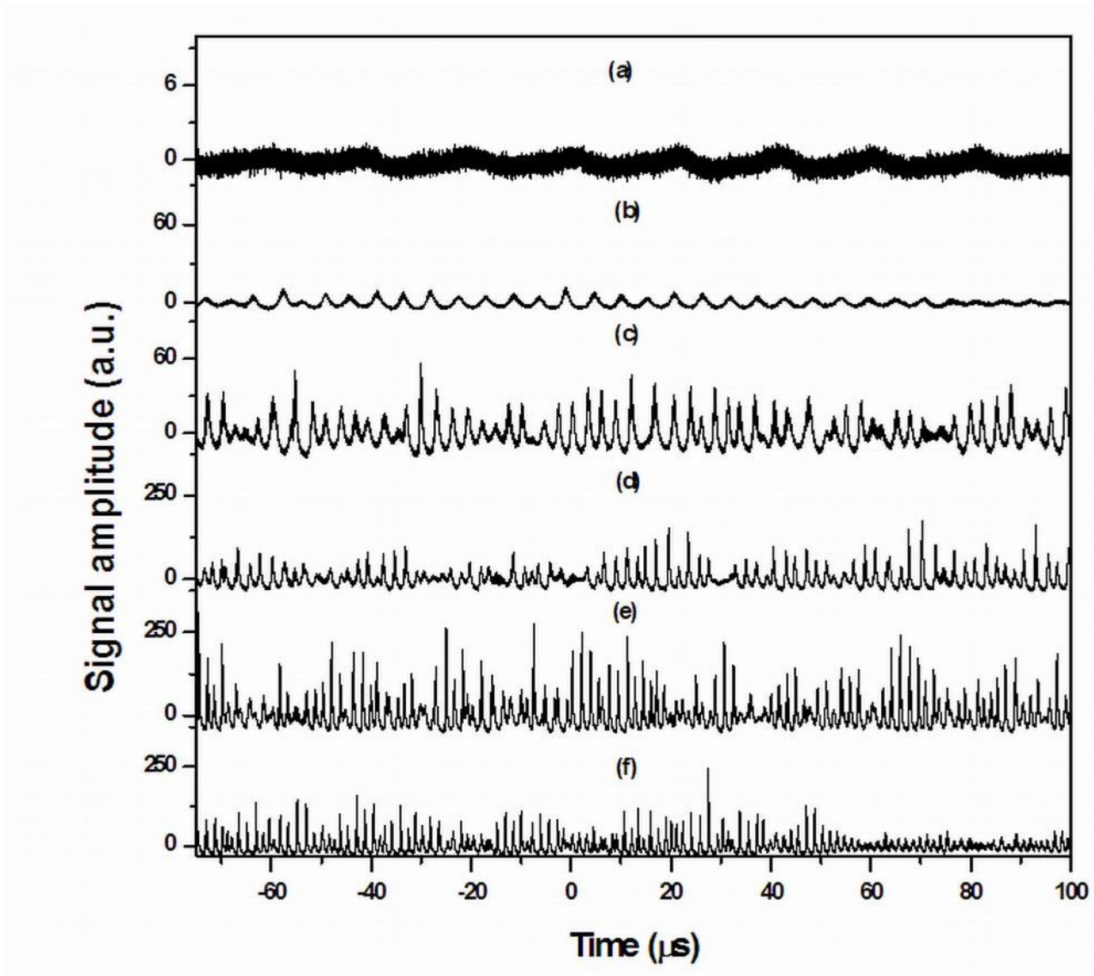

However, when the pump power was increased to 29.6 W, it was observed that the peak intensity of the pulses reduced from ~250 a.u. to ~150 a.u.. Also, the frequency of occurrence of the self-pulses was reduced comparatively. Further increase in the pump power was limited due to the non-availability of high power laser diodes with us.

To study the effect of self-pulsing in the double end pumping configuration, Yb-doped polarizing PCF was pumped from both the ends by the fiber pigtailed diode laser. Fig. 2.5(a–f) shows the self-pulsing behavior at various values of absorbed pump powers in the range from 7.71 W to 59.30 W for the double end pumping configuration. As the pump power was increased from 7.7 W to 27 W of the absorbed power, the peak intensity increased from ∼3 to ∼60. Frequency of the pulses also increases from 100–150 kHz to 350–400 kHz range. Between pump power levels of 27 W and 40 W, the amplitude of pulses remains constant at ∼40. However, when the absorbed pump power was increased further to 59.3 W, a significant decrease in the peak pulse intensity to ∼7 was recorded. Self-pulses at the absorbed power of 59.3 W were also recorded with better resolution so as to have a clear pulse structure. It is expected that further increase in the pump power would remove the self-pulsing completely and pure CW behavior can be expected as also reported by Shenggui et al. [64] in normal Yb-doped fiber. Comparing the pulsing behavior in the single and double end pumping configuration (figures 2.4 and 2.5), it is observed that the maximum intensity of pulses in single end pumping configuration rises up to ∼250, whereas in double end pumping configuration it is limited up to ∼60 at the same pump power of ~30 W. If intensity of the pulses is compared for the same amount of absorbed pump power in the single and double end pumping case, it can be seen that for 8 W of absorbed pump power, the peak amplitude is 10 in case of single end pumping configuration and is only 2.5 for double end pumping configuration. For an absorbed pump power of 13.5 W in single end pumping configuration, the peak intensity is 40; however in double end pumping configuration, for most of the peaks the amplitude is 20 with very few peaks reaching amplitude of 40. At 24 W of pump power, the peak intensity is nearly 150 in single end pumping configuration while in double end pumping configuration at an absorbed pump power of 27 W the peak intensity is only 50. It was also observed that if the pump power in double end pumping is reduced to half, the self-pulsing behavior in double end pumping configuration will not be similar to the single end pumping configuration because self-pulsing behavior depends upon the non-uniform steady state single pass distribution of upper laser level population at a particular pump power. This result can be inferred from self-pulsing traces in Figs. 2.4 and 2.5. At an absorbed pump power of 13.5 W in single end pumping configuration, the observed peak of self-pulses is ~60 and the peak of self-pulses at 7.7 W of absorbed pump power in double end pumping configuration is ~5. The values of pump power and peak intensity mentioned are to show the trend of the self-pulsing with increase in the pump power and the corresponding values can vary with the experimental conditions maintaining the observed behavior.

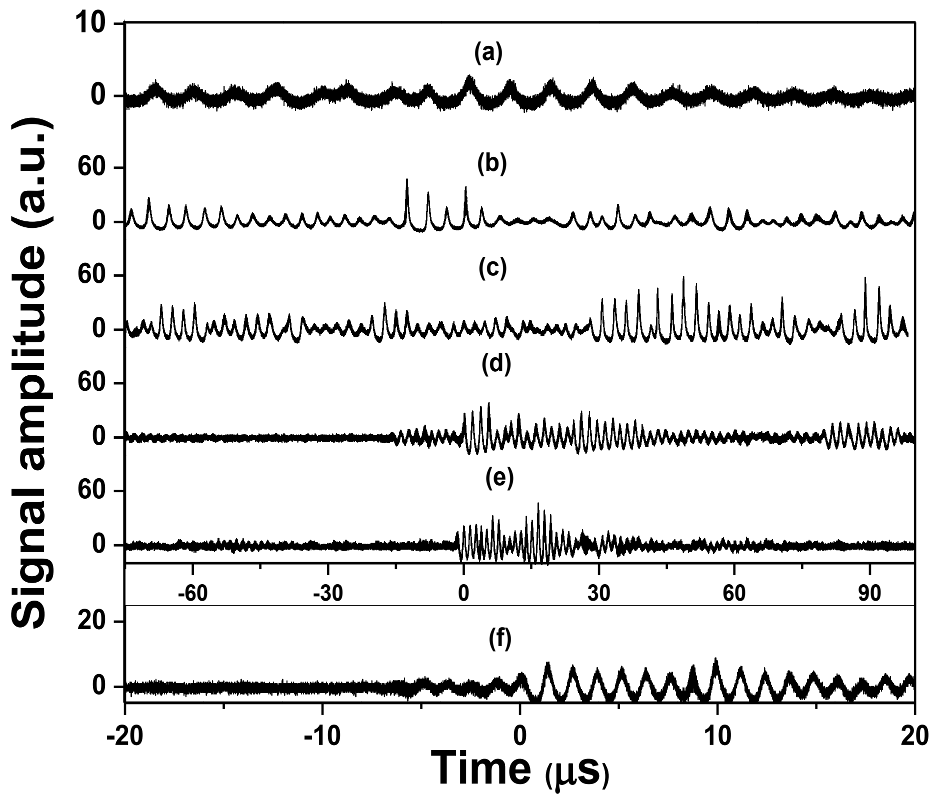

Fig. 2.5: *Self-pulses in the case of an Yb-doped double-clad PCF in the double end pumping configuration at pump powers of (a) 7.7 W, (b) 16.18 W, (c) 27 W, (d) 38.28 W, (e) 49.35 W, and (f) 59.3W.*

From these measurements, it is apparent that the pulsing phenomenon is more dominant in the single end pumping compared to double end pumping case and the pulses can be removed at sufficiently higher pump powers in both the configurations. In the single end pumping configuration, most of the pump power is absorbed near the pump end of the doped fiber and farther end of the fiber is un-pumped or weakly pumped. Whereas in the case of double end pumping configuration, fiber is pumped from both the ends so that the un-pumped portion or weakly pumped part of the fiber exists only in the middle portion of the fiber. As the Yb-doped fiber in silica is having quasi three level energy structure with lower lasing levels lying very near to the ground level, even at room temperature these levels are populated giving rise to signal re-absorption. Thus, in single end pumping configuration, long length of the fiber at the farther end is un-pumped or weakly pumped and would cause stronger "saturable absorption". However, in double end pumping configuration, the un-pumped or weakly pumped length of the gain fiber at the central region is small, leading to weak "saturable absorption" giving rise to low peak power pulses or fewer pulses compared to single end pumping configuration.

Figures 2.6(a) and (b) show the single pulse profile for single end and double end pumping configurations, respectively. It is observed that the envelop of the relaxation oscillation of the pulses are modulated and the modulation is similar to self-mode locking of large number of oscillating modes at a frequency separation close to free spectral range of the cavity which is 80 MHz. These pulses occur as soon as the lasing starts but, their occurrence is random. As the pump power is increased, it was noted that the modulation depth of the pulses inside the envelop increases. The formation of Q-switched mode-locked kind of pulses can be attributed to the coupling of the longitudinal modes existing inside the fiber due to the saturable absorption in the lower pumped part of the PCF [65]. Pulses with significantly lower depth of modulation will form when the large number of longitudinal modes inside the cavity oscillate at random phase.

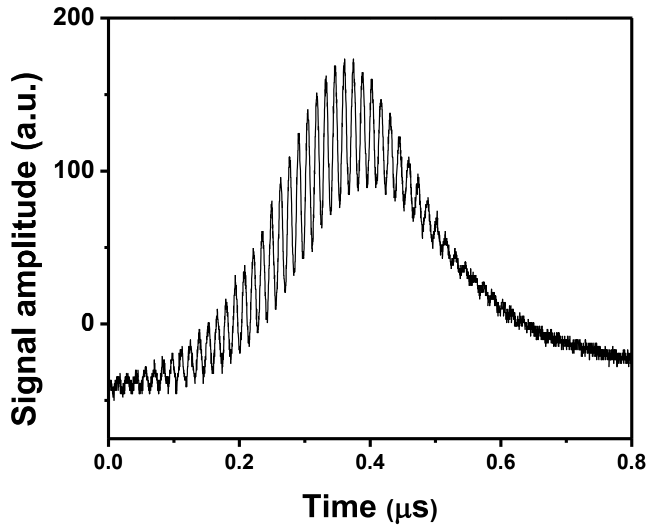

(a)

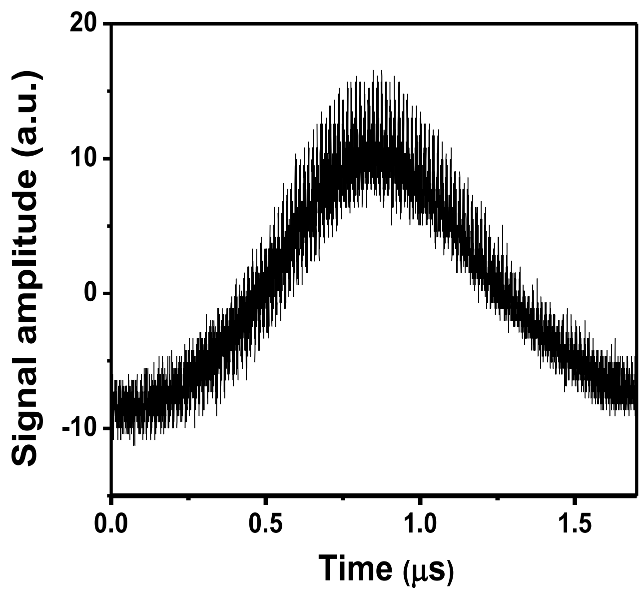

(b)

Fig. 2.6: *Temporal profile of an individual pulse of random self-pulsing at pump powers of (a) 24.68 W in the single end pumping configuration, and (b) 38.28 W in double end pumping configuration.*

Figure 2.7 shows the output spectrum of the Yb-doped PCF for single and double end pumping case at the absorbed pump power of 29 W and 59.6 W, respectively. In the single end pumping case, the spectrum ranges from 1028 nm to 1045 nm with the peak wavelength of 1038 nm. In the double end pumping case, the wavelength shifts toward the lower side and it ranges from 1026 nm to 1041 nm with the peak wavelength of 1035 nm.

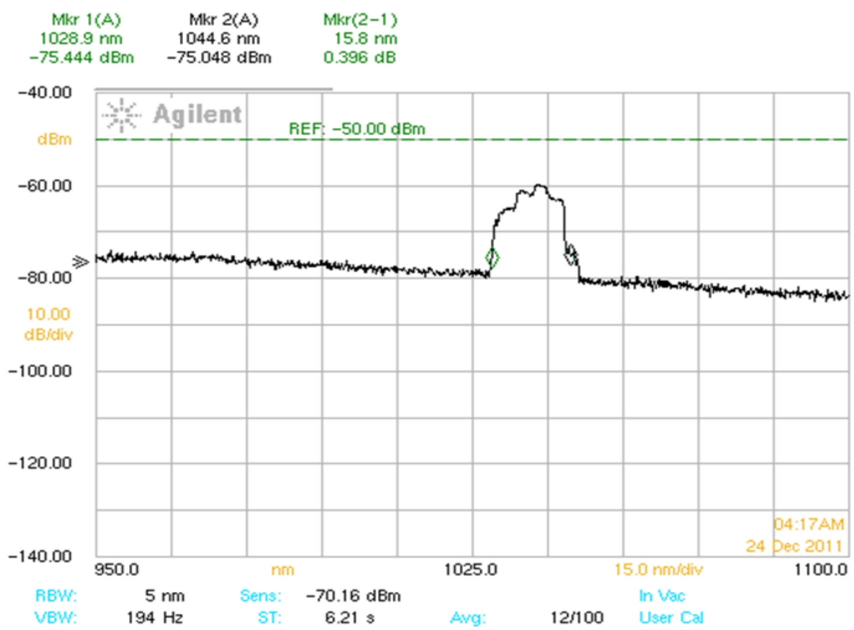

(a)

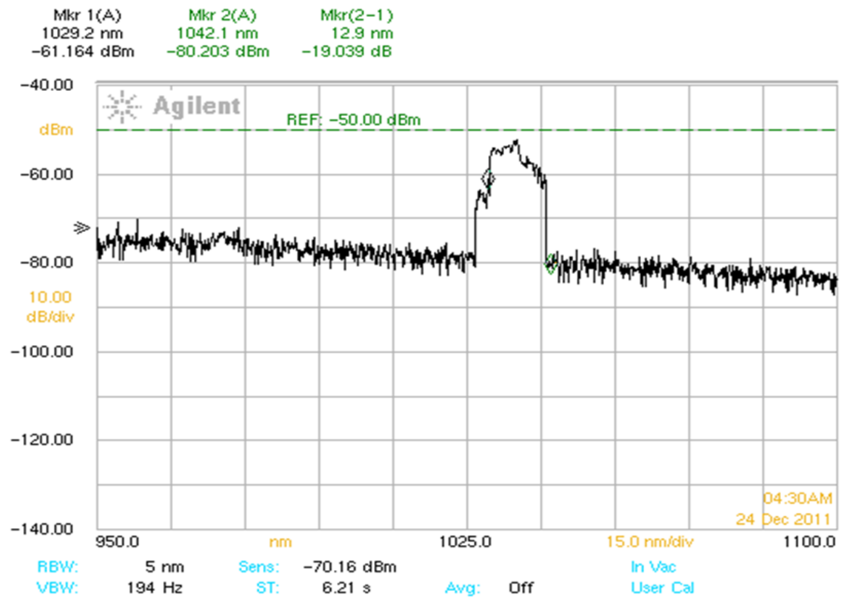

(b)

Fig. 2.7: *(a) Output spectrum of Yb-doped double-clad PC fiber at maximum values of absorbed pump power for single end pumping configuration and (b) double end pumping configuration.*

The wavelength is measured by taking a small reflected signal with the help of the glass wedge and it is given to the optical spectrum analyzer. The graph is only to measure the wavelength of the signal. The noise level appears to be high in double end pumping configuration, as it is not averaged signal value, but it doesn't affect the wavelength of the signal. Shift in the central wavelength toward the lower side at higher pump power stems due to the higher gain achieved at the lower wavelengths. There is no evidence of the SRS in the output spectrum and the broad bandwidth of ~15 nm also inhibits the appearance of any kind of SBS phenomenon inside the fiber laser. This confirms that the output pulses do not contain nonlinear contribution from the SBS or SRS. The calculated values of thresholds for nonlinear SBS and SRS phenomena are 160 kW and $5.9\text{x}10^{7}$ W, respectively for the Yb-doped PCF used in the experiment, with $A_{eff}=1.256\text{x}10^{-9}$ m^2 and L_{eff}~L=1.25 m [26]. Self-pulsing in Yb-doped fiber can cause damage at the end face of the fiber and initiate unwanted nonlinear effects when the peak power of self-pulses increases beyond the threshold values for nonlinear effects. For applications requiring pure CW output self-pulsing is not acceptable at any power level. These calculated threshold values are very high due to the small length and large core area of the PCF, and confirms the absence of nonlinearity in the Yb-doped PCF. Hence, it may be concluded that the observed self-pulsing in these lasers is primarily due to the saturable absorption.

Rate equations 2.1 to 2.7 have been solved in the single pass configuration, with no feedback from the mirrors and from the ends of the fiber to show the distribution of the upper level population in single end and double end pumping configuration. ASE term has also been taken into consideration. These rate equations in the single pass configuration have been used to explain the occurrence of self-pulses at the lower pump power and decrease in the amplitude of the pulses at a higher level of pump power. The parameters used in solving the rate equations are given in Table 2.2.

Table 2.2: *Various parameters used in the simulation of Yb-doped PCF laser [54, 55]*

Parameter	Value
λ_p	975 nm
λ_s	1050 nm
σ_{ap}	1.94×10^{-24} m^2
σ_{ep}	2.54×10^{-24} m^2
σ_{as}	2.74×10^{-26} m^2
σ_{es}	5.826×10^{-25} m^2
N	3×10^{25} atoms/m^3
τ	830 μs
Γ_p	0.04
Γ_s	0.82
A	1.256×10^{-9} m^2
L	1.25 m

Figures 2.8 and 2.9 show the upper level population along the length of the fiber for single and double end pumping configuration, respectively, when there is no feedback from the end mirrors. Significant difference in the single pass upper level population at the two ends of the fiber is estimated in single end pumping case. The portion of the fiber with lower values of upper level population poses possibility of higher re-absorption losses due to the presence of atoms at the lower lasing level. If the ratio of the maximum to minimum population is calculated, it is observed that at the lowest pump power of ∼5 W, the ratio is 5.43. With increase in the pump power to 30 W, this ratio decreases to 1.97. When the ratio is less than 2, it is observed that there is a decrease in the peak intensity of the pulses. Similarly, for the double end pumping case, the ratio of the maximum to minimum values of single pass upper level population at particular pump power is always less than 2. For the lowest value of the pump power, it is 1.36 and it decreases to 1.06 for 60 W of the absorbed pump power. As the ratio is approaching one, the peak intensity and the frequency of the occurrence of the pulses gets reduced. The reabsorption losses decrease as the number of atoms available instantaneously in the lower lasing level for causing re-absorption of the signal is small.

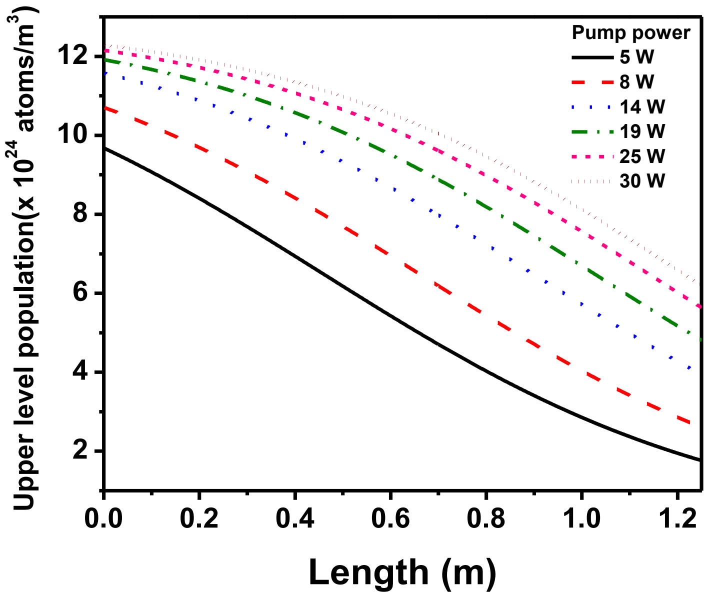

Fig. 2.8: *Variation of upper level population along the fiber length for various values of absorbed pump powers in the single end pumping configurations.*

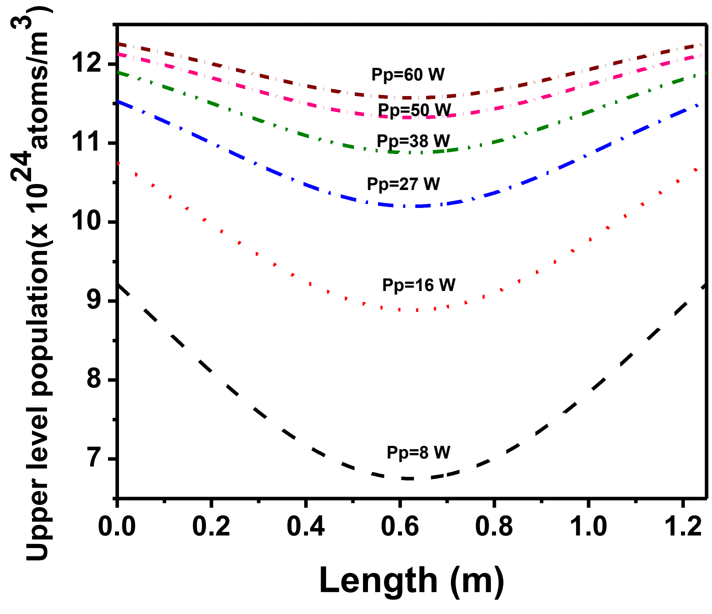

Fig. 2.9: *Variation of upper level population along the fiber length for various values of absorbed pump powers in the double end pumping configurations.*

In case of the lasing action, at steady state, population inversion is locked at about the threshold population inversion level. Stronger pumping increases the output signal power, but it does not change the population distribution of lower and upper lasing levels. The upper and lower level population distribution before the steady state thus determines the re-absorption losses inside the fiber and hence self-pulsing dynamics. Fu et al. [42] have also shown that at higher pump powers laser attains quasi-CW state. Marcuse et al. [49] has shown theoretically that three level laser with the saturable absorber will pass from the pulsed state to the stable CW operation by simply raising the pump. Time domain analysis in the transient condition may provide further insight; however it is beyond the scope of this work. Pump power and signal distribution along the length of the fiber was estimated theoretically using rate equations and was compared with the experimental results.

Figures 2.10(a) and 2.10(b) show the simulated pump profile and the signal profile along the length of the fiber for single end and double end pumping case. The theoretical value of the output power obtained by solving rate equations from 2.1 to 2.7 and experimental output power for single end pumping configuration are 22.8 W and 18.7 W, respectively. The resonator is formed with the mirrors of reflectivity 0.04 and .98. For double end pumping configuration, the theoretical and experimental output power are 45.6 W and 29.6 W, respectively. It is observed that for double end pumping configuration, there is a large difference in the theoretical and experimental values that can be assigned to the poor coupling losses from the other end of the PCF. From simulated pump profile of figures 2.10(a) and (b), it can be inferred that absorbed pump power distribution in case of double end pumping configuration is more uniform along the length of the fiber as compared to single end pumping configuration. Since the absorbed pump power profile is a measure of the thermal gradient along the length of the fiber, hence in double end pumping configuration, thermal effects are much reduced as compared to the single end pumping configuration at the same value of the pump power.

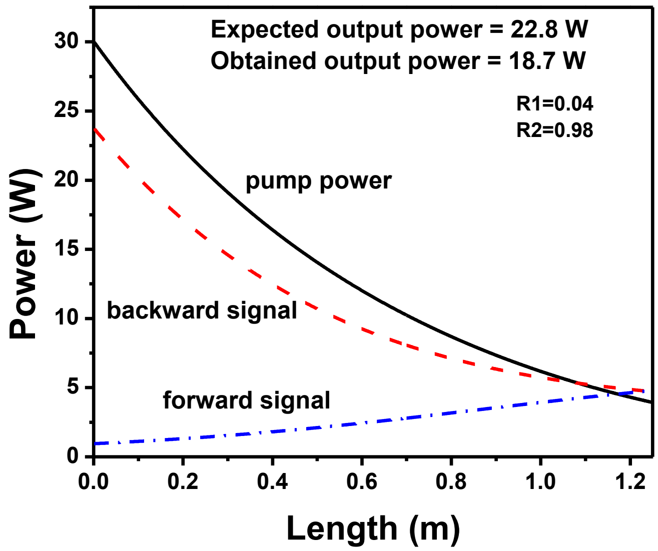

(a)

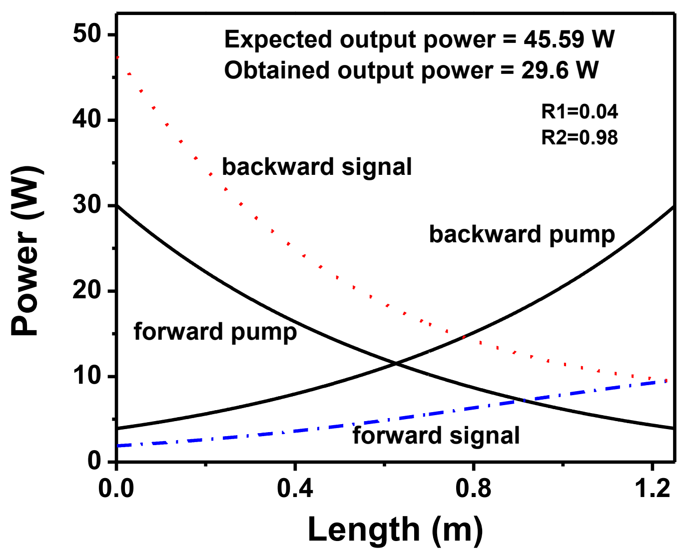

(b)

Fig. 2.10: *Pump and signal evolution in the case of (a) single end pumping configuration, (b) double end pumping configuration*

The another advantage of double end pumping configuration is that with the same power of available laser diodes, double end pumping configuration can be pumped to twice the pump level as compared to single end pumping configuration in the bulk coupling setup. However, single end pumping configuration is advantageous over double end pumping configuration in terms of its simple experimental setup.

2.4.2 Multi-wavelength generation in Yb-doped PCF laser

Multi-wavelength fiber lasers are useful in spectroscopy, wavelength division multiplexing, and fiber optical sensors [39, 40]. Yb-doped fiber lasers are potential candidate for high power multi-wavelength generation and its application in different areas because of its low quantum defect and broad gain bandwidth.

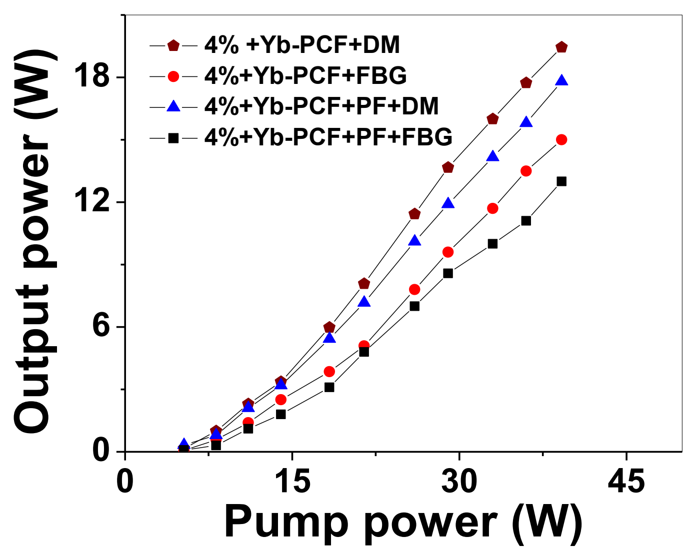

Fig. 2.11: *Output signal power vs input pump power for different experimental configurations. When dichroic mirror (DM) is used as the feedback mirror (pentagon shape). When Yb-PCF was spliced with passive fiber (PF) and DM was used (triangle). In case of FBG mirror with Yb-PCF (circle shape). When Yb-PCF was spliced with passive fiber (PF) and FBG mirror was used (square).*

Figure 2.11 shows the variation of the fiber laser output power as a function of the input pump power for different configurations. When dichroic mirror was used as a feedback mirror

(Fig. 2.2(a)), a maximum output power of 19.45 W was obtained at an incident pump power of ~40 W. In this configuration, the laser output spectrum of the Yb-PCF laser was in the range of 1040 nm to 1070 nm (Fig. 2.12).

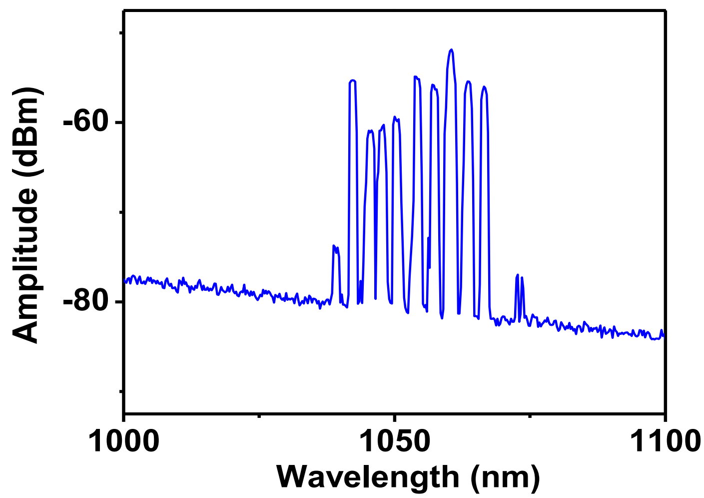

Fig. 2.12: *Spectrum of the output signal when the feedback is given by the dichroic mirror.*

The inhomogeneous broadening mechanism in silica host favours the broad bandwidth of the output signal. When Yb-PCF was spliced to the passive fiber and dichroic mirror was used as the feedback mirror (Fig. 2.2(b)), an output power of 17.76 W was obtained and the output spectrum remains the same as in the previous case. In this case, the gain is decided by the active fiber and mirror. Passive fiber increases the loss inside the cavity due to its core incompatibility with the Yb-PCF, which creates splicing loss and hence reduction in the output power was observed. To reduce the line-width of the output signal, FBG mirror (R= 99.9 % at 1090 nm, Fig. 2.2(c)) was fusion spliced to the Yb- PCF and an output power of ~15 W was obtained with the lasing wavelength at ~1090 nm as shown in Fig. 2.13. When passive fiber of length ~50 m was spliced in between the Yb-PCF and FBG mirror(Fig. 2.2(a)), then at the maximum value of pump power, ~12.9 W of output signal was obtained. There was a decrease in the output power due to loss at the two splice joints, one between the Yb-PCF and passive fiber and the other between the passive fiber and FBG. In this configuration, the lasing was observed in two wavelength regions, spectral wavelength region from 1040 nm to 1048 nm, which is at the gain peak of Yb-PCF and other wavelength at ~1090 nm (Fig. 2.13). The spectrum shown here is for the representation of wavelength of the signal and is taken by feeding few mW of the signal into the spectrum analyser. The spectrum looks noisy as it is the single shot spectrum from the analyser.

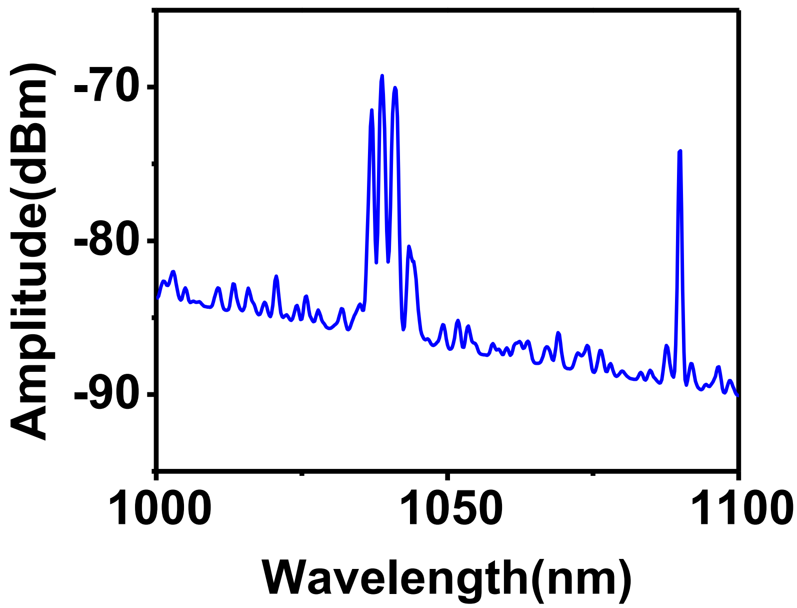

Fig.2.13: *Spectrum of the output signal when passive fiber is spliced between the Yb-PCF and FBG.*

This shows that spectrum is governed by both the gain bandwidth of the active medium and feedback provided by the FBG mirror. The output end of the FBG was angle cleaved to suppress the 4% feedback for the wavelength range from 1040 to 1070 nm. The lasing in the two wavelength range may be due to the Rayleigh scattering and scattering at the splice joints [66]. Although the Rayleigh scattering is week in silica fiber, but the long length of 50 m may provide a composite feedback. This was confirmed by splicing ~30 cm length of the passive fiber between Yb-PCF and FBG. It was observed that in this case only signal at 1090 nm was obtained. Higher gain at lower wavelength region compensates for its lower feedback due to Rayleigh scattering in long length of passive fiber and scattering from splice joints and higher feedback at 1090 nm due to high reflectivity FBG generates its lasing action even for lower gain region and hence both the regions of wavelength are generated simultaneously in the oscillator output.

2.4.3 Thermal studies in Yb-doped fiber laser

For high power fiber laser, thermal management is essential and for this to achieve, understanding the temperature distribution inside the fiber laser for efficient cooling mechanism is imperative.

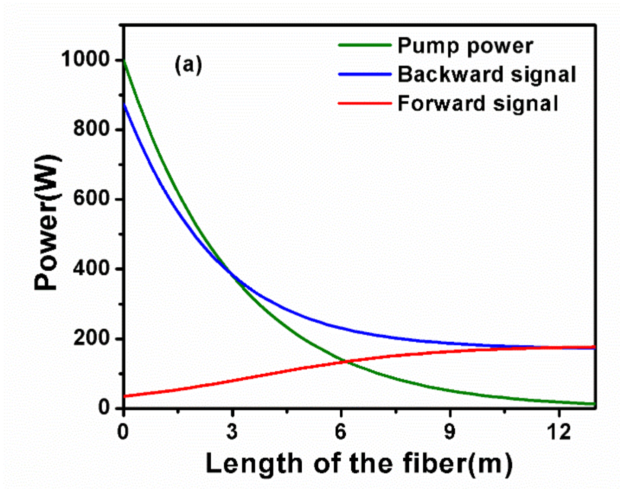

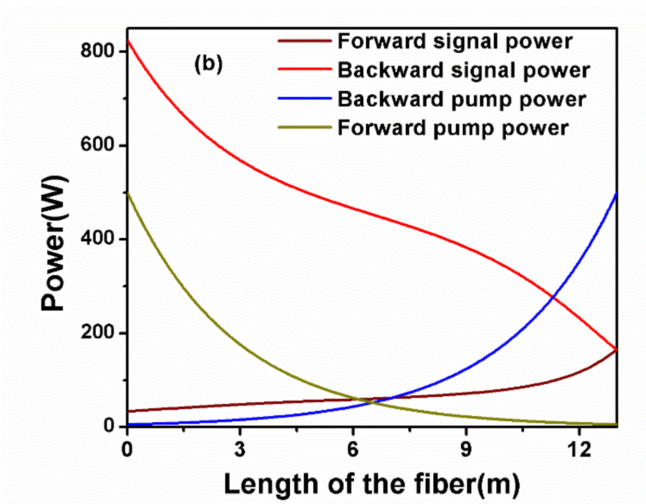

Fig. 2.14: *Pump power & signal power distribution in (a)* single end pumping configuration*, and (b)* double end pumping configuration *at 1000W of pump power.*

For theoretical simulation, a large mode area Yb-doped fiber having core/inner clad diameter of 20 µm/400 µm, with 1.5 dB/m absorption at 975 nm and a length of 13 m for efficient pump absorption has been used. Laser emission wavelength has been taken as 1090 nm, which is expected from this fiber. Thermal effects have been studied for pump power in the range of 200 W to 1000 W for 975 nm pump wavelength. In this simulation, rise in fiber core temperature has been considered only due to the quantum defect. One of the end of the fiber acts as the output coupler and its reflectivity is taken as 4% (R1) and the reflectivity of the highly reflecting mirror (HR mirror) is taken as ~98% (R2) for the simulation. Figures 2.14 (a) & (b) show pump power and signal power distribution along the length of the fiber for single end and double end pumping configurations which are obtained theoretically by solving equations from (2.1) to (2.7) . For both the cases, output signal power is nearly same which is about 830 W at input pump power of 1000 W, but the pump power distribution is different which gives rise to different temperature distribution inside the fiber.

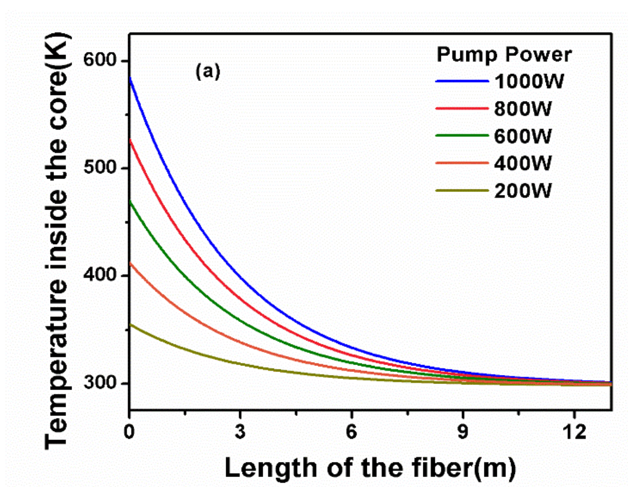

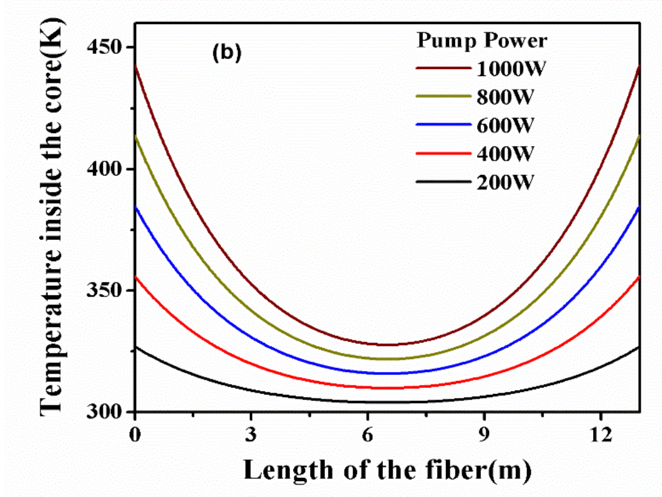

Fig. 2.15: *Temperature distribution inside the core in (a) SEPC and (b) DEPC for 200 W to 1000 W of pump power.*

Figures 2.15 (a) & (b) show the core temperature distribution for single end and double end pumping configurations from 200 W to 1000 W of pump power along the longitudinal direction which are obtained by solving equation 2.11. It shows that at 1000 W of input pump power for single end pumping configuration, temperature at the pump end is ~580K and at other end, it is at room temperature, whereas for double end pumping configuration (500 W pump from each ends), rise in the core temperature at the pump input end is ~ 442.7 K and at the center, it is ~ 327 K.

Temperature difference for single end pumping configuration is ~280K and for double end pumping configuration it is ~115K. This indicates a high temperature difference along the silica fiber in case of single end pumping configuration as compared to double end pumping configuration, which can degrade the fiber quality and laser beam quality due to thermal stresses and variation in the effective index of the fiber mode along the fiber length. Quantum efficiency of the fiber laser also decreases due to decrease in the population of the lower laser level because of temperature.

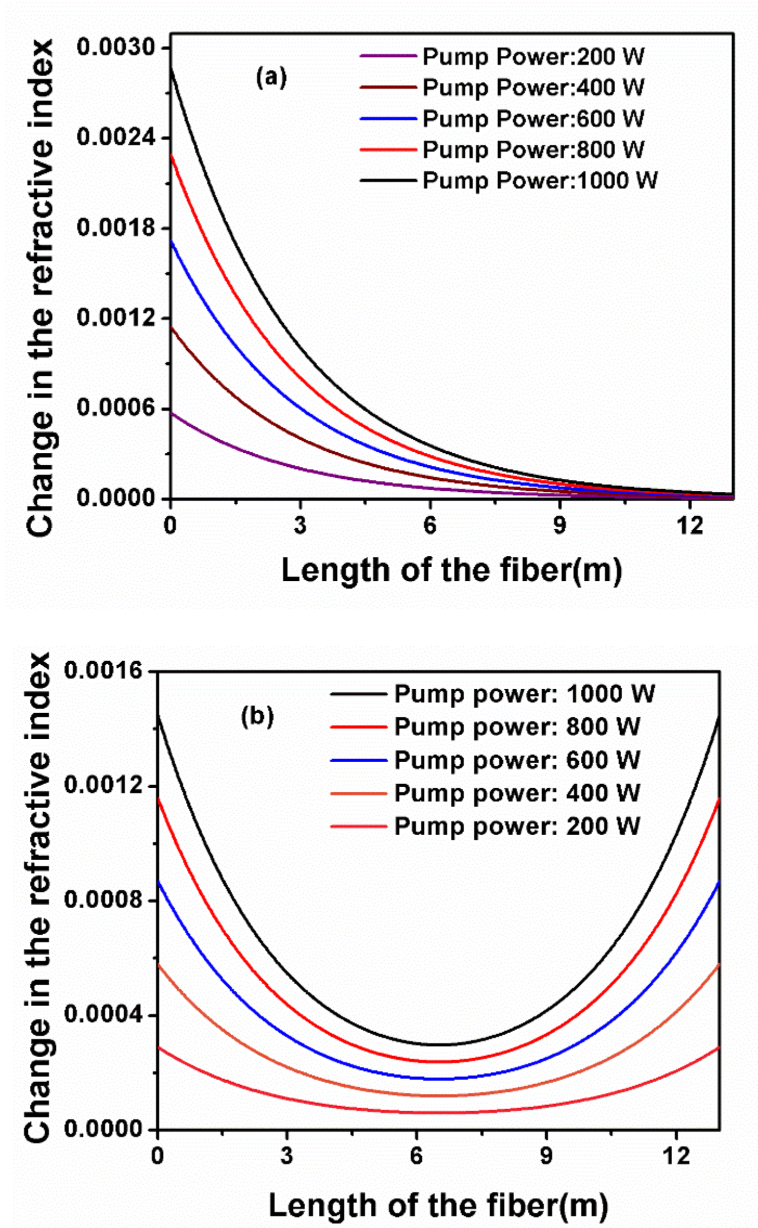

Fig. 2.16: *Change in the refractive index inside the core in (a) single end pumping configuration, and (b) double end pumping configuration for 200 W to 1000 W of pump power.*

Figure 2.16 shows change in the refractive index (RI) due to the temperature gradient which is obtained by solving equation 2.12. For silica β is positive and so RI increases with increase in temperature. For 1000 W of pump power, due to change in the RI for single end pumping configuration V-number becomes 3.2 and for the double end pumping configuration it attains the value of 3.1. Hence the fiber becomes multimode from single mode. Change in the population density due to the rise in the temperature was also simulated using Boltzmann distribution equations.

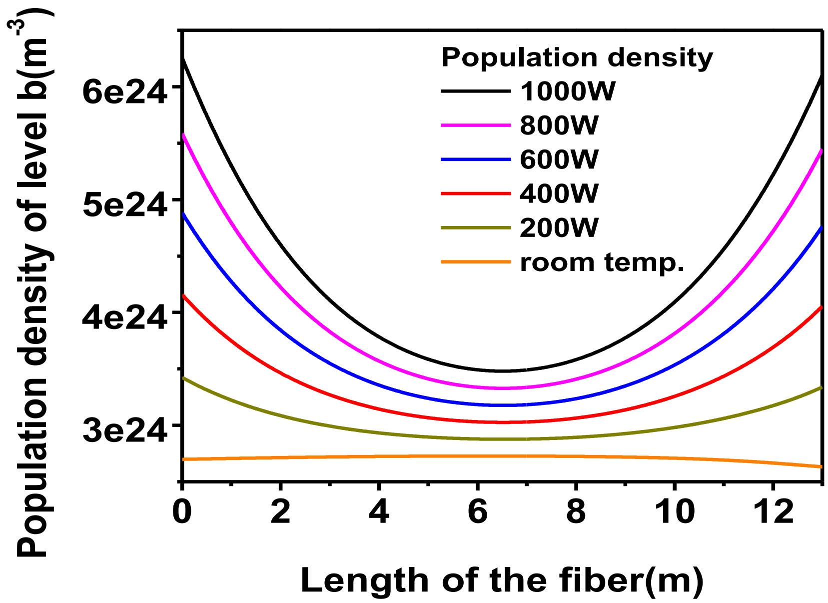

Fig. 2.17: *Population density of level 'b' vs fiber length in* double end pumping configuration

Figure 2.17 shows population density of level 'b' (Fig. 1.4 (a)) as a function of fiber length in double end pumping configuration. It is found that for double end pumping configuration, there is about two times rise in the population of the level 'b' at the pump input end. An increase in the population of level 'b' will cause stronger re-absorption in the short wavelength region (1020-1050 nm). This will make lasing more difficult in short wavelength region and simplify lasing in long wavelength region having small emission cross-section. Hence, optical-to-optical conversion efficiency of fiber laser will decrease.

2.5 Conclusion

We have presented an experimental and analytical study of self-pulsing dynamics, multi wavelength generation in the Yb-doped photonic crystal fiber laser and study of thermal effects in Yb-doped fiber laser. Self-pulsing dynamics was studied in the single end and double end pumping configurations with maximum signal power of 43 W in double end pumping configuration in a Yb-doped PCF with length of 1.5 m at an input pump power of 59.3 W with a slope efficiency of 80.9% and polarization extinction ratio of 10.5 dB. In the same gain medium, narrow linewidth and multi-wavelength generation was studied using passive fiber and FBG with lasing wavelength in the range of 1040 nm to 1048 nm and at 1090 nm with an output power of ~12.9 W in the single end pumping configuration. Multi-wavelength generation appears to be due to the Rayleigh scattering from the long length of the passive fiber. This was confirmed by splicing ~30 cm length of the passive fiber between Yb-PCF and FBG. It was observed that in this case only signal at 1090 nm was obtained.

In the self-pulsing study, it is observed that the intensity of the self-pulses are significant in the single end pumping configuration as compared to the double end pumping configuration. In both the cases, it was noted that when the pump power was sufficiently high, the amplitude and the occurrence of the self-pulses were reduced. The reduction in the amplitude of the self-pulses was much more appreciable in the double end pumping case. Even at the highest values of absorbed pump power, no signature of SBS or SRS was observed under the experimental conditions. The rate equation analysis showed the significant non-uniform single pass distribution of upper level population along the length of the fiber which could enhance the re-absorption losses, which can be one of the major causes for the self-pulsing inside the fiber. In the single end pumping, single pass distribution of upper level population is more non-uniform as compared to the double end pumping, so the intensity and the frequency of occurrence of the pulses are higher in single end pumping as compared to the double end pumping configuration.

In thermal studies, by solving the steady-state rate equations and heat equations, temperature distribution has been calculated for the single end and double end pumped configuration at different pump power levels for our fiber. Effect of the temperature gradient in the thermo-optical properties of fiber laser has been studied. It is concluded that due to rise in the temperature, fiber becomes multimode from single mode as V-number now exceeds beyond 2.404. Change in the population density of level ‘b’ has also been simulated for double end pumping configuration, which results in decrease in the output laser efficiency.

Chapter 3

Passive Q-switching in Ytterbium doped Q-switched fiber laser

3.1 Introduction

High-peak-power short-pulse Q-switched fiber lasers are highly promising in the field of industrial processing, range finding, remote sensing, and medicine owing to their higher efficiency, good beam quality, and compactness [67–75]. Passive Q-switching (PQS) is favored over active Q-switching due to its simple experimental configuration, compactness, and ease of operation. There are various reports on PQS operation of Yb-doped fiber (YDF) lasers using Cr^{4+}: YAG crystals as a saturable absorber [67–72]. Huang et al. [70] have reported maximum average power of 6.2 W at a repetition rate of 48 kHz by using Cr^{4+}: YAG crystal. For special applications of nonlinear frequency shifting like frequency doubling and optical parametric oscillation, linearly polarized Q-switched output is essential. Zhuang et al. [71] have reported polarized average output power of 3.4 W using Yb^{3+}-doped photonic crystal fiber (PCF) as a gain medium. Reports on PQS with AlGaInAs quantum wells as saturable absorber are also available in the literature [73-76]. Zhuang et al. [73] have also reported an average output power of 7.1 W with corresponding pulse energy of 1.1 mJ by using AlGaInAs quantum wells, which possess low non-saturable loss as compared to Cr^{4+}: YAG crystal, and Yb-doped PCF as a gain medium, which has the potential to store higher energy due to the larger available core diameter with single-mode operation. A hybrid Q-switched fiber laser has also been reported by Huang et al. [75]. In this work, active and passive Q-switching have been incorporated simultaneously to increase the pulse energy and pulse-to-pulse stability of the output, and an average output power of 14 W with pulse energy of 0.56 mJ has been achieved. Several other researchers have also worked extensively on all-fiber configurations using doped fibers as saturable absorber, such as Sm-doped fiber and small core un-pumped Yb-doped fiber

[77–80]. There are also reports on the use of graphene and few-layer topological insulator Bi_2Se_3 as saturable absorber [81–83]. However, high average power operation of a passively Q-switched YDF laser above 20 W has not yet been reported. This may be due to frequent damage of Q-switched fiber laser components when they are operated at higher average and peak powers. For high average power operation, Cr^{4+}:YAG crystals are the preferred saturable absorber as they have a large absorption cross-section and low saturation intensity at the signal wavelength. Cr^{4+}: YAG crystals are also thermally and chemically stable with higher damage threshold and, hence, are suitable for high power PQS operation. In most of the cited works, PQS fiber laser has been operated in single-end pumping configuration in which YDF has been pumped from one end. Spectral studies have also been performed in the PQS operation of Yb-doped fiber laser by Pan et al. [84, 85]. In these reports, laser operation has been demonstrated simultaneously at two wavelengths and spectral evolution has been observed up to input pump power of ~10 W.

In this chapter, initially, we have presented the generation of linearly polarized passively Q-switched output from Yb-doped PCF laser using Cr^{4+}: YAG crystal as a saturable absorber in single-end pumping configuration. An average power of 9.4 W with a pulse width of 63 ns and a pulse repetition rate of 60 kHz has been achieved. Output pulses are polarized with polarization extinction ratio (PER) of 10.5 dB. In later part of the chapter, PQS operation of Yb-doped fiber laser in a special T-type double-end pumping configuration (DEPC) has been studied. In this configuration, average output power of 41.6 W has been achieved, which is the maximum average output power in PQS Yb-doped fiber laser oscillator reported so far in the literature. It was possible to achieve such a high value of average output power by means of low-loss end caps spliced at both the ends of the doped fiber. The effect of saturable absorber on random self-pulsing dynamics and on the spectral behavior of the output signal near the threshold for Q-switching has also been investigated. Studies on output pulse characteristics with different linear transmission of saturable absorbers has also been performed. Our results show that with lower values of the initial transmission of the passive Q-switch crystal, output pulse energy increases and pulse-to-pulse stability also improves. Detailed studies were also performed to observe the spectral evolution of PQS Yb-doped fiber laser as a function of pump power as well as the dependence of output spectral characteristics on the length of the gain medium.

The contents of this chapter have been arranged as follows. The details of the experimental configuration of PQS in Yb-PCF laser and Yb-doped LMA fiber laser have been provided in Section 3.2 and Section 3.3 presents results and discussion.

3.2 Experimental Details

3.2.1 Experimental configuration of passively Q-switched Yb-doped photonic crystal fiber laser

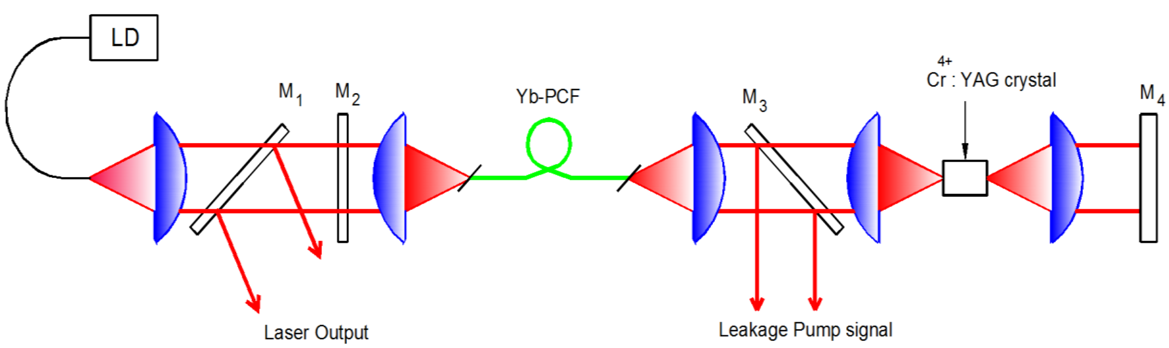

Fig. 3.1: *Schematic of the passively Q-switched Yb-doped PCF laser in single end pumping configuration.*

Figure 3.1 shows schematic of the experimental setup for passively Q-switched Yb-doped PCF laser consisting of a 1.5 m long Yb-doped PCF and an intracavity saturable absorber. A Yb-doped double-clad polarizing PCF (YDPCF) having a mode field diameter (MFD) of 29.5 µm at 1060 nm with numerical aperture (NA) of 0.03, and an inner-clad diameter of 200 μm with an NA of 0.55 has been used as the gain medium. Large NA of the inner clad relaxes the tolerances on coupling optics for coupling pump light into the inner clad of the PCF. The clad-pump absorption of the fiber is 10 dB/m at 976 nm. The transverse cross-section of the PCF is shown in Fig. 2.1 of chapter 2 and boron-doped silicate rods in the micro-structured inner clad provides a birefringence of $\sim 1\times10^{-4}$. Both the ends of the fiber are angle polished at 5º to prevent feedback from the end faces. Fiber-coupled laser diode having 30 W CW power at the center wavelength of 975 nm at 25ºC has been used as a pump source. The pump laser output through a fiber pigtail having 200 μm core diameter and 0.22 NA has been collimated using a lens of 20 mm focal length and then focused using another lens of 20 mm focal length to have a focused spot diameter of about 200 μm on the input end of the doped fiber.

A Cr^{4+}:YAG crystal has been used as a saturable absorber for passive Q-switching. Both the sides of the Cr^{4+}:YAG crystal are antireflection coated in a broadband from 1030 nm to 1100 nm (R< 0.2%). The edges of saturable absorber was made in contact with indium foil and conductively cooled. The focal lengths of the collimating and focusing lenses were chosen to have a focused beam diameter on the saturable absorber equal to the fibre core diameter. The saturable absorber was mounted on a translation stage to optimize the focus position depending on output performance of the Q-switched laser. Two dichroic mirrors M_2 and M_4, which form the resonator cavity were used in this configuration; both the mirrors have high transmission at 975 nm whereas M_2 has 4% reflection for the normal incidence and M_4 has high reflection in a broad range of 1035 nm – 1120 nm for normal incidence. Mirror M_1 has been used to take the beam out and has similar characteristics as M_4 for 25˚ angle of incidence. Mirror M_3 has high transmission for laser signal and high reflection for pump signal at 45° and has been used to remove the leakage pump power from the cavity to prevent the bleaching of the saturable absorber by the pump signal, as Cr^{4+}:YAG crystal is having absorption at the pump wavelength also. The pulse temporal behaviour was recorded by using a 1 GHz LeCroy digital storage oscilloscope and a 1 GHz InGaAs photoreceiver.

3.2.2 Experimental configuration of large mode area (LMA) Yb-doped passively Q-switched fiber laser in double-end pumping configuration

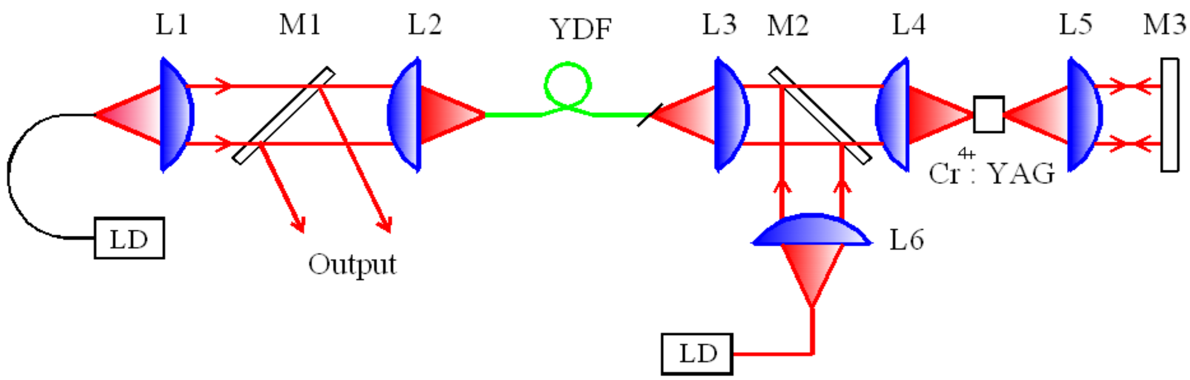

Fig.3.2: *Schematic of the experimental setup of passive Q-switching in large mode area Yb-doped fiber laser in a double-end pumping configuration.*

Figure 3.2 shows the schematic of the experimental setup for a passively Q-switched Yb-doped double-clad fiber laser in a specially designed T-type double-end pumping configuration (DEPC). Two fiber-coupled laser diodes (LDs) of 40 W output power at 976 nm pigtailed with fibers having core diameter of 200 μm and numerical aperture (NA) of 0.22 have been used as pump sources at both ends of the doped fiber. The gain medium consists of a Yb-doped double-clad fiber with an absorption coefficient of 1.8 dB/m at 976 nm. It has a circular core of 20 μm diameter with NA of 0.07, and an octagonal inner clad of 400 μm diameter with NA of 0.46. The outer cladding is a low index polymer with a diameter of 550 μm. To study the length dependence and spectrum of the Q-switched laser, three different lengths (6.5, 9, and 12 m) of the same fiber were used as the gain medium. To couple the pump beam into the inner clad of the doped fiber, collimating and focusing lenses L1 and L2, with 20 mm focal lengths, have been used to re-image the pump beam at the input facet of the YDF with a pump beam spot diameter of ~200 μm. Using this 1:1 imaging configuration, a pump coupling efficiency of 80% was achieved from each end of the fiber. During Q-switching experiments, even at low values of input pump power, end facet damage of the gain fiber was encountered. To avoid the damage of end facets, end caps were spliced at both ends of the fiber. End caps were taken as a section of silica fiber with a circular core diameter of 400 μm, which is compatible with the inner clad of the YDF. The length of the end cap is chosen in such a manner that the single-mode beam quality of the output signal is maintained. The calculated value of the maximum permissible length of the end cap is given by [86]

$$L_{\max} = \frac{d}{2nNA} \tag{3.1}$$

where, *d* is the diameter of the end cap, *n* is the refractive index of the silica end cap at the operating signal wavelength, and NA is the numerical aperture of the core of the YDF. The length of the silica end cap spliced to the YDF is ~1.5 mm. The length of the end-cap must be carefully chosen to maintain single-mode beam quality in the sense that, if the length of the end cap $L< L_{max}$, then the beam quality will be similar to that emerging from the YDF core. In contrast, if the length of the end-cap $L>L_{max}$, the beam emerging from the end cap will become multi-moded due to multiple reflections in the end cap and will not be able to maintain beam quality similar to that from the YDF fiber. Although the YDF fiber is itself slightly multi-moded, it has been coiled on a spool to achieve near diffraction limited beam quality. For build-up of population inversion and to prevent spurious lasing between the two ends of the fiber, one of the end caps was cleaved at an angle of 10°. It was observed that, with the spliced silica end caps, damage of the fiber ends was prevented due to an increase in the beam diameter from 20 μm to less than 400 μm at the fiber ends, thereby decreasing peak power density.

Passively Q-switched operation of the YDF laser was studied using Cr^{4+}:YAG crystals as a saturable absorber with linear transmission in the range of 20%–50%. Both sides of the Cr^{4+}:YAG crystals are antireflection coated in a broadband wavelength range from 1030 to 1100 nm (R< 0.2%). The saturable absorber is kept close to a 100% reflecting mirror, as shown in figure 3.2, and is mounted on a copper heat sink, which is conductively cooled with water. To re-image the signal beam from the Yb-doped fiber on the saturable absorber crystal, two lenses (L3 and L4) having focal lengths of 22 mm were used to maintain tight focus on the saturable absorber crystal with proper magnification. The saturable absorber is mounted on a translation stage to optimize the focal position on the crystal to obtain stable Q-switched laser pulses. The perpendicular end of the Yb-doped fiber and the dichroic mirror M3, which has high transmission at 975 nm of pump wavelength and high reflection for the signal wavelength in the broad range of 1035–1120 nm for normal incidence, forms the laser resonator. Mirror M1 has been used as the output coupler mirror and has characteristics similar to mirror M3 for 25° angle of incidence. A special T-type pumping configuration was designed to incorporate double-end pumping of the gain fiber and to avoid exposure of the pump beam on the saturable absorber crystal. The direct exposure of a pump beam on a saturable absorber crystal may result in its saturation, which may stop the Q-switching process. In this scheme, the pump beam was coupled into the angled fiber end with the help of mirror M2, which is kept at 45° with respect to the axis of the fiber. Mirror M2 has high reflection for the pump wavelength at a 45° angle of incidence and high transmission for the signal wavelength. Mirror M2 also helps to remove the leakage pump power from the YDF, and does not allow it to enter the saturable absorber crystal. The gain medium is pumped from both the ends in double end pumping configuration, the residual pump signal is not feedback into the gain medium. In the single end pumping configuration residual pump signal can be feedback into the gain medium.

3.3 Results and Discussion

3.3.1 Results of passive Q-switching in Yb-doped photonic crystal fiber laser

Figure 3.3 (a) shows the average output power with respect to the incident pump power in CW and passive Q-switching operations. In the CW regime, the PCF laser had a slope efficiency of 73.4% with an output power of 13.4 W at an incident pump power of 22.5 W.

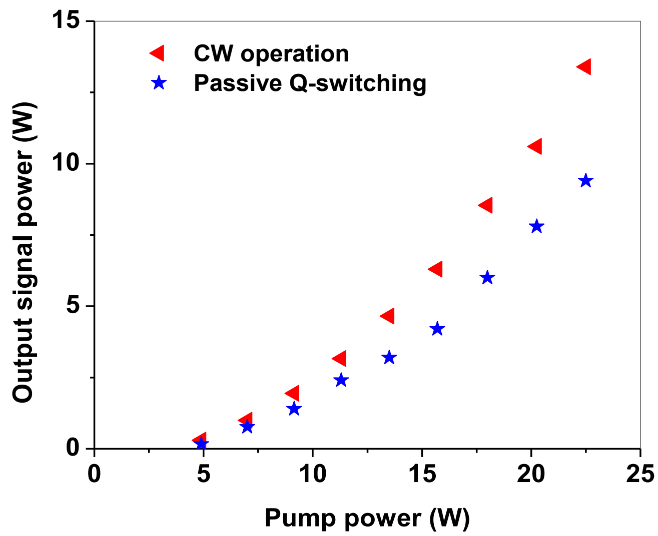

(a)

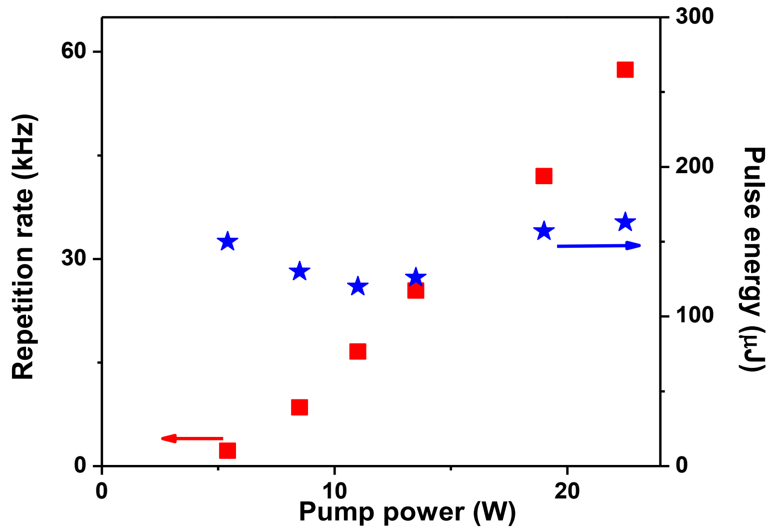

(b)

Fig. 3.3: *(a) Average output power with respect to the launched pump power in CW and passive Q-switching operations. (b) Pulse repetition rate and pulse energy as a function of launched pump power.*

In the passive Q-switching regime, an average output power of 9.4 W was obtained at the same value of the incident pump power with a slope efficiency of 52%. Polarization extinction ratio (PER) of the output pulse was recorded to be 10.5 dB. Figure 3.3(b) shows the variation of pulse repetition rate and pulse energy with the launched pump power. Pulse repetition rate increased from 2.2 kHz to 57.4 kHz with increase in the pump power from 5.4 W to 22.5W, which is the characteristic of typical passively Q-switched lasers. Pulse energy from the Q-switched laser depends upon the initial population density in the gain medium. For passively Q-switched laser, the initial population density achieved in the gain medium is determined by the initial transmission of the saturable absorber and reflectivity of the output coupler mirror. Hence, pulse energy achieved in passively Q-switched laser should remain constant for fixed choice of the satrable absorber and output coupler mirror. However, from figure 3.3(b), it can be seen that pulse energy varies from 120 μJ to 160 μJ with increase in pump power. The observed variation in the pulse energy can be attributed to the effect of self-pulsing phenomenon in Yb-doped polarizing PCF.

Figure 3.4 (a) and (b) show oscilloscope traces for single pulse and Q-switched pulse train at maximum value of pump power with repetition rate of 57.4 kHz. The passive Q-switching process inherently have amplitude fluctuations. Pulse to pulse energy change may be attributed to the self- pulsing phenomena occurring inside the fiber laser which itself generates random pulses due to saturable absorption taking place inside the gain medium. Self-pulsing may also lead to jitter in the repetition rate of the pulses. These kinds of fluctuations were also reported by various authors in Cr^{4+}:YAG crystal and AlGaInAs QWs structures as passive Q-switches [69]. It is expected that uniform pumping inside the fiber laser will form stable pulses in passive Q-switching.

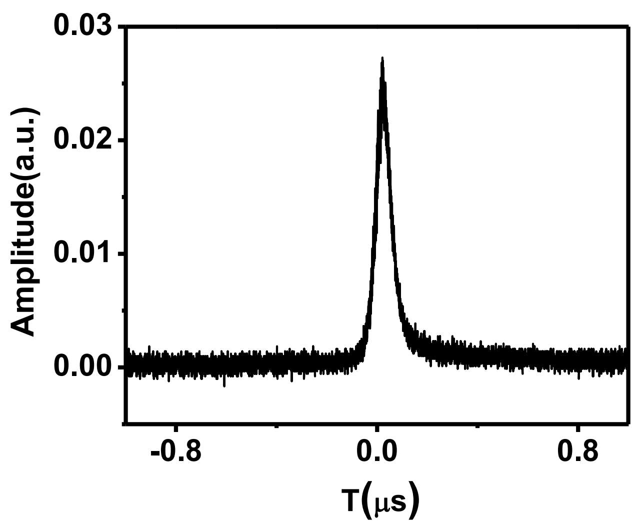

(a)

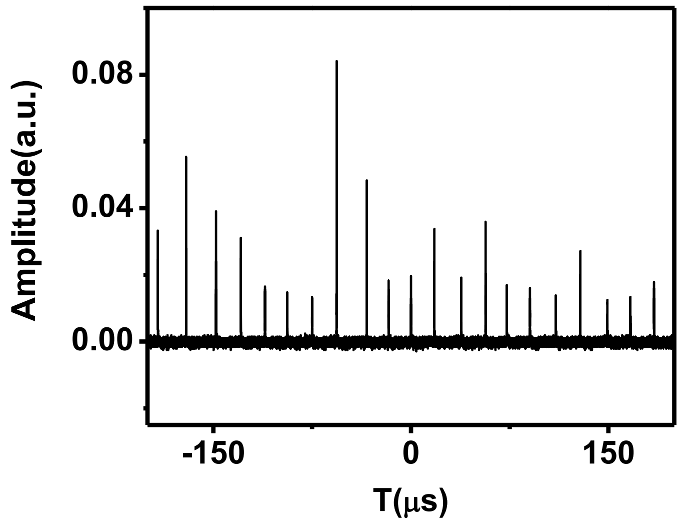

(b)

Fig. 3.4: *Typical oscilloscope traces for (a) single Q-switched pulse, (b) train of Q-switched pulses.*

3.3.2 Results and discussion of passively Q-switched LMA Yb-doped fiber laser

3.3.2.1 Effect of initial transmission of the saturable absorber

In this subsection, the effects of the initial transmission of the saturable absorber on output power, temporal characteristics, and spatial characteristics have been discussed.

A. Output Power

The experiments were performed to understand the effect of linear transmission of Cr^{4+}:YAG crystal on passive Q-switching operation of the YDF laser. For this study, crystals with linear transmission of 50%, 40%, 30%, and 20% were used. This was studied using gain fiber length of 12 m, to ensure sufficient pump power absorption in the doped fiber. In the PQS operation of YDF laser, maximum average power of 41.6 W with pulse duration of ∼410 ns and pulse repetition rate of 127 kHz was achieved using a Cr^{4+}:YAG crystal having linear transmission of 50%. Variation of the experimentally measured laser output characteristics, such as average output power, pulse repetition rate, pulse duration, and pulse energy with pump power, are shown in figures 3.5(a)–3.5(d) with different linear transmissions of the crystal. It can be seen from the figures that the average output power, pulse repetition rate, and pulse energy increases, whereas pulse duration decreases with an increase in pump power for all the crystals. Average output power corresponding to Cr^{4+}:YAG crystals with linear transmission of 40%, 30%, and 20% were measured to be 39.2 W, 38.0 W, and 36.7 W, respectively with corresponding slope efficiencies of 73.5%, 71.8%, and 68.7%. The pump thresholds for PQS for 50%, 40%, 30%, and 20% linear transmission crystals are 3.8 W, 4.5 W, 5W, and 5.6 W, respectively. With a decrease in linear transmission of the PQS crystal, the average output power decreases, since a decrease in the linear transmission induces more loss in the cavity and results in reduction of the average output power [86]. It was also observed that in PQS operation, the average output power is less than the CW power. This is because the final transmission of the Cr^{4+}:YAG crystal never reaches 100% due to the occurrence of un-saturable loss in the saturable absorber crystal from excited state absorption[22].

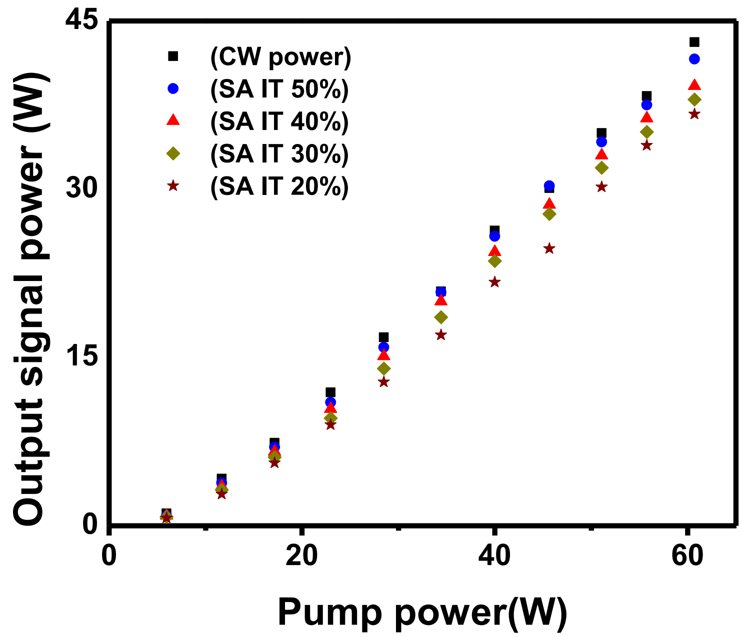
45
30
15
0
0
20
40
60
Output signal power (W)
Pump power(W)
(CW power)
(SA IT 50%)
(SA IT 40%)
(SA IT 30%)
(SA IT 20%)

(a)

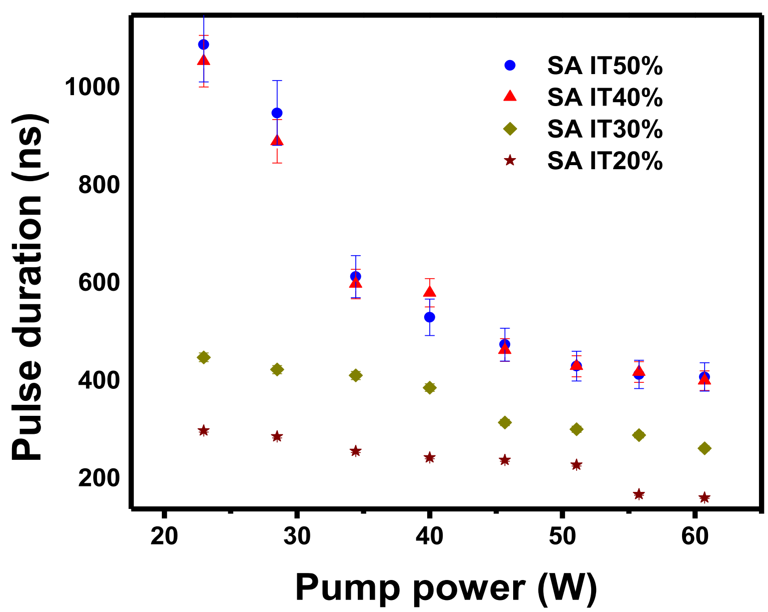
1000
800
600
400
200
20
30
40
50
60
Pulse duration (ns)
Pump power (W)
SA IT50%
SA IT40%
SA IT30%
SA IT20%

(b)

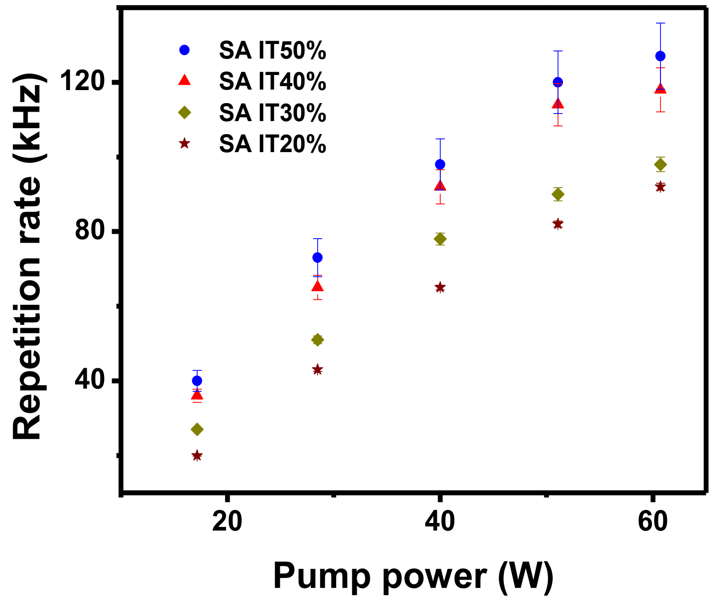

(c)

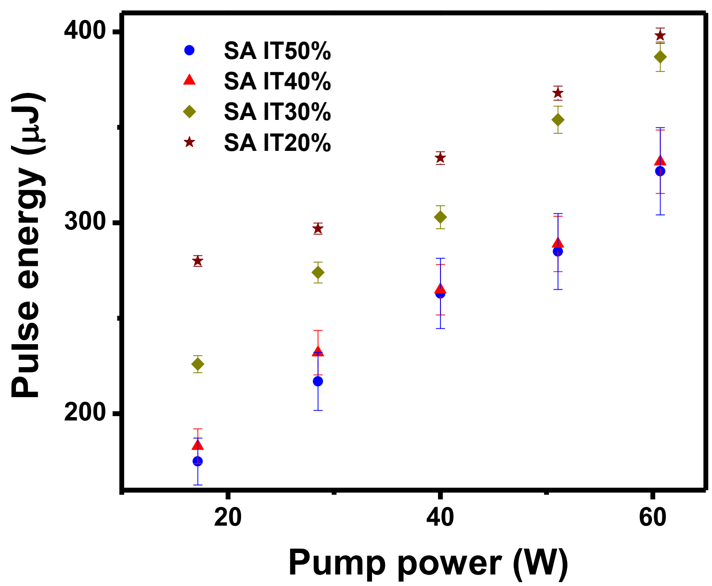

(d)

Fig.3.5: *(a) Average output power as a function of coupled pump power in CW (squares) and passively Q-switched operations. (b) Variations of pulse duration as a function of pump power for 50% (dots), 40% (triangles), 30% (diamonds), and 20% (stars) linear transmission of satrable absorbers.(c) Pulse repetition rate and (d) pulse energy as functions of pump power for 50%*

(squares), 40% (triangles), 30% (diamonds), and 20% (stars) linear transmission of saturable absorbers.

B. Temporal Characteristics

The minimum pulse duration obtained using Cr^{4+}:YAG crystals of linear transmission 50%, 40%, 30%, and 20% were measured to be 410 ns, 402 ns, 264 ns, and 163 ns, respectively. The lowest pulse duration of ∼163 ns is close to the cavity round- trip time ($2nL/c$) of 130 ns. The experimental data shows pulses of lower pulse duration are obtained for crystals of lower transmission. This is because the pulse duration and pulse energy depend upon the population inversion achieved before PQS is opened. For lower transmission of the crystal, population inversion achieved before opening of the Q-switch is higher as compared to that for higher linear transmission of the saturable absorber crystal. Hence, pulse duration is shorter and pulse energy is higher for crystal with lower values of linear transmission. Figure 3.5(c) shows the variation of pulse repetition rate as a function of coupled pump power. With an increase in pump power, the repetition rate increases for all PQS crystals, which is a characteristic of typical passively Q-switched lasers [22]. At fixed pump power, the repetition rate of pulses decreases with a decrease in the linear transmission of the crystal, owing to the higher linear loss created by a saturable absorber of low transmission. Figure 3.5(d) shows variation of output pulse energy with variation in coupled pump power. For a given pump power, it is observed that pulse energy increases with a decrease in linear transmission of the crystal. At the maximum value of pump power, for a crystal of 50% linear transmission, maximum pulse energy of 327 μJ was obtained, and it increases to 398 μJ for a PQS crystal of 20% linear transmission at the maximum value of pump power. The energy of the Q-switched pulse depends upon the difference between the initial and the final energy stored in the upper laser level during Q-switching, and, in turn, depends on population inversion just before switching (n_i) and final population inversion after the Q-switched pulse has burst out of the cavity (n_f). A transverse crosssectional area of the gain medium also decides its energy storage capability. Theoretical values of the pulse energies can be estimated by [87–89]

$$E = \frac{h\nu A}{2\sigma\gamma}\ln\left(\frac{1}{R}\right)\ln\left(\frac{n_i}{n_f}\right) \tag{3.2}$$

where, n_i is determined from the condition that the round-trip gain is exactly equal to the round-trip loss just before the Q-switch opens [87], but n_f cannot be directly calculated analytically. Degnan [89], has analytically derived a dimensionless parameter z on which pulse energy and pulse duration depends. The optimized output energy in terms of the dimension less parameter z is given by [89],

$$E = \frac{Ah\nu L}{2\sigma\gamma}\left[z - 1 - \ln z\right] \tag{3.3}$$

where, $z = \frac{2\sigma n_i l}{L}$

Here, σ is the stimulated emission cross-section of the gain medium, l is the length of the gain medium, L is the round-trip dissipative optical loss, R is the reflectivity of the output coupler, A is the core area of the gain medium, and γ is the inversion reduction factor. Population inversion density (n_i) in the passively Q-switched laser is given by [87]

$$n_i = \frac{\ln\left(1/R\right) + \ln\left(1/T_o^2\right) + L}{2\sigma l} \tag{3.4}$$

where T_0 is the linear transmission of the crystal. The output pulse duration in terms of the z parameter is given by [87]

$$t_p = \frac{t_R}{L}\left(\frac{\ln(z)}{z\left[1 - a(1 - \ln a)\right]}\right) \tag{3.5}$$

where, $a = \frac{z-1}{z \ln z}$

The values of the constants used for calculations are given in Table 3.1.

By using the above formulations, the theoretical values of the pulse energies for 50%, 40%, 30%, and 20% linear transmission of the crystals are 417 μJ, 459 μJ, 514 μJ, and 590 μJ, respectively. The corresponding experimental values of the pulse energies are 327 μJ, 332 μJ, 387 μJ, and 398 μJ, respectively. Similarly, the theoretical values of the pulse durations are 254, 233, 212, and 195 ns, and the corresponding pulse durations obtained experimentally are 410, 402, 264, and 163 ns for saturable absorbers of linear transmission of 50%, 40%, 30%, and 20%, respectively.

Table 3.1*: Values of the parameters used in the simulation [from nufern data sheet provided by the manufacturer].*

Parameters	Values	Parameters	Values
$\sigma_{sg,}$	8.7×10^{-23} m^2	λ_s	1080 nm
σ_{se}	2.2×10^{-23} m^2	λ_p	976 nm
σ_{as}	2.3x10-27 m^2	α_p	1.8 dB/m
σ_{es}	2.98x10-25 m^2	N	6.38×10^{25} m^2
σ_{ap}	26×10^{-25} m^2	Γ_p	2.5×10^{-3}
σ_{ep}	26×10^{-25} m^2	Γ_s	0.8

It is observed that the experimental values of pulse energies are lower than the theoretical values and the experimental values of pulse durations are higher than the theoretical value, except for the saturable absorber of 20% linear transmission. Discrepancy in the estimated and the calculated values of the pulse energy and pulse duration can be attributed to Fresnel reflection losses from different optics and from the fiber ends and loss of the signal due to the angle cleaving of the output end of the fiber, which affects the coupling of the signal into the PQS crystal and back into the fiber. Q-switched pulse width depends upon the cavity lifetime and the initial population inversion density. For higher linear absorption of the saturable absorber, the population inversion in the cavity will be high, which will lead to shorter pulses. In the theoretical estimation of the pulse energy, only round-trip loss and linear transmission of the saturable absorber has been taken into account. Other losses, such as non-saturable loss, induced by the saturable absorber at high intensity has not been considered. This may result in the experimentally measured value of the pulse width to be shorter than the theoretical value for 20% linear transmission of the crystal, whereas, for other crystals of higher transmission, non-saturable loss will not be considerable due to lower intra-cavity intensity.

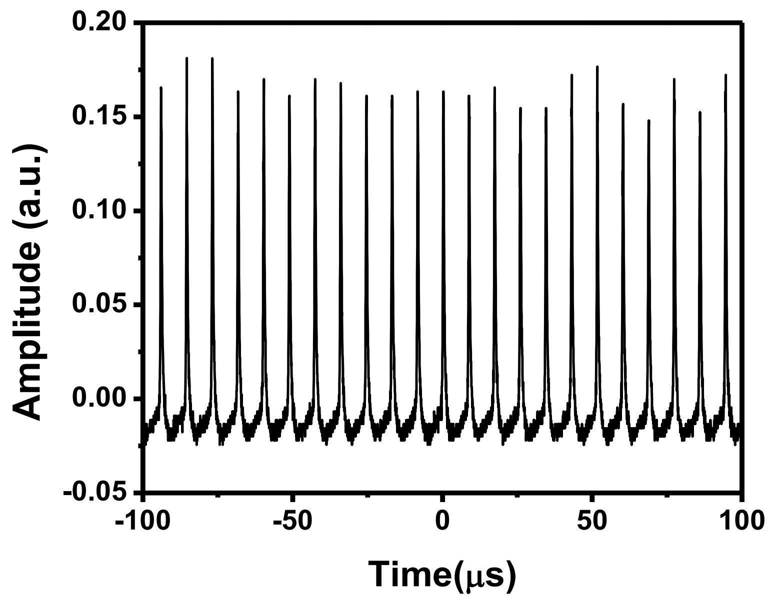

(a)

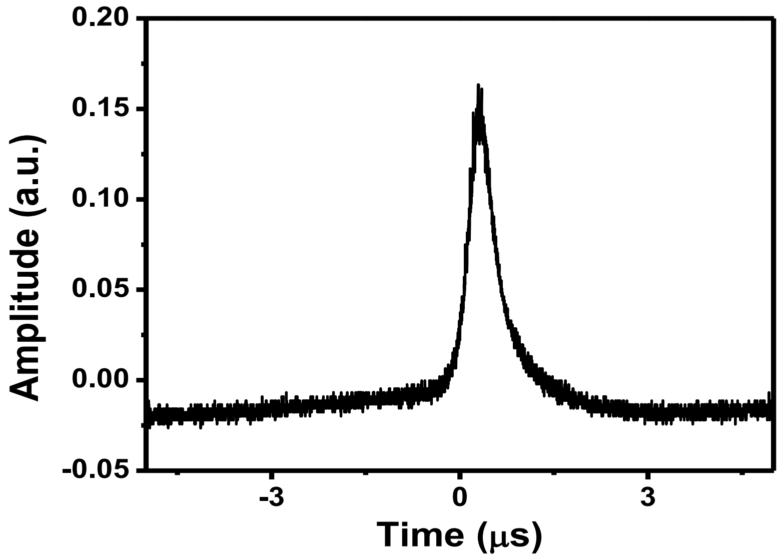

(b)

Fig. 3.6: *Oscilloscope trace of (a) a typical pulse train of PQS pulses at maximum pump power of 60 W, and (b) expanded view of a single pulse of the PQS pulse train in (a).*

During the passively Q-switched operation of the YDF laser, stability in pulse duration, repetition rate, and pulse energy was also measured. It was observed that pulse-to-pulse stability for PQS crystal of 50% linear transmission is ∼7%, and it improves to ∼1% by using crystal of 20% linear transmission. Figure 3.6(a) shows a typical Q-switched pulse train at the highest value of pump power with a repetition rate of ∼127 kHz for PQS crystal of 50% linear transmission, and figure 3.6(b) shows the oscilloscope trace for a single pulse at the same value of pump power.

C. Spatial Characteristics

Figure 3.7 shows the spatial profile of the PQS YDF laser close to the maximum output power of ∼41 W. This figure shows 2D and 3D profiles of the beam, which are Gaussian in nature, with single transverse mode output and measured value of the M^2 parameter of ∼1.04, which further confirms the single transverse mode beam quality of the laser output. Similar values of M^2 were obtained with similar 2D and 3D beam profiles for all the saturable absorber crystals. This value was measured using laser beam analyzer system (model: BEAMSTAR FX from Ophir Optronics) having a CCD camera and built-in software for image processing and Gaussian fit of 2D and 3D profiles. Beam quality measurement was also performed using a knife-edge method, in which a lens of 50 mm focal length was used to focus the beam and measure beam diameter. Beam waist of the real beam is given by,

$$W(z) = W_0\left[1 + (M^2)^2 \frac{\lambda^2}{\pi^2 W_0^4}(x - x_0)^2\right]^{1/2} \tag{3.6}$$

where, W_0 is the minimum waist of a real beam and is at x_0. $W(z)$ is the beam waist of the real laser beam at the position x. The factor M^2 describes the relationship of the real laser beam with an ideal Gaussian beam and is referred as propagation constant or propagation factor.

Through the knife edge method beam waist (y) at different values of x is measured and plotted. With the help of the curve fitting with the equation,

$$y = A\left[1 + B(x - x_0)^2\right]^{1/2} \tag{3.7}$$

values of A and B are calculated.

The relationship between M^2 and A, B is given by,

$$M^2 = A^2 \sqrt{B}\,\frac{\pi}{\lambda} \tag{3.8}$$

From the curve fitting, A and B values are obtained (A=3.75 e^{-5}; B=7.2e^{4}) which gives M^2 value of 1.07, which is very close to that measured using the beam analysis system.

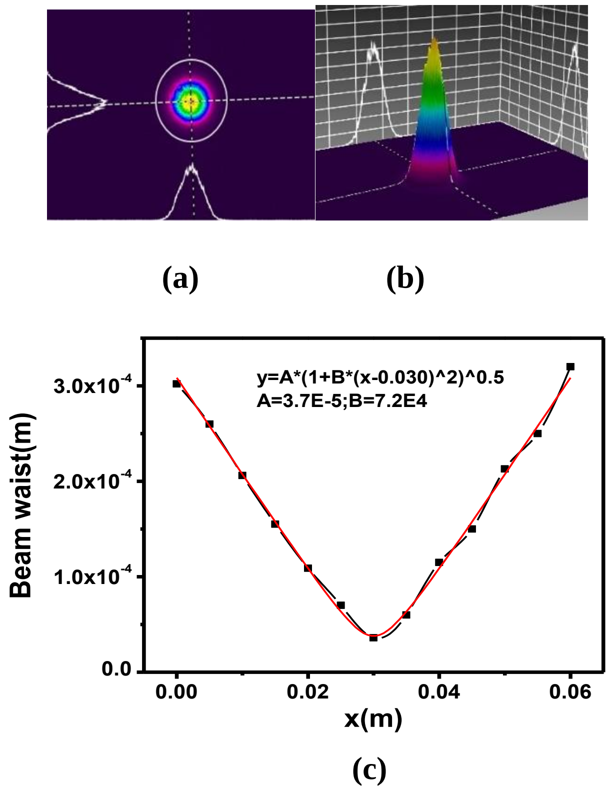

Fig. 3.7: *(a) Transverse 2D spatial beam profile, (b) 3D spatial beam profile. (c) Beam quality measurement curve of the passive Q-switched Yb-doped fiber laser using the knife edge method.*

3.3.2.2 Effect of saturable absorber on output pulse characteristics and spectrum

Before the Q-switching threshold is reached in PQS operation with 50% linear transmission of Cr^{4+}:YAG crystal, it was observed that, at low value of the pump power in the presence of a saturable absorber, recurrent damage of the fiber ends were taking place, when the saturable absorber was not at the focal spot of the beam. To prevent the fiber from damage, end caps were spliced at both fiber ends. To understand the underlying reason for the recurrent fiber end damage at very low value of pump power in the presence of the saturable absorber before start of Q-switching action, we simultaneously recorded the pulse and output spectral characteristics. When the laser was operated in the CW configuration, random self-pulses were observed, which has been reported in several Yb-doped fiber lasers.

Figure 3.8(a) shows the pulses at 7 W of pump power in the CW operation, and the amplitude of the pulses is about 0.02 arbitrary units (a.u.). Figure 3.8(b) shows the pulses when a saturable absorber was present inside the cavity at the same value of the pump power. The amplitude of the pulses enhanced by ~50 times. Figure 3.8(c) shows the spectrum of pulses when the saturable absorber is inside the cavity. Spectral peaks at 1116 nm and 1131 nm were also observed along with the signal peak, and these peaks in the output spectrum correspond to the primary and secondary Stokes component due to stimulated Raman scattering (SRS) in silica [26]. We estimated the threshold power for SRS, which is given by [26]

$$P_{out}^{SRS} = \frac{16A_{eff}}{g_R L_{eff}} \qquad (3.9)$$

Where, A_{eff} is the effective core area and L_{eff} is the effective fiber length and is given by,

$$L_{eff} = \frac{1}{\alpha_s}\left[1 - \exp(-\alpha_s L)\right] \qquad (3.10)$$

And g_r is the Raman gain coefficient in silica, given by $g_r = 1 \times 10^{-13}$ m/W. For our fiber, $A_{eff} = 3 \times 10^{-10}$ m^2 and L =12 m and, thus, the SRS threshold power is estimated as ~4 kW. From this value, it can be inferred that the peak power of the random self-pulses are enhanced to more than the threshold of SRS, so that nonlinear effects are initiated in the fiber laser. But, as the recurrent end damage of the fiber (without an end cap) were observed, the threshold value for the damage of the fiber end facets can also be calculated and is given by [24]

$$P_{laser}^{damage} = \Gamma^2 I_{damage} A_{eff} \qquad (3.11)$$

Where, Γ is the signal overlap factor, and I_{damage} is the upper limit of the intensity allowed in the fiber, the value of which is 10 W/μm^2 [90]. For our fiber, the calculated upper limit of peak power to prevent damage of the end facet of fiber is ~2 kW. The peak power of the pulses obtained due to the insertion of the saturable absorber inside the cavity, before the onset of Q-switching, is two times higher than the damage threshold of the fiber, resulting in recurrent damage of the fiber end facet. Thus, end caps were incorporated to prevent fiber end damage. As the pump power was further increased, PQS pulses were observed, indicating that the threshold for the PQS was achieved. Figure 3.8 (d) shows the regular PQS pulses at the threshold pump power. The amplitude of pulses is ~0.04 a.u., which is far lower than the amplitude of pulses before the onset of PQS. The frequency of the pulses is nearly uniform, but the amplitude jitter is very high, which is expected near the threshold. Figure 3.8 (e) shows the spectrum when Q-switching takes place and no Raman shift is observed in the spectrum. The presence of saturable absorber in the cavity before the Q-switching threshold is reached acts as a loss element, which enhances the peak power of random self-pulses [49, 52].

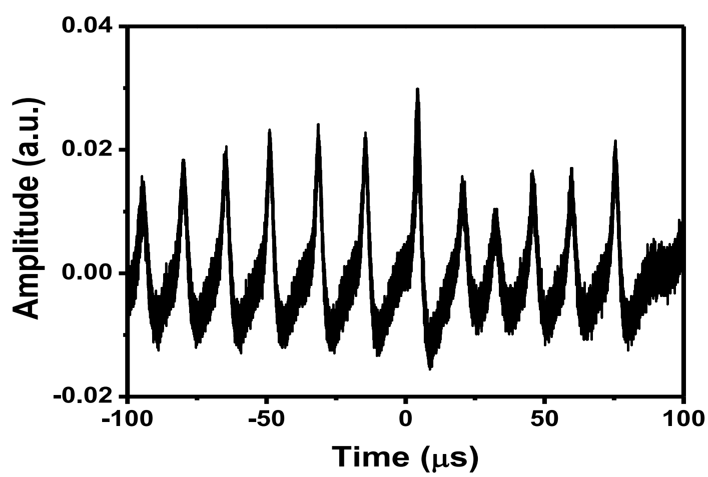

(a)

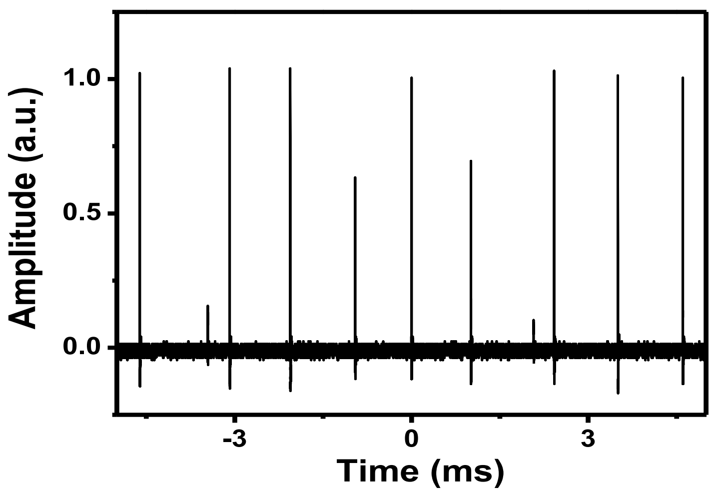

Amplitude (a.u.)
1.0
0.5
0.0
-3
0
3
Time (ms)

(b)

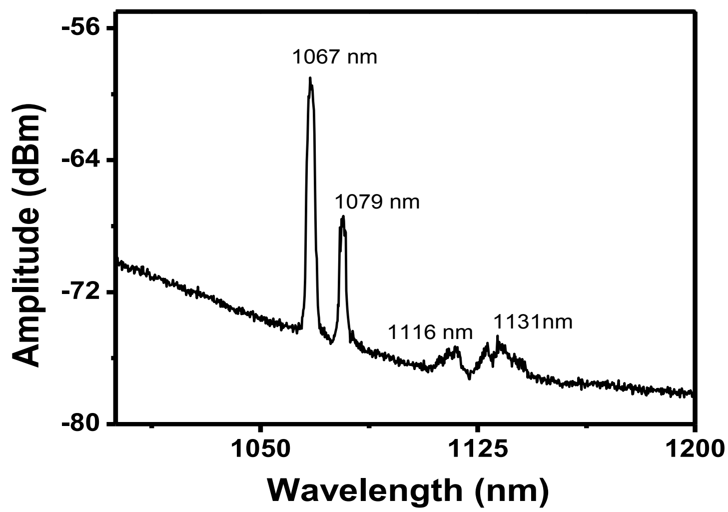

Amplitude (dBm)
-56
-64
-72
-80
1067 nm
1079 nm
1116 nm
1131nm
1050
1125
1200
Wavelength (nm)

(c)

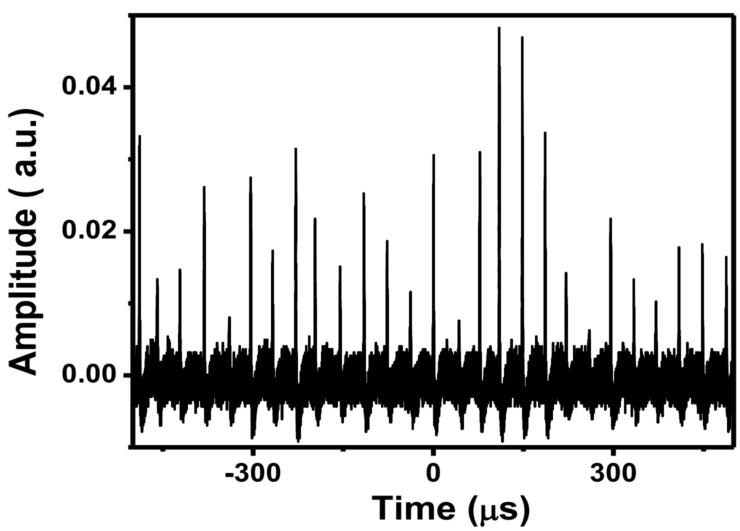

Amplitude (a.u.)
0.04
0.02
0.00
-300
0
300
Time (μs)

(d)

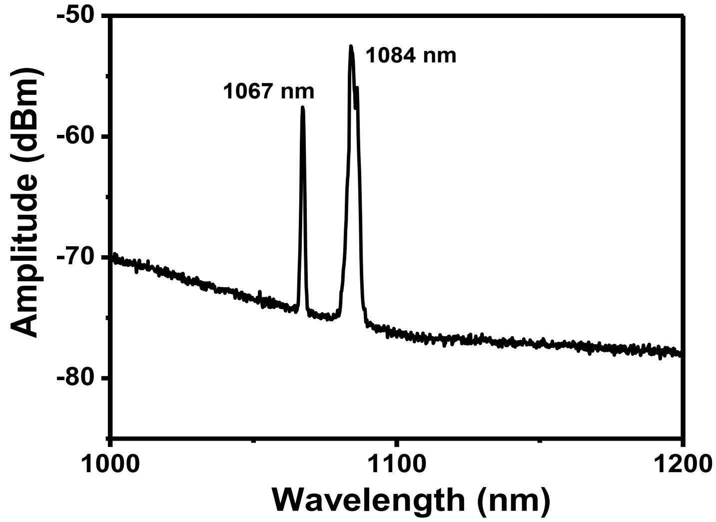

(e)

Fig. 3.8: *(a) Relaxation oscillations in the CW Yb-doped fiber laser in the absence of a saturable absorber, (b) Self-pulses in the YDF laser in the presence of a saturable absorber.(c) Spectrum corresponding to (b) showing SRS. (d) Q-switched pulses close to threshold pump power for Q-switching, (e) Spectrum corresponding to (d), showing absence of SRS signals.*

3.3.2.3 Effect of length of the gain medium on Q-switching

The effect of fiber length on PQS has also been studied with three different lengths of YDF gain medium, i.e., 6.5 m, 9 m, and 12 m, with a saturable absorber of 50% linear transmission. The absorption of the pump signal in 6.5 m, 9 m and 12 m is 11.7 dB, 16.2 dB and 21.6 dB respectively. In small length of fiber the pump signal absorption is less and will give rise to higher leakage power, which may damage the other pump diode, so the Q-switching studies were restricted to pump powers of less than 30 W. In CW operation, maximum output power of 13.7 W, 14.4 W, and 16.8 W at an input pump power of 28.5 W was obtained, respectively, for the 6.5 m, 9 m, and 12 m lengths of fiber. The pump thresholds for CW lasing for the three lengths of YDF are 2.9 W, 3.4 W, and 3.8 W, respectively. Figure 3.9(a) shows the average output power and pulse repetition rate of the Q-switched fiber laser for the three fiber lengths of 6.5 m, 9 m, and 12 m. Maximum average output power for the 6.5 m, 9 m, and 12 m fiber lasers are 7.2 W, 10.5 W, and 14 W, respectively, at the input pump power of 28.4 W with pump threshold values of 5.7 W, 5.3 W, and 5 W, respectively. The lowest output power is observed from the 6.5 m length of fiber, because the total pump absorption is expected to be lower. Pulse repetition rate for 6.5 m YDF ranges from 20 to 66 kHz, for 9 m it ranges from 16 to 57 kHz, and for the 12 m YDF, it ranges from 14 to 51 kHz. It is observed that, for the smallest length of gain medium, the repetition rate of the pulses is highest as the lasing threshold is lower compared to other lengths of the doped fiber.

Figure 3.9(b) shows the pulse duration at various values of pump power. For 12 m fiber, pulse duration ranges from 563 ns to 425 ns, for 9 m it ranges from 434 ns to 230 ns, and for the 6.5 m length of the fiber it ranges from 185 ns to 130 ns, with increase in the pump power from 11.6 W to 28.4 W. Pulse widths in the range from 130 ns to 550 ns can be easily obtained from the existing setup, and the smallest pulse width was obtained from the 6.5 m length of YDF due to the small cavity length. Still shorter pulses can be generated by reducing the length of the gain fiber, but at the expense of output power. Pulse energy increases from 109 □J to 274 μJ with increase in the length of the gain medium at pump power of 28.4 W, which is expected as the maximum gain is in the 12 m length of fiber.

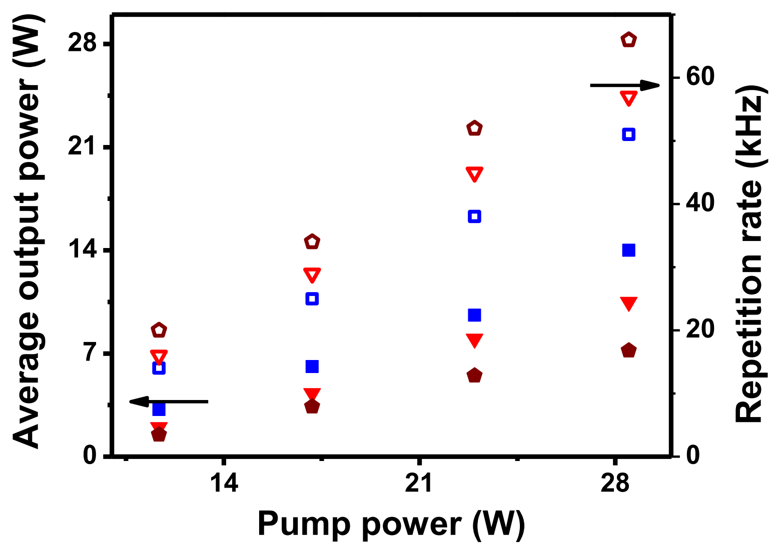

(a)

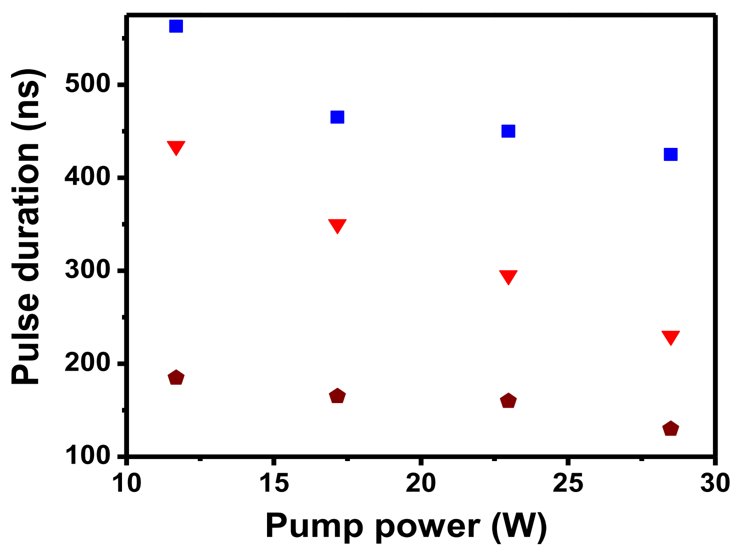

(b)

Fig. 3.9: *Variation of (a) average output power, repetition rate, and (b) pulse duration as a function of pump power for 6.5m (pentagons), 9 m (triangles), and 12 m (squares) lengths of YDF.*

3.3.2.4 Spectral evolution in Yb-doped fiber laser

The output spectrum evolution was also studied for three different lengths of YDF at different input pump powers. At low pump powers, lasing at two distinct wavelengths was observed, which merges into a broadband spectrum at higher pump power. Figures 3.10 (a) – (h) show the spectral evolution in PQS mode in all the three lengths of the YDF gain medium. For each length of the YDF, a single wavelength peak is generated close to the threshold pump power, and the wavelength of the peak depends upon the length of the gain fiber. An additional wavelength peak at the higher wavelength side emerges when the pump power is increased. Further increase in the pump power gives rise to multi-wavelength generation. A similar spectral evolution was observed during CW operation of the laser.

Figure 3.10 (a) shows the spectrum for the case of the 6.5 m length of YDF. Close to the threshold pump power of 5.7 W, the wavelength peak is generated at 1062.4 nm and spans within a range of 1 nm from 1062 nm to 1063 nm. As the pump power is increased to ~11 W, an additional wavelength peak appears in the spectrum at 1079 nm, with a wavelength range of 1.5 nm, as shown in Fig. 3.10 (b). The lower wavelength peak becomes slightly broader, with a wavelength range of 2.9 nm. At highest pump power of 28.4 W [Fig. 3.10 (c)], the linewidths of the two signals broaden, and an additional wavelength peak at 1056 nm emerge with base bandwidth of 14 nm and a 1080 nm peak. Here, the wavelength range spans from 1077 nm to 1082 nm with base bandwidth of 5 nm. It is observed that the two peaks at 1062 nm and 1080 nm have nearly the same amplitude at the highest pump power value of 28.4 W. For the 9 m length of YDF, Fig. 3.10 (d) shows the spectrum at the highest value of pump power of ~28.5 W, and the two wavelength peaks are at 1065 nm and 1079 nm with base bandwidths of 7 nm and 14 nm, respectively. The trend of the spectral evolution from the 6.5 m and 9 m lengths of YDF is similar, except that the spectral peaks are at different wavelengths. For the 12 m length of the YDF, we have studied the spectral evolution up to the highest pump power of 60 W. Initially, at threshold pump power of 5 W, only 1067 nm is generated; with an increase in the pump power, a 1084 nm signal also emerges in the spectrum, as shown in figure 3.10 (e). Further increase in the pump power to a level of ~28.4 W increases the bandwidth of 1084 nm signal, as shown in figure 3.10 (f). It was also observed that the peak of the lower wavelength signal at 1067 nm is re-absorbed, and a higher wavelength peak emerges at 1095 nm along with the signal at 1086 nm in the spectrum. The wavelength ranges from 1078 nm to 1099 nm with base bandwidth of ~21 nm. It may be noted that the re-absorption of the signal at lower wavelengths is not observed for the 6.5 m and 9 m lengths of the gain medium. Thus, re-absorption at lower wavelengths is predominant in the longer length of the fiber. With further increase in pump power, the spectrum becomes broad, with base bandwidths of 27 nm and 36 nm at pump powers of 51 and 60 W, respectively, with peak wavelength at 1083 nm, as shown in Figs. 3.10 (g) and 3.10 (h). The spectral evolution was also recorded for CW operation and was found qualitatively similar to that of the Q-switched mode of operation. Pan et al. [84, 85] have also reported two-wavelength generation in PQS operation of a fiber laser. However, they have observed the spectrum of the passively Q-switched laser at low pump powers only, at which the wavelength peaks were separated, and inferred that the two-wavelength generation is due to Q-switching of the fiber laser. In contrast, our results show that two-wavelength or multi-wavelength generation is associated with the pump power, gain medium, and resonator characteristics. It was noted that the shorter length of fiber generates marginally lower wavelength as compared to the longer length of gain medium. This is due to the quasi-three level energy structure of Yb-doped ions in silica, in which the ground level is the lower lasing level. The lower lasing levels lie close to the ground level and, hence, they are populated, giving rise to signal re-absorption. For shorter wavelengths, the reabsorption effect is more dominant compared to the longer wavelengths along the length of the fiber. Thus, for shorter fiber lengths, lower wavelength peaks will lase, and for long fiber lengths, higher wavelengths will lase, giving rise to a length-dependent signal wavelength effect in the YDF laser. The multi-wavelength generation in a Yb-doped fiber laser may be attributed to the broad reflection bandwidth of the bulk mirror used and due to inhomogeneous broadening effect in the silica-based fiber laser [91]

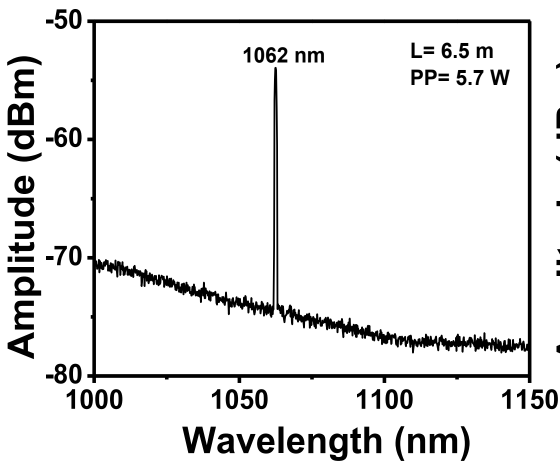

(a)

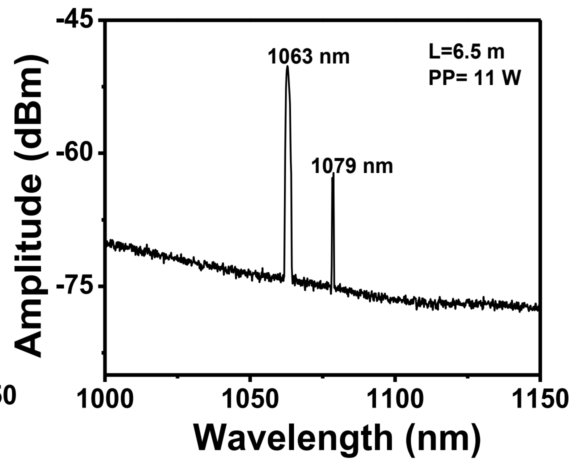

(b)

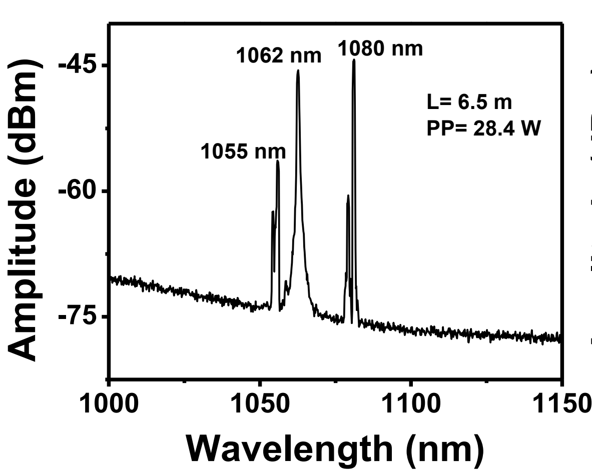

(c)

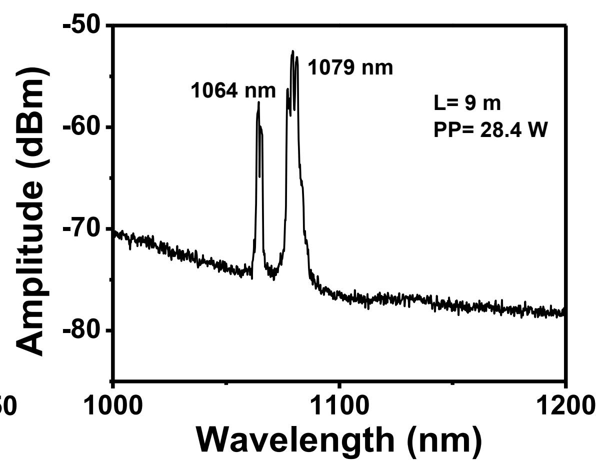

(d)

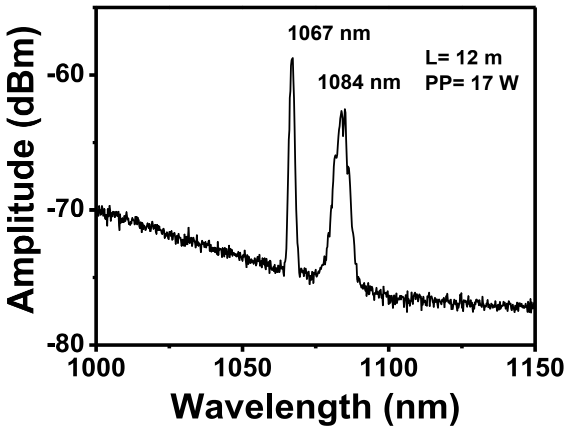

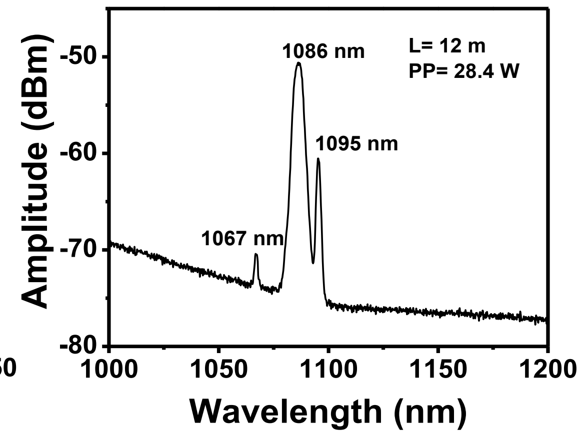

(e) **(f)**

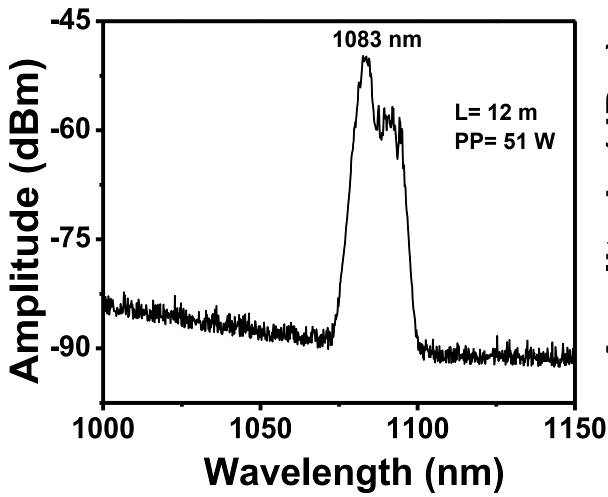

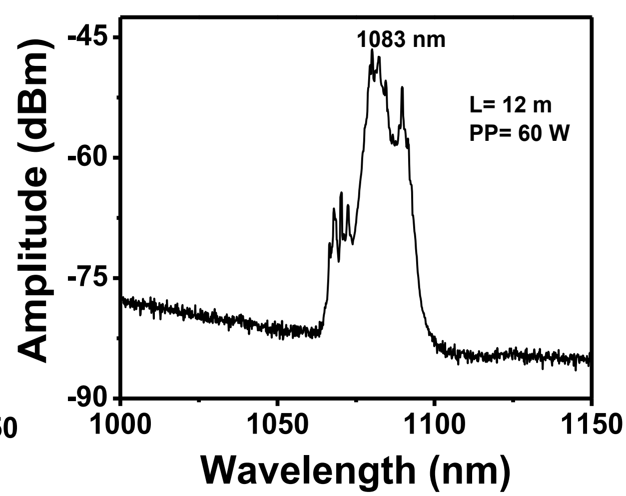

(g) **(h)**

Fig. 3.10: *Spectrum corresponding to fiber length (L) of 6.5 m at pump power (PP) of (a) 5.7 W, (b) 11 W, and (c) 28.4 W. (d) Spectrum corresponding to fiber length of 9 m at pump power of 28.4 W. Spectrum corresponding to fiber length of 12 m at pump power of (e) 17 W, (f) 28.4 W, (g) 51 W, and (h) 60 W.*

3. 4 Conclusion

In this chapter, we have demonstrated passive Q-switching operation in Yb-doped PCF laser and in LMA Yb-doped fiber laser with an average polarized output power of 9.4 W with PER of 10.5 dB and 40 W, respectively using Cr^{4+}:YAG crystal as a satrable absorber. Average power in Yb-doped polarizing PCF laser was limited by the available pump power in the single-end pumping configuration. Average power was increased in LMA fiber to 41.6 W by designing a special T-type double-end pumping configuration and splicing fiber end caps to avoid end damages. Variations in average power, pulse energy, pulse duration, pulse frequency, and pulse-to-pulse stability were also studied as function of linear transmission of saturable absorbers. The effect of the saturable absorber has been examined at a low value of pump power before the onset of Q-switching, and it was observed that the saturable absorber enhances random self-pulses generated in the Yb-doped fiber laser. The peak power of the self-pulses become high enough to a value such that it induces generation of stimulated Raman scattering inside the gain fiber, even at a very low value of pump power. With the onset of Q-switching, high peak power random pulses get converted to low-amplitude regular Q-switched pulses. We have also explored the effect of the length of the gain medium on dual wavelength generation at very low power, and of broadband generation at a sufficiently higher value of the pump power.

Chapter 4

Narrow-linewidth broadly tunable Yb-doped Q-switched fiber laser using multimode interference filter

4.1 Introduction

Pulsed fiber lasers with narrow linewidth and tunable output are useful in nonlinear frequency conversion applications, spectroscopic detection, remote sensing, wavelength division multiplexing, and Lidar systems [21, 39, 40, 71, 92-94]. Various methods have been employed to generate Q-switched pulses with narrow line- widths and tunable output. One of the preferred methods to tune the Q-switched output is via bulk grating [95], but it requires precise alignment and is not compatible with an all-fiber configuration. However, the use of in-line fiber Bragg grating (FBG) can overcome the disadvantage of free space bulk grating. There are a few papers in which FBG has been used as a Q-switching element to generate Q-switched pulses with narrow linewidths, however, the whole mechanism of Q-switching with the FBG as a Q-switch element looks cumbersome and the wavelength tunability is also limited to less than 1 nm range [96–98]. FBG written in Er-doped gain fibers and magnetostrictive mechanisms has been used as a Q-switching element to generate a narrow-linewidth Q-switched fiber laser having a linewidth of ∼6 MHz at 1532.3 nm [96]. Further, FBG has also been tuned optically to achieve a narrow-linewidth Q-switched Er-doped fiber laser having a linewidth of the order of tens of picometers [97]. However, wavelength tunability has not been achieved in the above papers [96, 97] by using FBG. Q-switching was done by the piezoelectric transducer and FBG, and tunability in the range of 0.05 nm was achieved, which is very low [98]. For narrow-linewidth generation in an Er-doped fiber laser, the seed injection technique using an all-fiber acousto-optic modulator (AOM) has been reported, but in this setup, wavelength tunability was not possible [99]. For passive Q-switching, graphene has also been used as a saturable absorber (SA) in an Er-doped fiber laser, and the wavelength tunability has been achieved by using a tunable band-pass filter (TBPF), which provides tunability in the range of 32 nm and a bandwidth of 0.3 nm [100]. Further, topological insulator Bi_2Se_3 has also been used as a SA for Q-switching and TBPF has been used to tune the wavelength in the range from 1493.6 to 1508.9 nm [101]. However, in these reported works, specialized optical filters were used to generate the narrow linewidth tunable output from the Q-switched fiber laser.

Recently, filters based on multimode interference (MMI) effects, which comprise of single-mode–multimode-single-mode fibers, have created a lot of interest for narrow-linewidth and tunable-output signal generation due to their adaptability with an all-fiber configuration and simple construction. In a Yb-doped CW fiber laser, tunability of 8 nm has been achieved by using a multimode interference filter (MMIF) and a broad- band mirror [102], and tunability of more than 60 nm has been reported by using a MMIF and ferrule-based technique [103] in the bulk configuration. In the all-fiber ring cavity configuration, tunability of more than 30 nm with a spectral bandwidth of 0.05 nm in a single-mode fiber has also been reported [104]. MMIF has also been used for the tuning of an Er-doped fiber laser and a semiconductor optical amplifier, with the tuning ranges of 55 nm and 90 nm, respectively, by using opto-fluidically tunable MMIF [105]. An all-fiber passively Q-switched fiber laser was demonstrated in an Er–Yb co-doped fiber laser with an MMIF and TBPF [106]. A MMIF has also been used for tuning of a mode-locked Er-doped fiber laser [107]. In a thulium-doped CW fiber laser, dual wavelength operation at the 1950 nm region was demonstrated by using an MMIF [108]. Tunability in a mode-locked thulium-doped laser was demonstrated using an MMIF [109, 110]. A compact laser diode was also demonstrated with a 1 × 2 MMI with a 25 nm tuning range and linewidth of ~750 kHz [111]. However, to the best of our knowledge, there are no reports showing tunability and narrow-linewidth generation in a Yb-doped Q-switched fiber laser using MMIF in the linear and ring cavity configurations. In this chapter, we report for the first time narrow-linewidth generation and broadly tunable output from a Yb-doped Q-switched fiber laser using an acousto-optic modulator (AOM) and MMIF in the linear bulk cavity and all-fiber ring cavity configurations. In the linear bulk cavity configuration, the spectral bandwidth of the Q-switched signal decreased by two orders of magnitude from 11 to less than 0.1 nm by insertion of an MMIF. Spectral tunability of more than 16 nm has also been achieved by the combination of MMIF and a standard polarization controller (SPC). The experimental observation showed a decrease in the pulse duration with a decrease in the spectral bandwidth of the output signal. The pulse duration was reduced by a factor of about two with the introduction of MMIF in the cavity. As the linear bulk cavity was not compatible with the all-fiber configuration, Q-switching was carried out in an all-fiber ring cavity using fiber optic AOM to exploit the feasibility of MMIF in the all-fiber Q-switched fiber laser configuration. In this configuration, the spectral bandwidth of the Q-switched signal was decreased from 17 to less than 0.1 nm and pulse duration was reduced by a factor of about three due to the introduction of the MMIF. The spectral tunability of more than 12 nm was also achieved by means of an MMIF and an SPC. The contents of this chapter are arranged as follows. After the introduction of MMIF, the details of experimental configuration are given in Section 4.2, which is subdivided into three sub-sections. The first subsection explains the experimental setup of the linear AO Q-switched fiber laser. The second subsection deals with the experimental configuration of the ring cavity, and the third subsection discusses the design part of the MMIF. Results and discussion are presented in Section 4.3, which is further subdivided into two subsections. In the first subsection, results of the linear cavity are presented, and in the second subsection, results of the ring cavity have been discussed.

4.2 Experimental details

4.2.1 Linear cavity using bulk AO Q-Switch

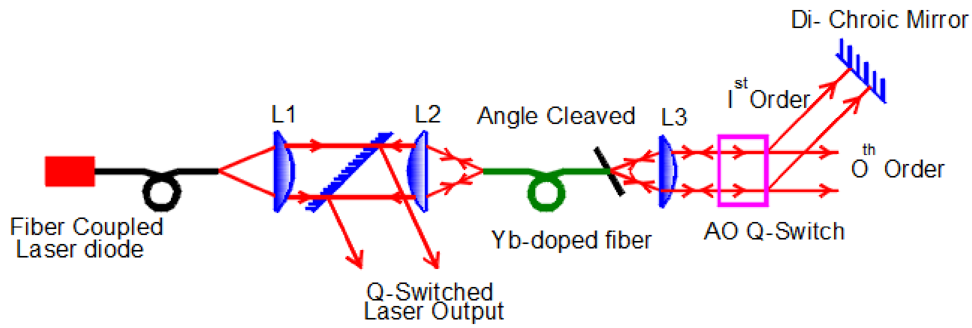

(a)

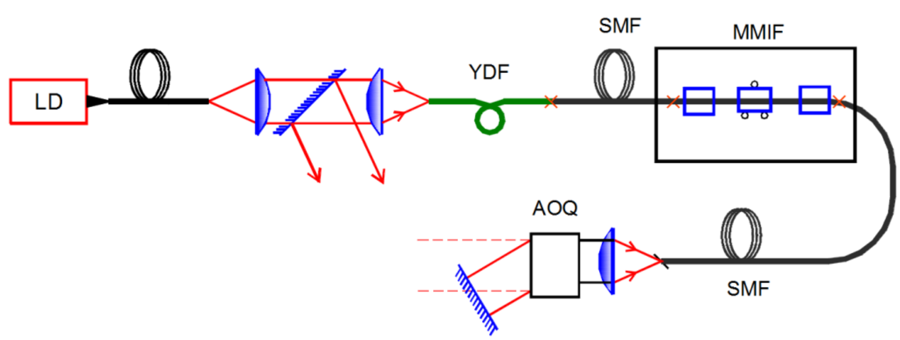

(b)

Fig. 4.1: *Schematic of (a) AOQ-switched fiber laser in the bulk linear cavity configuration; (b) AO Q-switched fiber laser in the bulk linear cavity configuration with MMIF.*

Figure 4.1(a) shows the schematic of the AO Q-switched fiber laser in the linear cavity configuration. The pump source consists of a 20 W fiber-coupled laser diode (LD) at 976 nm pigtailed with fiber having a core diameter of 200 μm and a numerical aperture (NA) of 0.22. A Yb-doped double-clad fiber (YDF), with a core diameter of 5 μm and NA of 0.14, an inner cladding diameter of 125 μm and NA of 0.46 has been used as the gain medium. This fiber has an inner clad pump absorption of 1.76 dB/m at 975 nm. The 9 m length of the gain medium led to pump absorption of ∼15.84 dB along the fiber length. Pump power from the laser diode was coupled to the gain medium with coupling efficiency of 50% using the combination of plano-convex lenses L1 and L2 with the focal lengths of 20 mm and 10 mm, respectively. The input end of the fiber was perpendicularly cleaved, and the output end of the fiber was cleaved at an angle of 8° to avoid lasing between the two ends of the fiber surfaces. The signal beam from the angle cleaved end of the fiber was collimated using lens L3 of the focal length 10 mm. For active Q-switching, AOM was kept after the lens L3. A broadband high reflectivity (HR) mirror with ∼99% reflectivity in the wavelength range of 1040–1110 nm was kept at a distance of ∼0.75 m from the AOM to adequately separate the zeroth-order and first-order beams, and feedback only from first-order beam was ensured. A radio frequency (RF) signal at 27.12 MHz was given to the AOM for diffraction of the laser beam and it was modulated in the kilohertz range for the generation of Q-switched pulses. The diffraction efficiency of the AOM was ∼60% and the corresponding Bragg angle for the Bragg diffraction was 7.68 mrad. For Q-switched operation, the HR mirror was aligned at the first-order diffracted beam. Figure 4.1(b) shows the schematic of the AOQ-switched fiber laser with the MMIF. The MMIF consists of single mode fiber (SMF), followed by a multimode fiber and a single-mode fiber. Both the ends of the MMF are spliced with the SMF to splice it with the other components. The core/clad diameters of the SMF and MMF used were 6/125 μm and 100/125 μm, respectively. Both the SMF and MMF were mounted on a straight block. The middle portion of the MMF was mounted on the standard polarization controller mount to provide axial rotation and pressure. The output end of the SMF towards the AO Q-switch was angle cleaved at an angle of 8°.

4.2.2 All-fiber ring cavity using fiber optic AO Q-switch

The studies were carried out in all fiber ring cavity AO Q-switch laser using MMIF. Figure 4.2(a) shows the experimental setup of the all-fiber AO Q-switched, tunable Yb-doped ring fiber laser. The pump source was a fiber-coupled laser diode with a maximum output power of 10 W, with a fiber pigtail having core/clad diameter of 105/125 μm. The fiber pigtail of the pump diode was fusion spliced to one of the pump ports of the pump combiner (2 × 1+1). The pump combiner comprises of two pump ports, one signal port, and one output port. The two pump ports of the combiner are fiber with core/clad diameter of 105/125 μm. The output port and signal port of the combiner are double-clad fibers, having core/inner clad diameters of 10/125 μm. The output port of the pump combiner (PC) was connected to the YDF. The other end of the YDF was fusion spliced to the all-fiber AO Q-switch, which was connected to the 50/50 coupler through the polarization-insensitive fiber optic isolator.

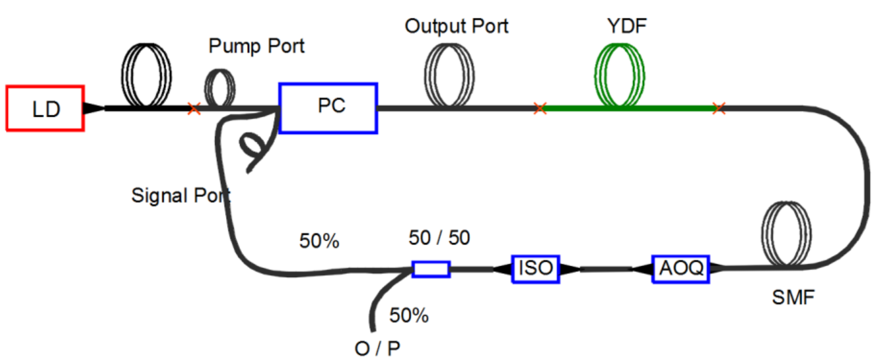

(a)

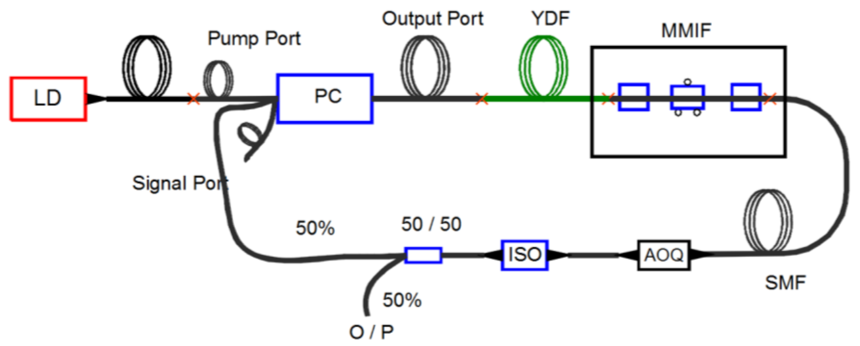

(b)

Fig.4.2: *Schematic of (a) all-fiber Q-switched fiber laser with fiber optic AO Q-switch in the ring cavity configuration; (b) all-fiber Q-switched fiber laser with MMIF.*

The all-fiber AO Q-switch, coupler, and fiber optic isolator are based on the single-mode fiber HI 1060. The fiber optic AO Q-switch operates at a RF signal of 80 MHz, to diffract the signal beam in the first order. One port of the 50/50 coupler was used as the output signal port and the other port of the coupler was spliced to the signal port of the combiner to make the ring cavity unidirectional. For the cavity with MMIF, the MMIF as explained in the previous section was spliced between the YDF and AO Q-switch [figure 4.2(b)]. Q-switched pulses were recorded using a 1 GHz photo-receiver and a 1 GHz, 2GSa⁄s digital storage oscilloscope. The wavelength spectrum of the laser output was observed using an optical spectrum analyzer from M/s Agilent Technologies (model No. 86146B) with a resolution of 0.06 nm, and output power was measured using a 50 W thermal power meter from M/s Ophir (model No. L50A-SH).

4.2.3 Design of the MMIF

To design the MMIF for the Q-switched narrow-linewidth and tunable Yb-doped fiber laser, the critical parameters are the length and diameter of the MMF [104]. If L is the length of the MMF segment such that

$$L = pZ_{img} \tag{4.1}$$

where, p is the order of the self-images of the input field formed, Z_{img} is the reimaging length, where the first image of the input field is formed, and this image repeats itself along the length of the multimode fiber. The reimaging length is given by [104]

$$Z_{img} = 4n_{MMF} d_{MMF}{}^{2} / \lambda_0 \tag{4.2}$$

where, λ_0 is the designed wavelength for which the transmission is maximum, n_{MMF} is the refractive index of the core of the MMF and d_{MMF} is the core diameter of the MMF. The transmission spectrum of the MMI filter is given as,

$$\begin{aligned} T(\lambda, L) &= \left| \sum_{m=1}^{M} c_m^2 \exp[i\beta_m(\lambda)L] \right|^2 \\ &= \left| \sum_{m=1}^{M} c_m^2 \exp[i\beta_m(\lambda) pZ_{img}] \right|^2 \end{aligned} \tag{4.3}$$

where, T is the transmission of the MMIF for given λ, m is the mode index, M is the total number of modes excited in the MMF, c_m is the excitation coefficient, and β_m is the propagation constant of the m^{th} order mode. The central wavelength λ_0 is taken as 1070 nm. It can be seen in Eq. (4.3) that the wavelength response of the MMIF depends on the order of self-image p. The wavelength separation between two consecutive transmission peaks of the MMIF, the self-image wavelength interval ($\Delta\lambda_{int}$), depends inversely on p and is given by [104]

$$\Delta\lambda_{\text{int}} = \lambda_0 / 2p \tag{4.4}$$

The gain spectrum of the YDF spans from ∼1010 to ∼1120 nm; hence for a designed wavelength of around 1070 nm, $\Delta\lambda_{int}$ > 60 nm is required to ensure single wavelength operation from the laser. This corresponds to a self-imaging order p = 8. Now the transmission bandwidth of the MMIF decreases with increase of the diameter of the MMF [104].

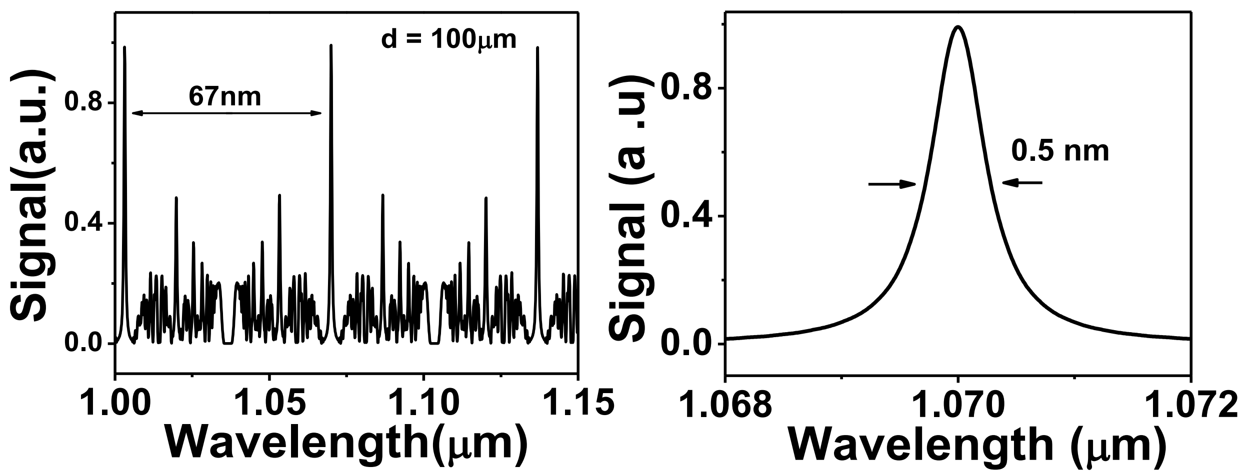

(a) **(b)**

Fig. 4.3: *(a) Transmission spectrum of MMIF with* d_{MMF} *=100 μm and for* p *= 8; (b) transmission peak at 1070 nm with FWHM width of 0.5 nm.*

In order to obtain low-loss fusion splicing between the SMF and MMF, we have chosen a MMF of core diameter 100 μm, which is available commercially having a refractive index of 1.4504. Thus for p = 8, the Z_{img} is estimated to be 54.22 mm and the MMF length of 43.376 mm is required to obtain single-wavelength and narrow-linewidth operation. However, the precise cleaving at this wavelength is not essential as the MMIF is placed inside the cavity. The computed wavelength response and the transmission bandwidth for the designed wavelength are shown in figure 4.3.

4.3 Results and Discussion

4.3.1 Results of the Q-Switched fiber laser with bulk AO Q-switch and MMIF in the linear cavity configuration

In this configuration, the CW output power of 1.8 W and an average Q-switched power of 1.15 W at the repetition rate of 100 kHz were obtained at an input pump power of ∼5 W. The spectral bandwidth of the Q-switched signal was very broad with the full width at half maximum (FWHM) bandwidth of ∼11 nm and ranges from 1066 nm to 1077 nm with the peak wavelength at 1070 nm, as shown in figure 4.4(a). When the MMIF was spliced to the output end of the YDF, the average output power was reduced to 0.51 W at the pump power of 5 W. With the introduction of the MMIF in the cavity, the FWHM bandwidth of the output spectrum was reduced by a factor of more than 100 times to a value of 0.08 nm with a peak wavelength at 1060 nm, as shown in figure 4(b). For tuning of the output spectrum of the Q-switched fiber laser, the actuator knob of the standard polarization controller mount was twisted[104], which tuned the output wavelength from 1057 to 1073 nm with the FWHM bandwidth of ≤ 0.1 nm at the signal output power of ∼500 mW [as shown in figure 4.4(c)]. The applied stress by the actuator knob of the polarization controller changed the refractive index of the core of the MMF, due to which the path length corresponding to each wavelength changed. This modifies the phase relationship between the different transverse modes for each wavelength inside the multimode fiber.

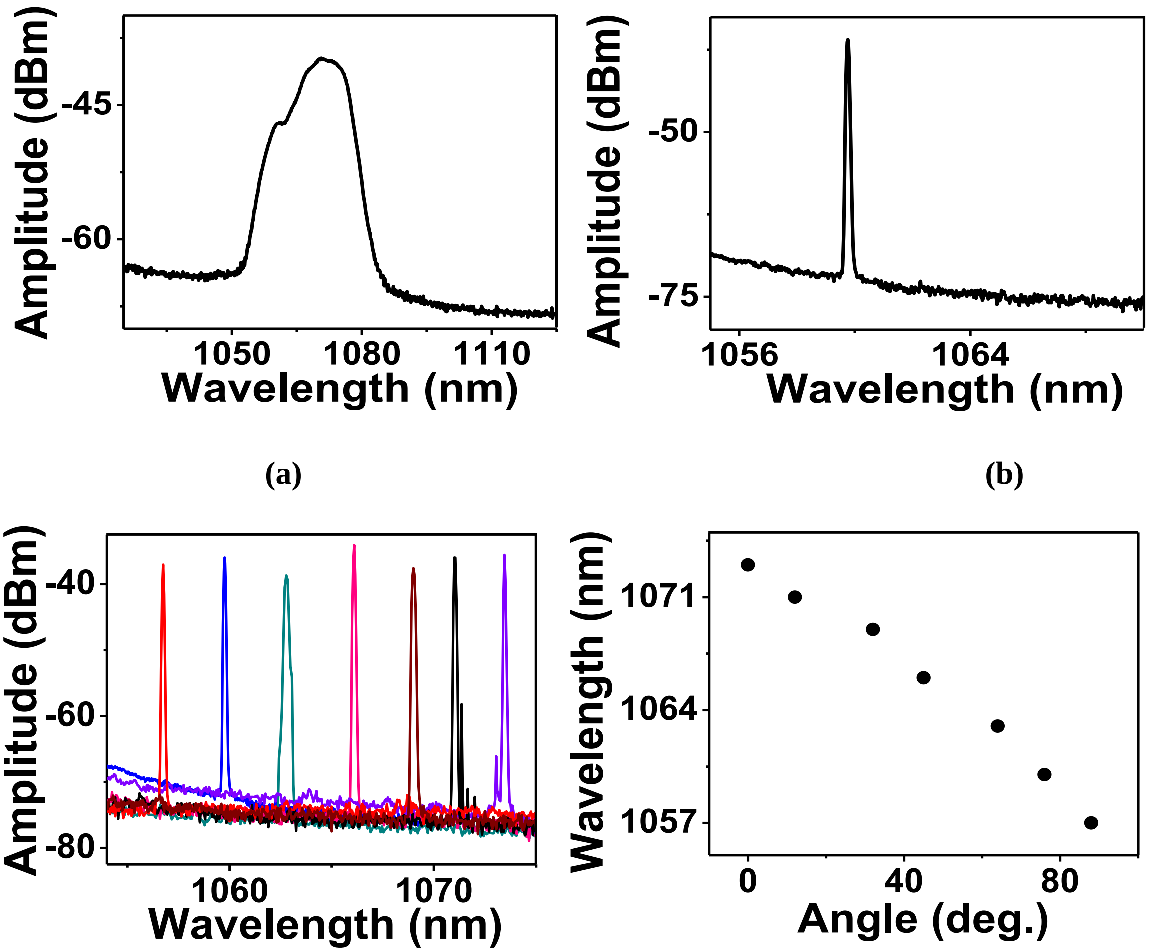

Fig. 4.4: (a) *Spectrum of the Q-switched signal with FWHM bandwidth of ~11 nm and peak wavelength at 1070 nm in the bulk linear cavity configuration without MMIF; (b) spectrum of the Q-switched signal with the FWHM bandwidth of 0.08 nm and peak wavelength at 1060 nm in the bulk linear cavity configuration with intra-cavity MMIF; (c) wavelength tuning in the range from 1057 to 1073 nm of Q-switched linear fiber laser with intra-cavity MMIF and SPC; (d) variation of the output wavelength of the signal with the angle of actuator knob of the SPC.*

The wavelength having the maximum transmission peak at the splice joint between the SMF and the MMF appears at the output. As the phase relationship changes, the output wavelength changes, resulting in the tuning of the output signal. Variation of output wavelength with the tuning angle of the actuator knob is shown in figure 4.4(d). Wavelength decreases with increase in the tuning angle of the actuator knob of the polarization controller. The variation in the tuning angle from 0° to 90° varies the wavelength from 1073 to 1057 nm. The presence of the MMIF in the resonator not only reduced the spectral bandwidth as contemplated, but temporal pulse shortening was also recorded. Figure 4.5(a) shows the Q-switched pulse with a FWHM pulse width of~305 ns at the pump power of 5 W.

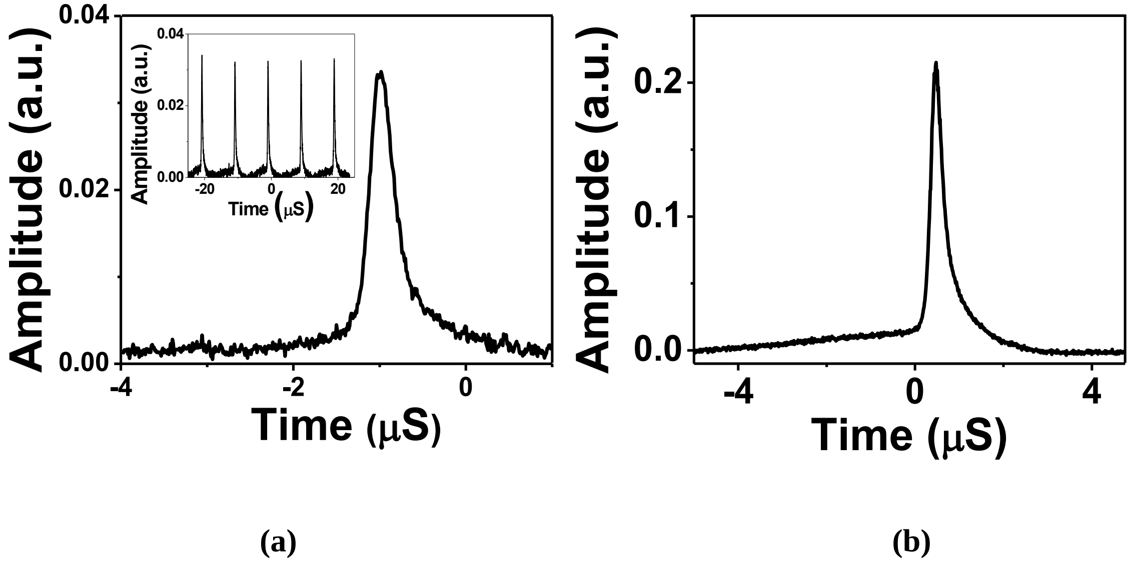

Fig. 4.5: *(a) Single Q-switched pulse with FWHM pulsewidth of ~305 ns in the bulk linear cavity configuration without MMIF (inset shows Q-switched pulse train at 100 kHz); (b) single Q-switched pulse with FWHM pulsewidth of ~240 ns in the bulk linear cavity configuration with MMIF.*

The inset shows the train of pulses at 100 kHz at the same value of the pump power. However, it is expected that there would be an increase in the pulse width of the output Q-switched signal with the insertion of the MMIF in the resonator, as the length of the cavity is increased and the output signal power is reduced from 1.15 W to 500 mW. Without the MMIF in the resonator, at the pump power of ~5 W, the FWHM pulsewidth of the Q-switched signal was ~305 ns, which was reduced to ~260 ns [as shown in figure 4.5(b)], when the MMIF was spliced to the YDF. The observed reduction in the pulse duration can be attributed to the spectral narrowing of the output spectrum by the introduction of the MMIF in the resonator. In the Q-switched resonator without the MMIF, the spectral bandwidth was very broad at ~11 nm. Each wavelength component possess different values of loss and gain depending upon the gain spectrum curve of the Yb-doped fiber. This results in the difference in the pulse buildup time for different wavelength components. The wavelength experiencing high gain will have a small pulse buildup time, and a shorter FWHM pulsewidth. The spectral component with slightly low gain in the cavity will have a large pulse buildup time, and also a large FWHM pulse width. The net output pulse, which appears at the output, will be an envelope of all the pulses corresponding to each wavelength component, and hence results in a longer pulse duration. In the presence of the MMIF, there is spectral narrowing, and hence the spread of the pulse for each wavelength component will be absent, resulting in a smaller FWHM pulse width of the Q-switched pulses [22]. The Q-switched operation was performed in the repetition rate frequency range from 5 to 100 kHz. The lower frequency range was decided by the appearance of the amplified spontaneous emission (ASE) signal, and the higher frequency range was limited by the operating frequency of the Q-switched modulator. The trend of the results were same irrespective of operating frequency range of the Q-switch.

4.3.2 Results of the all fiber Q-Switched fiber laser in the ring cavity configuration

In the all-fiber ring cavity configuration without an AO Q-switch [as shown in figure 4.2(a)], the resonator operates in the CW mode with a signal output power of 500 mW at the input pump power of 5 W. When all-fiber AO Q-switch was fusion spliced in between the YDF and fiber optic isolator, the output average power was reduced to 100 mW at 20 kHz repetition rate when operated at the same value of the input pump power. Figure 4.6(a) shows the spectral linewidth of the output

Q-switched signal without MMIF, which was broad, ranging from 1040 nm to 1078 nm with the FWHM linewidth of ~17 nm at the peak wavelength of 1070 nm.

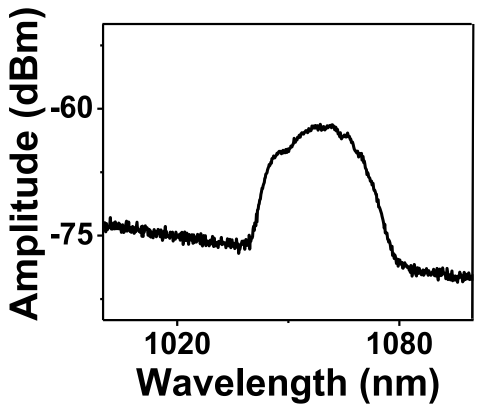

(a)

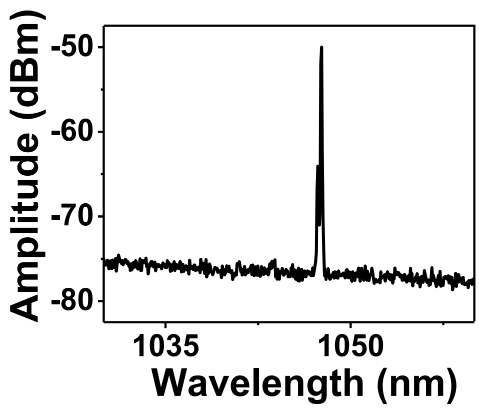

(b)

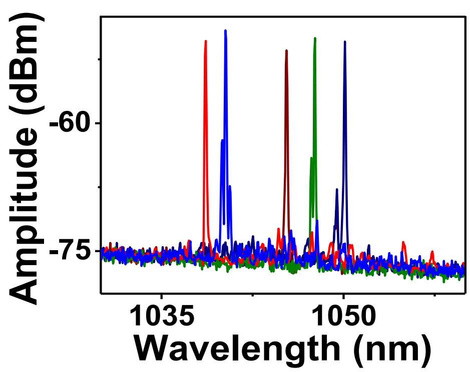

(c)

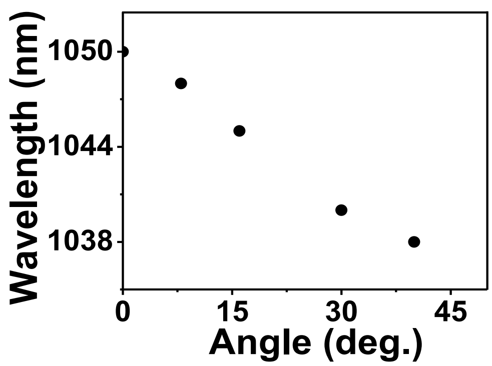

(d)

Fig.4. 6: *(a) Q-switched spectrum of YDF ring laser with FWHM bandwidth of 17 nm and peak wavelength at 1070 nm without intra-cavity MMIF; (b) Q-switched spectrum of YDF ring laser with MMIF, having FWHM bandwidth of less than 0.1 nm and peak wavelength at 1048 nm; (c) wavelength tuning in the range from 1038 to 1050 nm of Q-switched fiber ring laser with MMIF and standard polarization controller; (d) variation of the output wavelength of the signal with the angle of actuator knob of the polarization controller in the all-fiber ring cavity configuration.*

When the MMIF was introduced in the ring resonator between the YDF and the fiber optic AO Q-switch [figure 4.2(b)], the spectral linewidth of the signal reduced drastically from ~17 to less than 0.1 nm at the peak wavelength of 1048 nm as shown in figure 4.6(b). For the wavelength tunability of the output signal, the standard polarization controller mount in which the MMF was mounted was twisted, and the wavelength varied in the range of 1038 nm to 1050 nm as shown in figure 4.6(c). In the all-fiber ring cavity resonator, operating signals are towards the lower wavelength side compared to the linear bulk cavity resonator. This is because in the all-fiber ring cavity resonator, the signal power is low and the gain for the YDF is higher at the lower wavelength side, so the operating signal shifts towards the lower wavelength region. Variation of output wavelength with the tuning angle of the actuator knob followed the same trend as for the bulk cavity resonator.

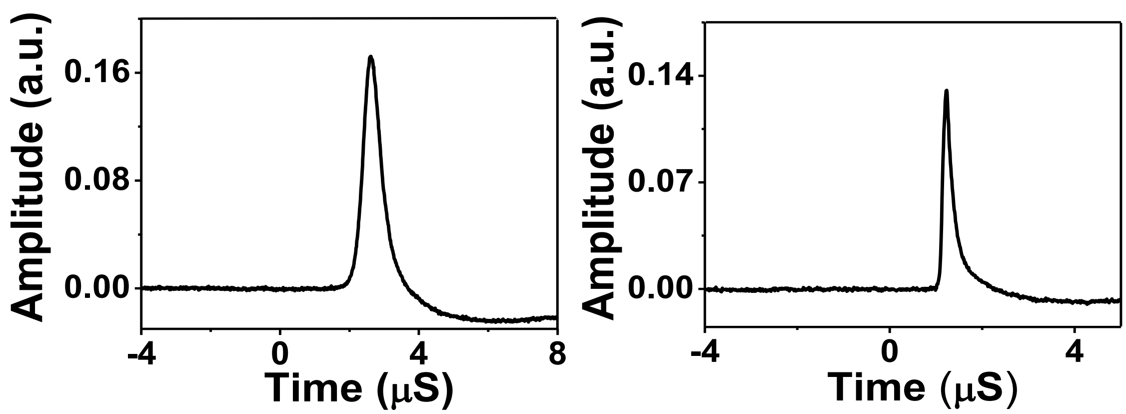

(a) **(b)**

Fig. 4.7: *(a). Single Q-switched pulse having a pulsewidth of ~200 ns at the input pump power of 5W in the YDF ring laser without intra-cavity MMIF; (b) single Q-switched pulse having a pulsewidth of ~185 ns at the input pump power of 5 W from the YDF ring laser with MMIF.*

With the variation in the tuning angle from 0° to 40°, wavelength varies in the range of 1050 nm to 1038 nm. In the ring resonator, reduction in the pulse width was also recorded, as in the linear cavity configuration. A single Q-switched pulse with a FWHM pulse width of ∼200 ns was obtained by the adjustment of the duty cycle of the modulating signal [figure 4.7(a)] [112]. With the insertion of the MMIF, FWHM pulse width of the output signal was reduced from 200 ns to 185 ns at the same value of the pump power [figure 4.7(b)]. The reduction in the average signal power and the spectral bandwidth of the signal has been explained in the previous section.

4.4 Conclusion

Narrow linewidth and tunable operation of an AO Q-switched YDF laser using an AOM and MMIF in the linear bulk resonator and all-fiber ring resonator has been demonstrated. In the linear resonator, the spectral bandwidth of the Q-switched signal decreased by two orders of magnitude from a value of 11 nm to less than 0.1 nm by the insertion of the MMIF in the cavity. Spectral tunability of more than 16 nm in the range of 1057 nm to 1073 nm has also been achieved by the combination of the MMIF and an SPC. Decrease in the pulse duration with a decrease in the spectral bandwidth of the output signal from ∼305 ns to ∼240 ns was also recorded. In the case of the all-fiber ring resonator with the MMIF, the spectral bandwidth of the output Q-switched signal was decreased from 17 to less than 0.1 nm. A spectral tunability of more than 12 nm in the range of 1038 nm to 1050 nm was achieved by an MMIF and an SPC. The pulse duration was reduced from ∼200 ns to ∼185 ns. The average output power in the linear resonator with the MMIF is ∼500 mW, which is much higher than the average power obtained in the all-fiber AO Q-switched ring resonator with the MMIF, in which the power is ∼10 mW. However, the tunability range in both the configurations are comparable. Due to the all-fiber nature, the ring cavity resonator with a narrow linewidth and tunable operation can be potentially used as an oscillator for further amplification of output power in the master oscillator power amplifier (MOPA) configuration.

Chapter 5

Short pulse generation in actively Q-switched Yb-doped all-fiber laser and its amplification

5.1 Introduction

In recent times, fiber lasers have been a field of intense research and development due to its diverse path breaking applications in industries and medicine owing to high beam quality, ease of beam delivery and feasibility of high output power. Pulsed Yb-doped fiber lasers with high energy and high peak power are inevitable in the fields of material processing [113], remote sensing, nonlinear frequency conversion [114], super continuum generation [115, 116] and spectroscopy due to their low quantum defect and large upper state lifetime. These vivid applications require high power lasers and one of the approach is through master oscillator power amplifier (MOPA) configuration. For the nanosecond pulse generation and its amplification through MOPA based systems, seed laser diodes (SLD) are the preferred choice [117,118,119], but seed diode lasers are vulnerable due to damages from back reflection of the amplified signal, heating and electronic disruption. In this regard, Q-switched fiber lasers as oscillators are rugged and compatible with all-fiber amplifier configuration. All-fiber Q-switched Yb-doped fiber lasers have been recently used as an oscillator for generation of high energy pulses [120, 121]. Although acousto-optic (AO) Q-switched fiber lasers are preferable for the generation of high energy pulses, the achievable minimum pulse duration is limited by the cavity round-trip time. As a rule of thumb, minimum pulse width achieved is always greater than or equal to the cavity round-trip time of the fiber laser in the conventional AO Q-switching process [4]. There are a few reports on Er-doped fiber laser in which pulses shorter than the cavity round-trip time have been generated [122,123]. In these reported works, symmetric experimental set-up has been designed such that AOM is kept at the center and gain fiber is spliced at both of its ends. Secondary pulses were generated, which were then suppressed by applying special modulation signal to AOM, which is a complex scheme [122]. In Yb-doped fiber lasers, shorter pulses of a few nanosecond duration have also been generated irrespective of length of the cavity by stimulated Brillouin scattering (SBS) based Q-switching [124,125], but the pulses generated using SBS Q-switching have large temporal and amplitude variations making it rather unsuitable for various applications.

A lot of work has also been reported on the study of AO Q-switched pulse shapes, multiple pulsing, multi-peak pulses and mode-locked resembling pulses [126] in the normal Q-switching regime in which the Q-switched pulses appear during the modulation signal ON-time of the AOM. In the normal Q-switching regime with AOM, the pulse duration depends on the cavity life time, pump power, and repetition rate of the modulation signal.

In this chapter, we report for the first time, to the best of our knowledge, generation of sub-cavity round-trip time pulses seems to be appearing after the modulation window ON-time of AOM (anomalous pulses). The experimental results show that the anomalous pulses actually are generated at the falling edge of modulation off time of AOM. The studies of generation of anomalous pulses have been performed in four different experimental configurations (see Fig. 5.1) depending upon the position of AOM and pumping configuration. In two similar setups with higher cavity loss in which the AOM is placed near the 100% FBG, the pulse duration of anomalous pulses are in the range of 50-55 ns. For the other two setups with lower cavity loss obtained by placing AOM near the 10% output coupler FBG, the pulse durations are in the range of 80-85 ns. The anomalous pulses are more than ~24 times shorter than the normal pulses obtained with conventional Q-switching at the same value of the pump power. Maximum average power of 12 mW with ~55 ns pulse duration has been obtained in one of the experimental setups. These anomalous pulses have been amplified in the pre-amplifier stage to reach the average power level of more than 3.4 W. Since the amplitude of amplified spontaneous emission (ASE) was large at 3.4 W output of the pre-amplifier stage, output power from pre-amplifier stage was set at the level of ~500 mW and amplified in the power amplifier stage to achieve ~19 W of average output power at 80 kHz of repetition rate with slope efficiency of 29% at an input pump power of 60 W.

5.2 Experimental Details

The schematics of four all-fiber Yb-doped Q-switched fiber laser (QYFL) setups are shown in figures 5.1(a)-5.1(d). Generation of short pulses have been studied in four different configurations with respect to the position of the AOM, fiber Bragg grating (FBG) mirrors, pump direction and Yb-doped fiber. Yb-doped double-clad fiber of length ~9 m with product number SM-YDF-5/130-VIII, having a core/cladding diameter of 5/125 μm and clad-pump absorption of 1.7 dB/m at 975 nm acts as the gain medium. This length has been used for the efficient pump absorption in gain medium. For all the four experiments same length of the fiber has been used. If the length of the fiber is changed, it will change the output signal power, and characteristics of normal AO Q-switched pulses will also change due to change in round-trip time. For the case of anomalous pulses, as the pulse duration is independent of the cavity round-trip time, change in the gain fiber length will only change the output signal power.

Yb-doped fiber is pumped using 10 W of fiber coupled laser diode (LD) at 975 nm through a (2+1) x1 pump to signal combiner (PSC). The PSC has a signal port and a common port which are compatible with YDF and two pump input ports having core/clad diameters of 100/125 μm, which are compatible with the pump laser diode. The two fiber Bragg grating (FBG) mirrors FBG1 and FBG2, which are inscribed in the core of the double-clad fiber with 10/130μm core/clad diameter, form the laser resonator. FBG1 is highly reflecting with 99.6% reflectivity and full width half maximum (FWHM) reflection linewidth of 0.2 nm at the central wavelength of 1064 nm, while FBG2 is 10% reflecting at the same wavelength and has FWHM linewidth of 2 nm and it acts as the output coupler (OC).

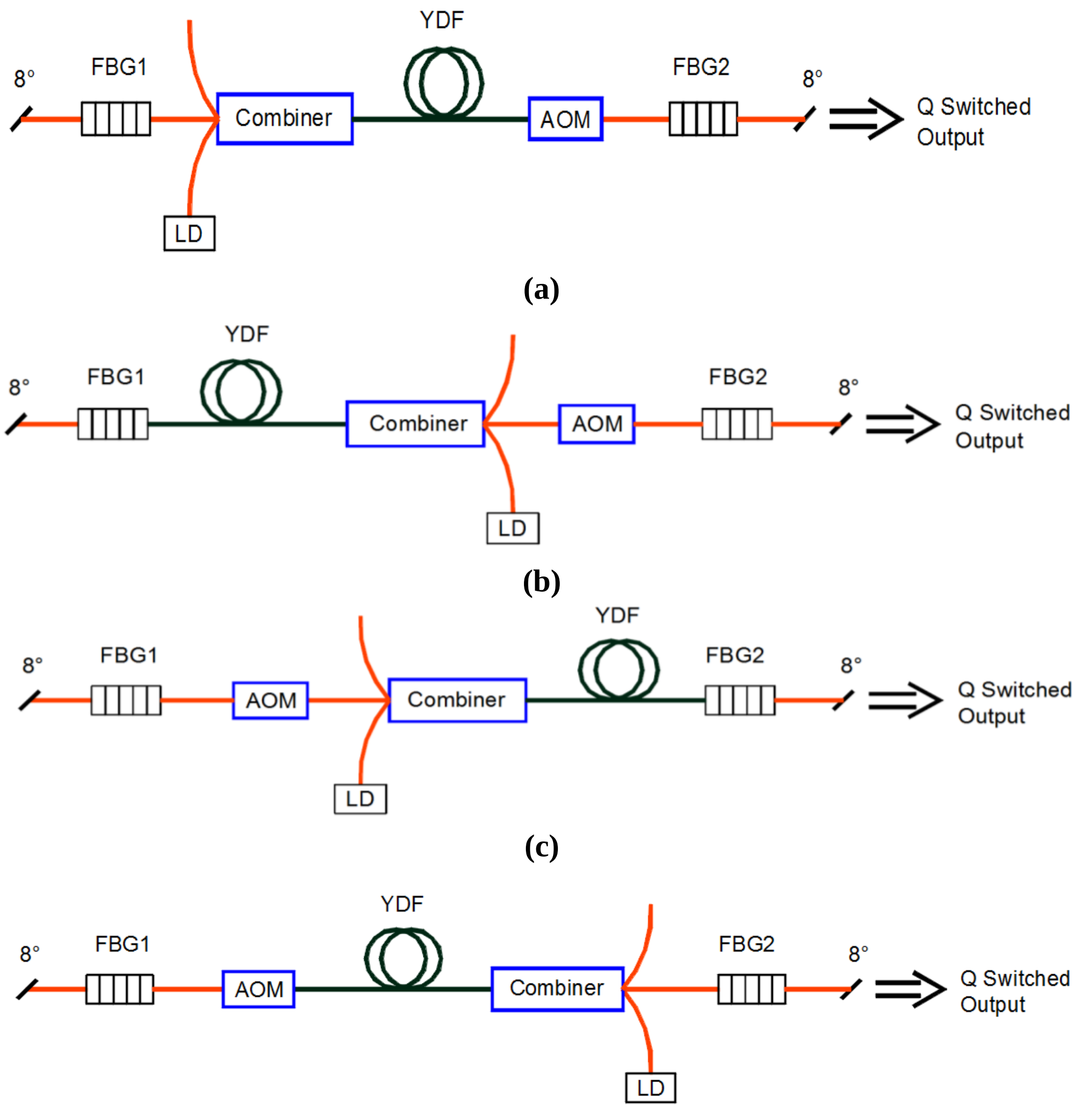

Fig. 5.1: *Experimental configurations for the study of anomalous pulse generation in (a) forward pumping configuration and AOM is placed just before the output coupler FBG2 (10%), (b) backward pumping configuration and AOM is placed just before the output coupler FBG2 (10%),*

(c) forward pumping configuration and AOM is placed just after the 100% FBG1, and (d) backward pumping configuration and AOM is placed just after the 100% FBG1.

The free ends of both the FBG's are angle cleaved to avoid Fresnel's reflection. The two pumping configurations discussed are forward pumping configuration (FPC) and backward pumping configurations (BPC). FPC and BPC are decided by the pumping direction and the relative direction of the signal output. In the forward pumping configuration, the signal beam and the pump beam both propagate in the same direction. In this case, the leakage pump has to be separated from the signal. Figures 5.1(a) and 5.1(c) are in FPC in which pump and signal both are co-propagating. In these two experimental configurations (figures 5.1(a) and 5.1(c)), the leakage pump from the YDF was stripped off after FBG2 by using a high index coating in a length of about 50 mm and heat sink was also provided in this region. However, in the backward pumping configuration (figures 5.1(b) and 5.1(d)), the pump beam and the signal beam both propagate in the opposite direction and hence are counter-propagating. There is no leakage of pump in the direction of signal output and only signal power is ejected. Figures 5.1(b) and 5.1(d) are in BPC in which pump and signal are counter-propagating to each other. In figures 5.1(a) & 5.1(b), AOM is kept near the output coupler FBG (FBG2), whereas in figures 5.1(c) & 5.1(d), AOM is placed near the 100% FBG (FBG1). The all-fiber AOM with fiber pigtails of HI1060 was operated at radio frequency (RF) of 100 MHz and can be modulated in the frequency range of 1 - 100 kHz.

The pulses from these oscillators can be further amplified in the pre-amplifier and power amplifier stages as shown in Fig. 5.2. Output from one of the above oscillator is first amplified in the pre-amplifier stage, which is isolated by means of fiber optic isolator at 1064 nm. In the pre-amplifier stage, isolator is spliced with the signal input port of the pump combiner. Two pump laser diodes of 10 W at 975 nm are spliced with the two pump ports of the pump combiner and the output of the PSC (pump to signal combiner) is spliced with the YDF with product number of LMA-YDF-10/130-VIII, having core/clad diameter of 10/130 µm. The pump clad absorption of the YDF in pre-amplifier is 4.5 dB/m at 975 nm and 2.5 m length has been chosen for sufficient pump absorption.

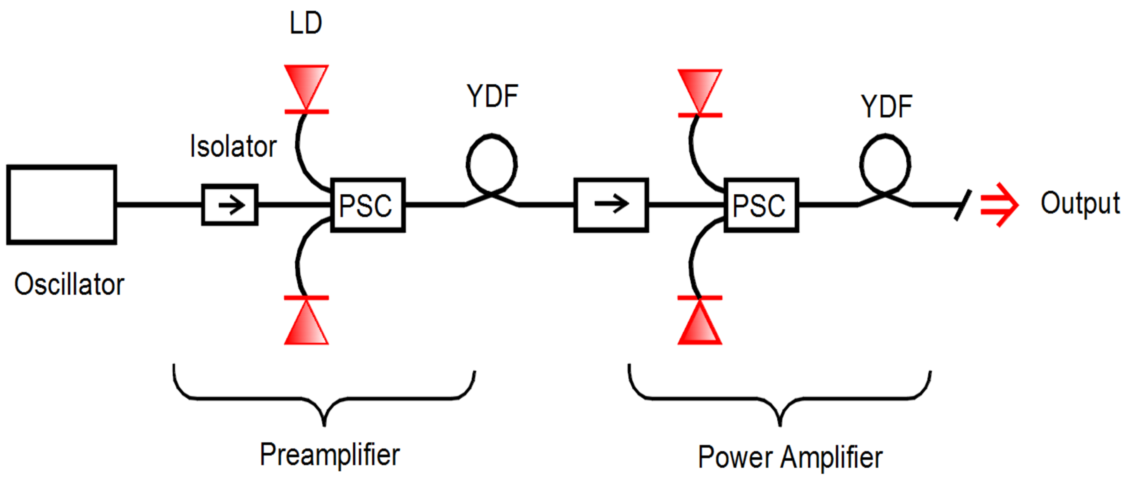

Fig. 5.2: *Experimental configuration with oscillator, pre-amplifier and power amplifier. Oscillator, pre-amplifier and power amplifier are separated from each other by fiber optic isolator at 1064 nm to prevent the signal from travelling in the backward direction towards the oscillator.*

The output end of the gain medium in the pre-amplifier stage is spliced to the second isolator before the power amplifier stage. In the power amplifier stage, the gain medium is similar to the pre-amplifier stage with the product code of LMA-YDF-10/130-VIII and length of 2.5 m. For the pump source two laser diodes at 975 nm with total output power of 70 W are spliced with the two pump ports of the PSC. Output end of the Yb-doped fiber in the final stage is angled to avoid any feedback in the backward direction. The output is diffraction limited as the Yb-doped fiber is pure single mode double clad fiber. Leakage pump is separated by using dichroic mirror with high transmission for the signal and high reflection for the pump at 45° angle of incidence.

5.3 Results & Discussion

This section provides details of experimental results and discussion about the results. It contains three subsections, which provide results of anomalous pulse generation in different cavity configurations, delay in appearance of anomalous pulses, and amplification of anomalous pulses.

5.3.1 Generation of anomalous pulses in different cavity configuration of Yb-doped fiber laser

In normal mode of Q-switching operation with AOM operated in the frequency range of 20-80 kHz, the pulse duration obtained is in the range of 350 ns to 2 μs. The pulses are generated during the modulation window ON-time of AOM and typical build-up time observed are 1.5 μs to 5 μs.

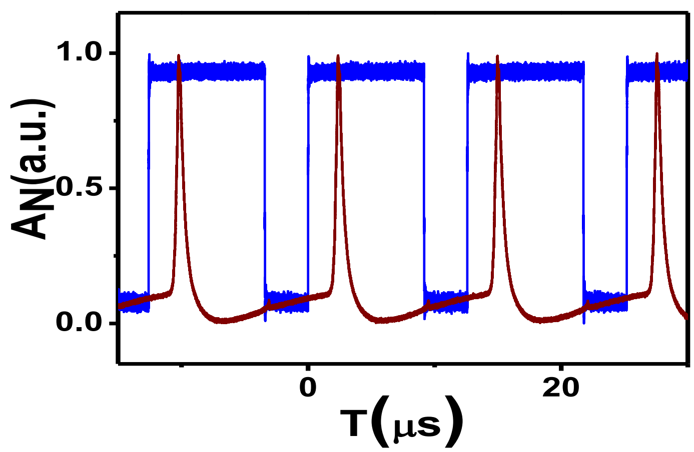

Fig. 5.3: *Train of AO Q-switched pulses of duration ~600 ns with pulse energy of 0.94 μJ. Rectangular pulse indicates the modulation ON-time of AOM and the Q-switched pulses appear within ON-time of AOM.*

Figure 5.3 shows the train of AO Q-switched pulses at 80 kHz repetition rate with the pulse duration of 600 ns and average power of ~75 mW at 4 W of input pump power. In normal Q-switching operation, single pulse could not be obtained below 20 kHz of modulation frequency of AOM. This is due to the fact that at lower modulation frequencies, when the modulation window ON-time is kept long multiple pulses get generated due to continuous pumping and slow Q-switching, and when the modulation window ON-time is reduced to obtain a single Q-switched pulse, peak power is enhanced to a level above the stimulated Raman scattering (SRS) threshold and leads to SRS signal and unstable pulses in the output. Above 80 kHz of modulation frequency, the pulse energy and average power was not enough for the generation of anomalous pulses. Thus, studies were carried out in the modulation frequency range of 20 kHz-80 kHz of AOM.

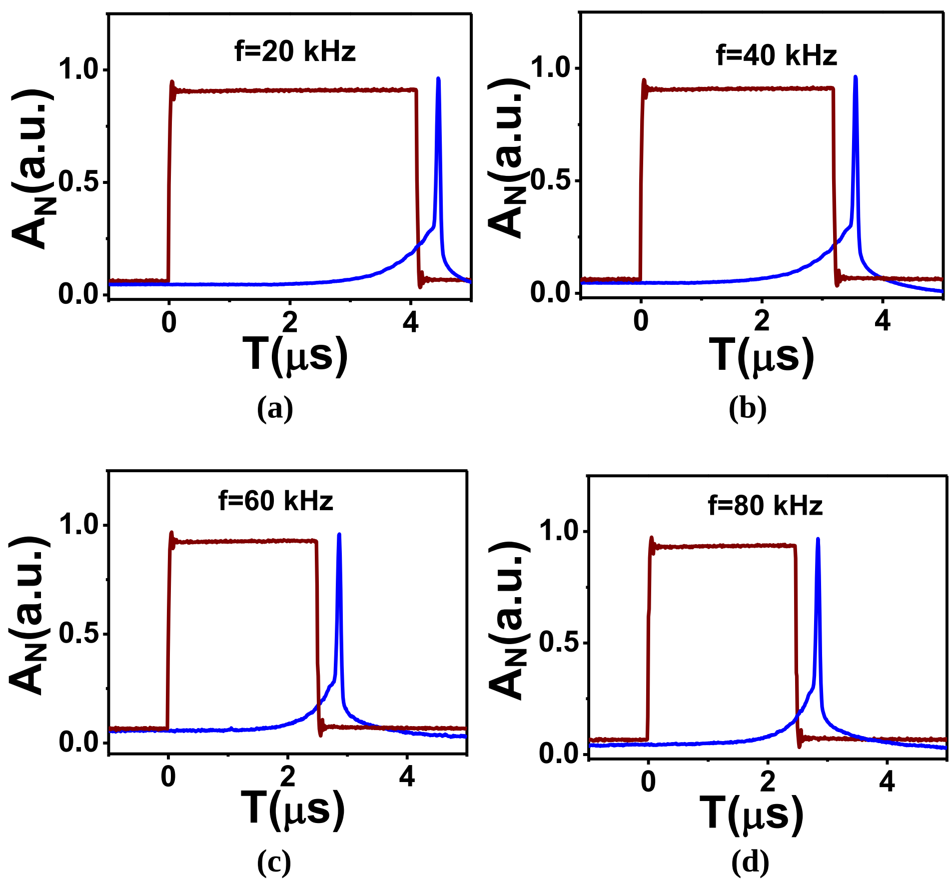

Fig. 5.4: *Anomalous pulses with pulse-width of ~80 ns generated from the experimental setup 5.1(a) at various repetition rates of (a) 20 kHz, (b) 40 kHz, (c) 60 kHz, and (d) 80 kHz. (A_N is normalized amplitude, a.u. is arbitrary unit, T is time, rectangular pulse indicates the modulation window ON-time of AOM).*

Figure 5.4 shows the “anomalous” pulses recorded at modulation frequency of AOM in the range from 20 kHz to 80 kHz in the experimental configuration of Fig. 5.1(a) at 1 W of pump power. It is apparent from the figure that at all the modulation frequencies, the “anomalous” pulses appear after the modulation window ON-time of the AOM, in contrast to the conventional Q-switching behavior, where Q-switched pulses appear within modulation window ON-time of the AOM.

These "anomalous" pulses were produced when the ON-time of AOM was reduced to less than the typical pulse build-up time of normal pulses. The pulse duration of the "anomalous" pulses at different modulation frequency ranges from 80-85 ns, which is smaller than the cavity round-trip time of 130 ns. Both the modulation signal of AOM and the pulse shape have been normalized to have a clear pictorial representation of "anomalous" pulses. Results at all the frequencies from 20 kHz to 80 kHz have been summarized in Table 5.1. For the fixed experimental configuration and pump power, as the operating frequency of the AOM is changed, the build-up time of the Q-switched pulses will be different and hence the modulation window ON-time has to be adjusted accordingly for the formation of Q-switched pulses. As the anomalous pulses are produced when the modulation window ON-time of the AOM is just close to the build-up time of the normal AO Q-switched pulses, thus modulation window ON-time of AOM will vary with the frequency of operation. Although pulses have appeared in the OFF-time of AOM, however, it may be noted that in principle it is not possible to generate the pulses in OFF-time of the AOM, since during OFF-time, AOM is not aligned with the cavity axis. The clarification on this point is discussed in Section 5.3.2.

Table 5.1*: Results for the experimental configuration of figure 5.1(a)*

Sr. No.	Frequency (kHz)	Average power (mW)	Pulse energy (nJ)	Pulse duration (ns)	Delay of the short pulse from falling edge of the modulation signal (ns)
1.	20	0.34	17	81	372
2.	40	0.58	14.5	81	370
3.	60	0.83	13.8	80	373
4.	80	1.05	13.1	80	375

Table 5.1 shows that the pulse energy is maximum at 20 kHz and at 80 kHz average power is maximum. It was also observed that the delay of the “anomalous” pulses from the falling edge of the modulation signal is in the range of 370-375 ns. To understand the underlying reason behind the appearance of pulses beyond the ON-time of AOM and fixed delay of the anomalous pulses three more experimental configurations were investigated.

Figure 5.1(b) represents the schematic of the second experimental configuration in which the position of YDF was changed such that the whole setup is in backward pumping configuration. The position of the AOM with respect to the output coupler FBG (FBG2) remained same and the other end is spliced to the signal port of the pump combiner. It was observed that the delay of the anomalous pulses from the falling edge of the modulation signal (370-375 ns) and the pulse duration (80-85 ns) was similar to that observed in Fig. 5.1(a) configuration. This may be attributed to the fact that the delay of the anomalous pulses and pulse duration depends upon the position of the AOM with respect to the output coupler FBG (FBG2) which is same in both the experimental setups (Fig. 5.1(a) & Fig. 5.1(b)). In figure 5.1(a), the signal is taken from the end of the fiber where population inversion is small due to the exponential decay of the pump signal along the length of the fiber. Whereas, in Fig. 5.1(b), the output signal is taken out from the direction where population inversion is large [60, 54]. Hence, the pulse energy and the peak power of the anomalous pulses from Fig. 5.1(b) are slightly more than the results of experimental setup from Fig. 5.1(a), at the same value of the pump power.

In the experimental configurations of Fig. 5.1(c) & 5.1(d), the position of the AOM was changed from the previous two setups (Fig. 5.1(a) & Fig. 5.1(b)) and positioned near the 100% FBG mirror (FBG1), Fig. 5.1(c) corresponds to forward pumping configuration and other setup in

Fig. 5.1(d) corresponds to backward pumping configuration, respectively. Figure 5.5 summarizes the generation of anomalous pulses from experimental configuration of Fig. 5.1(d) from frequency 20 kHz to 80 kHz at pump power of 2 W. Table 5.2 represents the result of Fig. 5.1(d) in detail. It was noted that the delay of the anomalous pulses in the experimental configurations is in the range of 450-455 ns for all modulation frequencies from 20-80 kHz and the output pulse duration is in the range of 50-55 ns. At 20 kHz of modulation frequency of AOM, the average power is minimum, which is 3.8 mW with maximum pulse energy of 190 nJ, and at 80 kHz, the average power is maximum with the value of 12 mW and pulse energy of 150 nJ. For higher value of pump power, we could not achieve stable anomalous pulses for the whole range of modulation frequency.

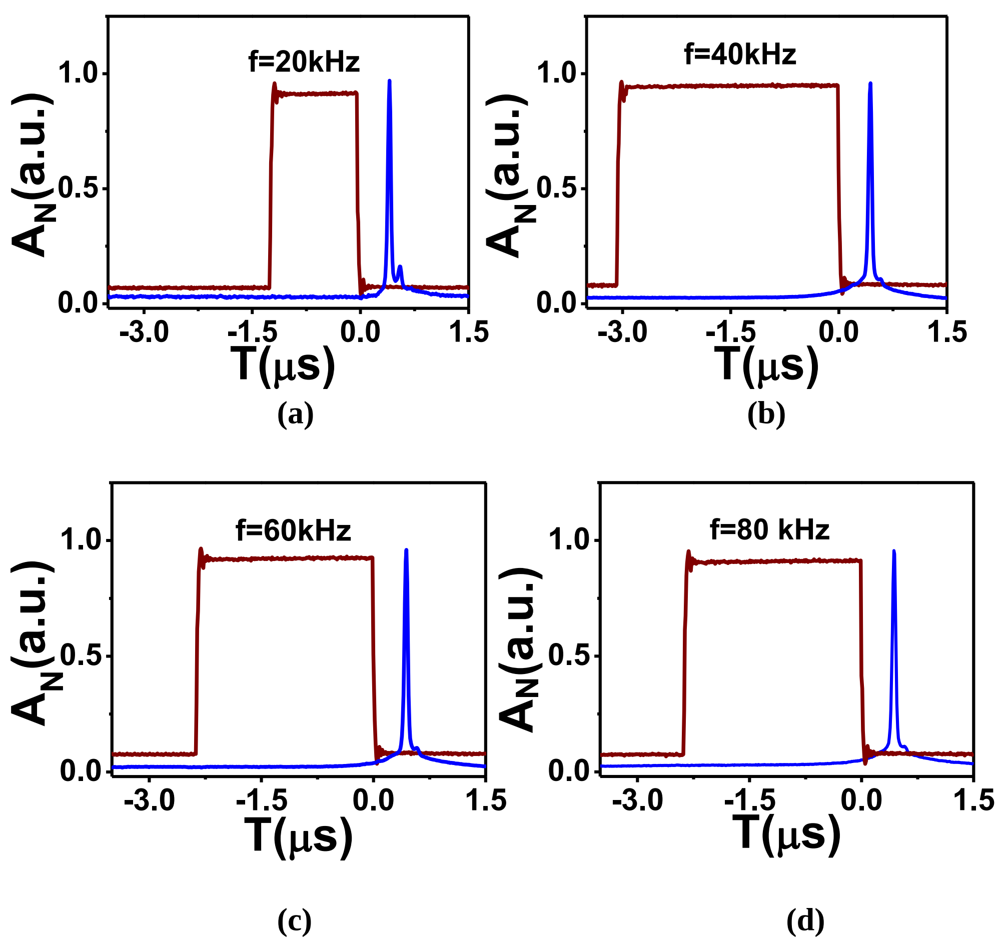

Fig. 5.5: *Anomalous pulses with pulse duration in the range of ~50-55 ns generated from experimental setup 5.1(d) at various repetition rates of (a) 20 kHz, (b) 40 kHz, (c) 60 kHz, and (d) 80 kHz.(Rectangular pulse indicates the modulation ON-time of AOM).*

For 80 kHz of modulation frequency, stable pulses were possible even at pump power of 4 W, but at lower values of frequency as the created population inversion is high, while decreasing the modulation window ON-time of AOM, unstable pulses were generated instead of the anomalous pulses. The pulse duration and delay of the anomalous pulses from the falling edge of the modulating signal in the experimental setup of Fig. 5.1 (a) & 5.1(b) are ~80-85 ns and ~370-375 ns, respectively irrespective of the different pumping configurations (FPC and BPC). Similarly, in the experimental setup of figures 5.1(c) and 5.1(d), the pulse duration of anomalous pulses are in the range of ~50-55 ns and the delay of the anomalous pulses from the falling edge of the modulating signal is ~450-455 ns, which is greater than the previous observed delay of ~370 ns at modulation frequencies from 20 kHz to 80 kHz.

In the configurations of figures 5.1(a) & 5.1(b), AOM is positioned near 10% FBG (FBG2), and in figures 5.1(c) & 5.1(d), the AOM is near 100% FBG (FBG1). In figures 5.1(a) and 5.1(b), when AOM is in OFF-state, then the cavity may be formed between 100% FBG and scattered signal (low feedback) from the AOM. Whereas, in figures 5.1(c) and 5.1(d), the cavity is formed between 10% FBG and low feedback from AOM. In principle, during AOM OFF-state, it is expected that population inversion will build-up and ideally the cavity will have 100% loss and no photon flux will build-up.

Table 5.2*: Results of experimental configuration of Fig. 5.1(d).*

S.No.	Frequency (kHz)	Average power (mW)	Pulse energy (nJ)	Pulse duration (ns)	Delay of the pulses from falling edge of the modulation signal (ns)
1.	20	3.8	190	51	452
2.	40	7.2	180	51	450
3.	60	9.4	157	52	455
4.	80	12	150	55	454

The output pulse energy will be proportional to the population inversion. However, the formation of resonator cavity (FBG and low feedback from AOM) during AOM OFF-state, will reduce the magnitude of population inversion. In figures 5.1(c) and 5.1(d), during AOM OFF-state, the photon flux build-up will be relatively smaller and hence the population inversion build-up will be large resulting in higher output power in these cases. Hence, pulses with higher average power and shorter pulse duration of ~50-55 ns are generated from the experimental configurations of figures 5.1(c) &5.1(d).

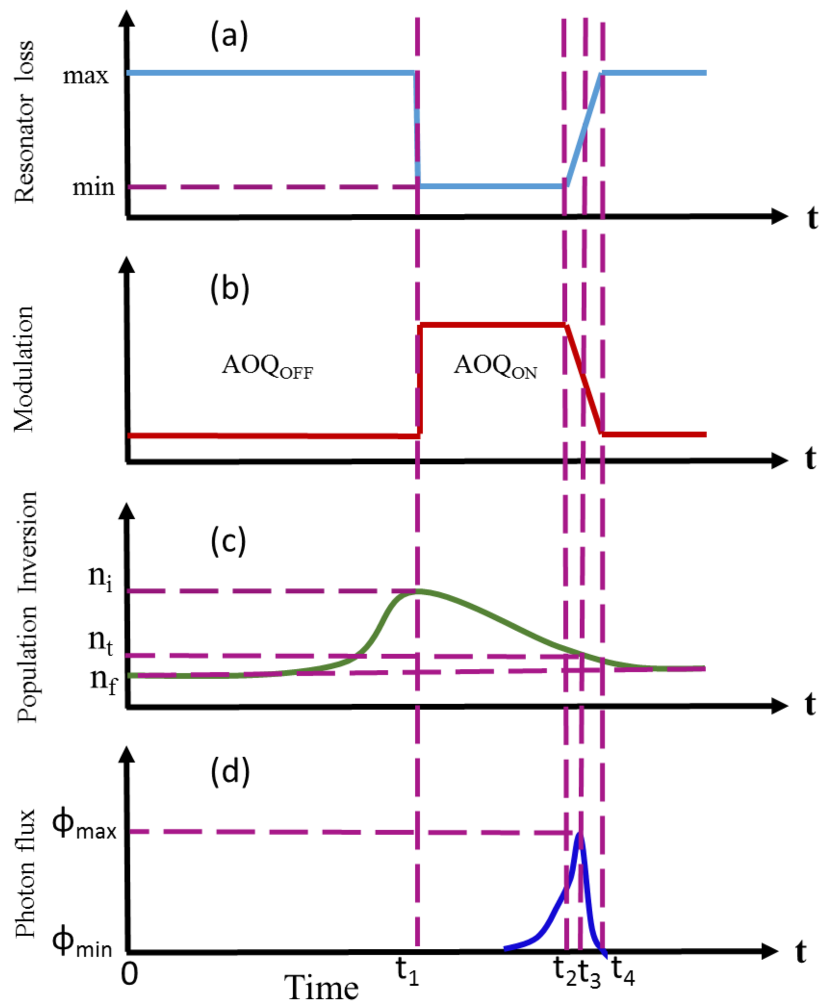

Fig. 5.6: *Qualitative representation of generation of anomalous pulses. (a) Resonator loss vs time, (b) Modulation signal showing AOQ-switch OFF and ON time, (c) variation of population inversion with time, and (d) formation of anomalous pulse in the falling time of AOQ-switch.*

The anomalous pulses are generated at the falling edge of the modulation window ON-time of AOM which will be described experimentally in section 5.3.2. Its generation is related with the fall time of the AOM and build-up time of the normal AO Q-switched pulses. For the generation of anomalous pulses, modulation window ON-time of AOM is kept just smaller than the pulse build-up time of the normal AO Q-switched pulses. The generation of anomalous pulses is shown qualitatively in Fig. 5.6. From 0 to t_1 time AO Q-switch is OFF and the population inversion build-up takes place. At time t_1, AO Q-switch is switched ON and the loss decreases from maximum value to the minimum value. There is a finite rise time of AO Q-switch from OFF state to the ON state, but as it doesn't contribute to the generation of anomalous pulses, it is not shown in the diagram. Photon flux starts building up inside the cavity during the AO Q-switch ON time, however small it may be and depletes the population inversion from the maximum value n_i. At time t_2, AO Q-switch is switched off and it has a finite fall time from t_2 to t_4. During fall time of AO Q-switch, loss inside the cavity starts increasing. During t_2 to t_3 time, since population inversion is greater than the threshold population inversion, photon flux continues building up, till the gain is higher than total loss inside the cavity. The rise time of the anomalous pulses depends on the population inversion created. At point t_3, population inversion is equal to the threshold population inversion and peak of the anomalous pulse is formed. At this point, total loss is equal to the gain inside the cavity. From t_3 to t_4 the loss is greater than the gain in the cavity and pulse decays and it follows the fall time of the AO Q-switch. In the case of normal AO Q-switched pulses, it is the photon flux build-up inside the cavity which depletes the gain by reducing the population inversion below the threshold value and the falling edge of the pulse is decided by the cavity life time and it is large as compared to the rise time of the pulse. Whereas, in the case of anomalous pulses, the pulse generation is determined by the loss created by the switching of AOM from ON-state to OFF-state. Hence, the pulse duration of the anomalous pulses is decided by the switching time or fall time of the AOM. The variation in the pulse duration for the experimental configuration of figures 5.1(a) and 5.1(b), which is in the range of 80-85 ns, and for figures 5.1(c) and 5.1(d), which is in the range of 50-55 ns, is decided by the rise time of the anomalous pulses which in turn depends on the population inversion before the AOM is switched ON. For higher population inversion, it is expected that rise time of the pulses would be small. Since, for figures

5.1(c) and 5.1(d), population inversion achieved is higher, hence the rise time for anomalous pulses is small and hence shorter pulses are achieved.

Figures 5.7 (a)-(c) show the experimental evolution of anomalous pulse from the normal AO Q-switched pulse at modulation frequency of 40 kHz in the experimental configuration of 5.1(d). Figure 5.6(a) represents normal AO Q-switched pulse with the pulse duration of ~500 ns, when the modulation window ON-time of the AOM is ~10 μs.

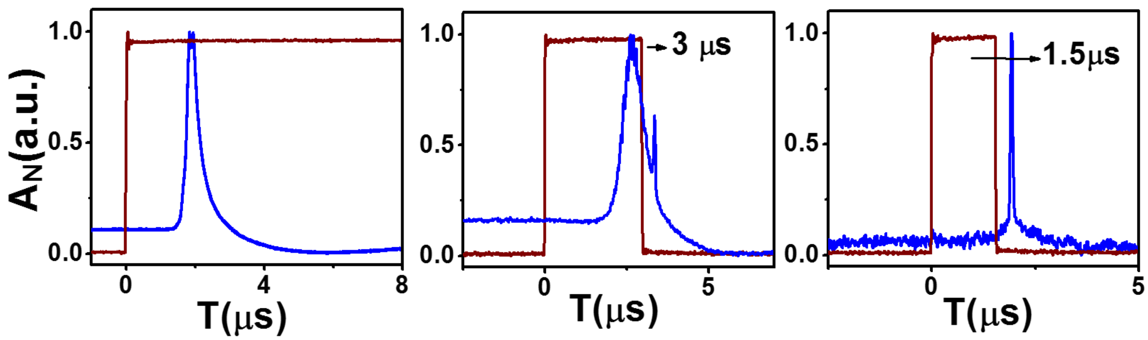

Fig. 5.7: *Evolution of anomalous pulses from normal AO Q-switched pulse, (a) normal AO Q-switched pulse (~500 ns), (b) pulse with a low peak appearing at the edge of modulation signal, and (c) anomalous pulse with pulse duration of ~55 ns.*

As the modulation window ON-time of the AOM was decreased slowly, initially the pulse was stable, with further decrease, low peak power pulse appears during the falling time of the normal AO Q-switched pulse and near the falling edge of the modulation signal of the AOM, as shown in Figure 5.6(b). At the peak of the normal AO Q-switched pulse, the photon flux is maximum and the population inversion corresponds to the threshold inversion for the normal lasing operation. During the fall time of the pulse, population inversion decreases below the threshold inversion value. When AOM is switched OFF, it induces extra loss in the cavity and this happens just after the formation of peak of the normal AO Q-switched pulse.

At this point, it may be noted that the population inversion is just below the threshold inversion. Due to the continuous pumping by pump laser diode, population inversion build-up takes place during the fall time of AOM, and it may cross the threshold inversion value. As the population inversion is more than the threshold inversion value, how so ever small it may be, pulse formation takes place. Hence, low peak power pulse appears near the falling edge of modulation signal of AOM. Further decrease in the modulation window ON-time makes the Q-switching process chaotic with unstable pulse train. By the slight adjustment of pump power and modulation window ON-time of the AOM, stable anomalous pulses of shorter pulse duration are generated during modulation window OFF-time, as shown in the figure 5.7(c).

5.3.2 Delay of anomalous pulses from falling edge of the modulation signal

The delay in the anomalous pulses from the falling edge of the modulating signal of the AOM can be explained using figure 5.7. When the modulating signal is applied to AOM, to either switch-ON or switch-off the AO Q-switch, finite time is required for the acoustic waves to travel from the front edge of the Q-switch crystal to its center. The delay in the anomalous pulses from the falling edge of the modulating signal of the AOM can be explained using figure 5.7. When the modulating signal is applied to AOM, to either switch-ON or switch-off the AO Q-switch, finite time is required for the acoustic waves to travel from the front edge of the Q-switch crystal to its center.

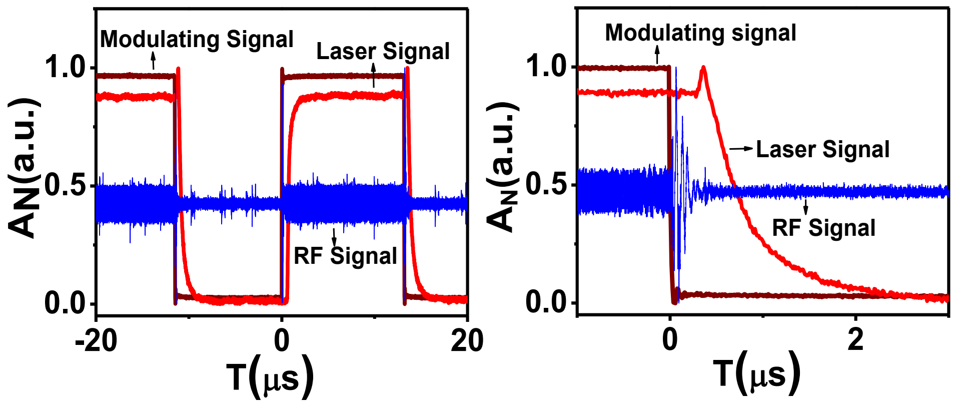

(a) **(b)**

Fig.5.8: *(a) Measured traces of modulating signal, modulated RF signal and transmission response of AOM to the CW laser signal, (b) expanded view of (a) showing delay of transmission response of AOM and the modulating signal to the CW laser beam fed into the AOM.*

Diffraction of the CW laser beam by the Q-switch crystal will take place after the acoustic wave reaches its center. This travel time of the acoustic wave from edge to the center of the crystal causes delay between the applied modulating signal and diffraction of the CW laser beam. Delay time depends upon the length of the Q-switch crystal and velocity of the shear acoustic waves in the medium. To measure this delay, CW laser beam was passed through the AOM, and RF waves, modulating signal and diffracted beam were recorded simultaneously as shown in figure 5.8. The measured delay of peak of the laser signal is ~ 350 ns from falling edge of the modulating signal. In the generation of the anomalous pulses, the additional delay is also added due to the length of the cavity from the AOM to the output coupler which corresponds to the travel time of the pulses from AOM to the output coupler. In principle, the pulses are generated at the falling edge of modulating signal. Delay (T) in the output pulse from falling edge of the modulation signal is given by,

$$T = \frac{n_g l}{c} + 350ns \tag{5.1}$$

where, l is the length of the cavity from AOM to the output coupler, n_g is the refractive index of the silica fiber and c is the speed of light in vacuum. In the experimental configurations of figure 5.1(a) and 5.1(b), the delay is ~370 ns, which is due to the additional ~4 m length of the fiber from AOM to the OC (figure 5.9(a)) in addition to 350 ns. In the experimental configurations of figure 5.1(c) and 5.1(d), the delay is ~450 ns (figure 5.8(b)), which corresponds to the additional ~10 m length of the Yb-doped fiber from AOM to the OC.

To further confirm that the pulse-duration is independent of the cavity round-trip time, 20 m of extra passive fiber length was spliced with the YDF in the experimental configuration of figure 5.1(d). Pulse-duration of anomalous pulses remained same with value of ~55 ns, but the delay of the pulse from the falling edge of the modulating signal increased from 440 ns to 550 ns (figure 5.9(c)), which corresponds to additional travel time of 20 m length of the passive fiber. Losses in the single mode passive fiber at 1064 nm is very less (< 1 dB/km), thus the addition of extra passive fiber will not contribute to the substantial amount of loss inside the cavity. For the normal AO Q-switched pulses, addition of extra passive length of the fiber will contribute to change in its pulse duration as the pulse duration depends upon the round-trip time of the cavity. But, for the anomalous pulses, the pulse duration is independent of the cavity round-trip time and is only dependent on the AOM fall time and position of the AOM inside the cavity, which doesn't change in adding 20 m of extra passive fiber length and hence there is no change in the pulse duration of the anomalous pulses.

Thus for a given configuration, the delay between output pulse from falling edge of modulation signal is constant and is independent of modulation frequency. The above results indicate that actually the short Q-switched output pulse is generated at the falling edge of the modulation signal in figures 5.4(a-d) and 5.5(a-d).

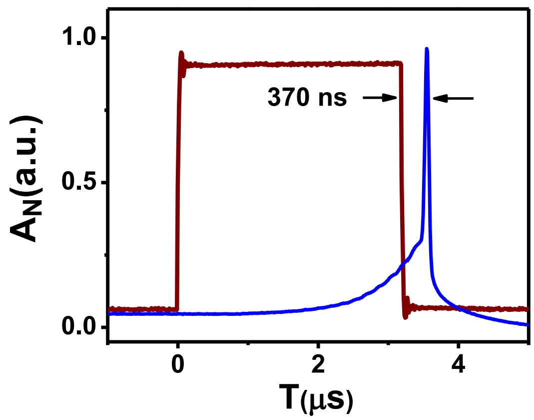

(a)

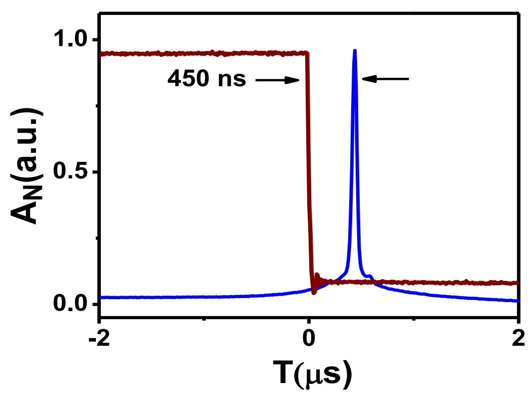

(b)

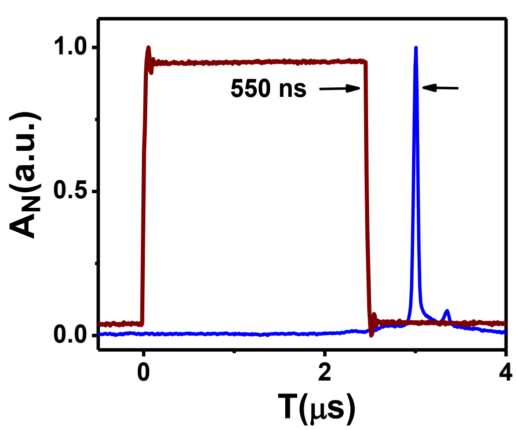

(c)

Fig.5.9: *Measured delay of anomalous pulses from the falling edge of the modulating signal of AOM in different experimental setups. (a) In experimental setup 5.1(a) in which AOM is positioned just before the output coupler FBG, (b) in experimental setup 5.1(d) in which AOM is positioned*

just after the 100% FBG, (c) in experimental setup 5.1(d) in which YDF is spliced with 20 m length of the passive fiber.

Figure 5.10 shows variation of pulse duration of the AO Q-switched pulses when modulation window ON-time is decreased from 22 μs to 1.4 μs at repetition rate of 20 kHz and pump powers of 1 W and 2 W in the experimental setup of figure 5.1(d).

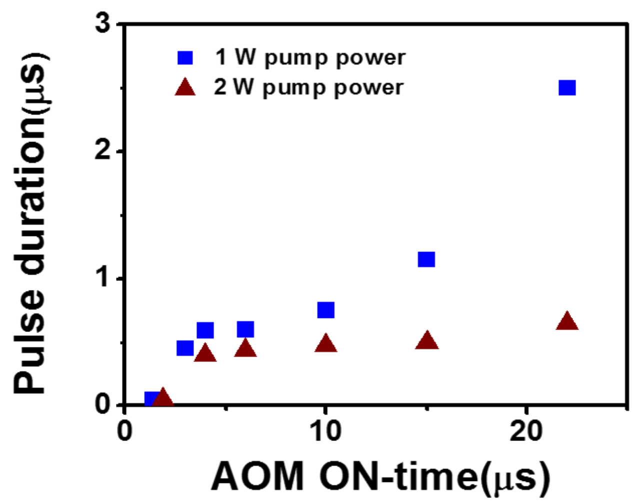

Fig. 5.10: *Variation of output pulse duration with the modulation window ON-time of AOM at 1 W and 2 W of pump power.*

At ~1 W of pump power, duration of the pulses are reduced by the factor of 50 from 2.5 μs (normal pulse) to ~51 ns (anomalous pulse) when the modulation window ON-time of the AOM is decreased from 22 μs to 1.4 μs. The minimum build-up time of the pulse is more than 1.4 μs. Thus, when the modulation window ON-time is less than 1.4 μs, no Q-switched pulses are observed. At ~2 W of pump power, reduction in the pulse duration is from ~650 ns to ~51 ns with corresponding reduction in the modulation window ON-time from 22 μs to 1.9 μs. For modulation ON-time between 2 μs to 4 μs region, pulses are unstable and random high peak power pulses are generated. During ~2 to 4 μs region, modulation window ON-time of AOM falls in the range of pulse build-up time of normal AO Q-switched pulses, however, modulation window ON-time is not sufficient for the formation of the normal AOQ pulses. Although, pulse formation starts taking place, but the modulation window ON-time is not enough for the release of full pulse energy. This leads to the generation of high peak power pulses with random frequency and pulse duration. These random pulses with high peak power initiates the generation of nonlinear effects like stimulated Raman scattering (SRS).

5.3.3 Amplification of anomalous pulses

In the experimental configuration of figure 5.1(d), shortest pulses with high average power were recorded. For the amplification, input signal of 12 mW average power with ~55 ns pulse duration at 80 kHz repetition rate from the oscillator was fed to the pre-amplifier. The average signal power was amplified to an output average power of 3.4 W and the pulse energy was enhanced from 125 nJ to 45 μJ. For further enhancement of the average power and pulse energy, 500 mW input signal from the pre-amplifier stage was fed into the power amplifier and was amplified to ~19 W of average output power with the pulse energy of ~240 μJ and peak power of 4.4 kW at ~ 60 W of input pump power. There was no notable variation in the pulse duration after amplification. Figure 5.11 shows the dependence of the output average power of power amplifier on the input pump power at 80 kHz of repetition rate with slope efficiency of ~29%.

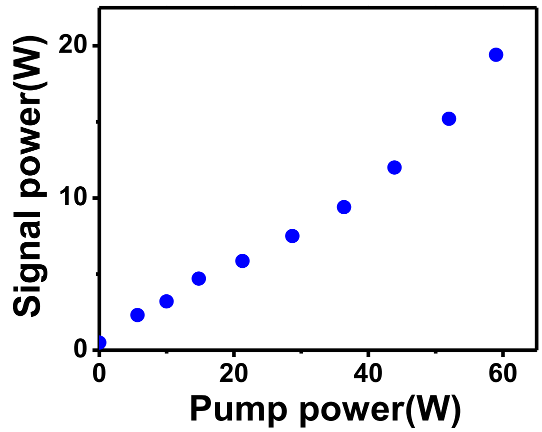

Fig. 5.11: *The variation of output average power of power amplifier as a function of the input pump power at 80 kHz repetition rate. Maximum output average power of ~19 W was achieved with the slope efficiency of 29%.*

For the extraction of pulse energy from the amplifier system, the limitations are imposed by the saturation energy of the doped fiber, nonlinear effects like stimulated Raman scattering (SRS) and amplified spontaneous emission (ASE). The maximum pulse energy which can be extracted from a fiber is ~10 times the saturation energy of the YDF [127]. The saturation energy of the doped fiber is given by [127]

$$E_{sat} = \frac{h\nu_s A}{(\sigma_{es} + \sigma_{as})\Gamma_s} \tag{5.2}$$

where, $h\nu_s$ is the signal photon energy, σ_{es} and σ_{as} are the emission and absorption cross-sections, respectively at the signal wavelength, A is the core area, and Γ_s is the signal overlap factor with active dopant core. The calculated value of saturation energy for 10 µm core diameter fiber used in the power amplifier at 1064 nm is ~55 µJ. Hence the maximum possible extractable energy from the power amplifier is ~550 µJ. Similarly, limitation from SRS generation can be calculated by the threshold signal power for the SRS generation which is given by [26],

$$P_{out}^{SRS} = \frac{16A}{g_R L} \tag{5.3}$$

where, A is the core area and L is the fiber length, g_R is the Raman gain coefficient in silica and is given by, g_R = $1x10^{-13}$ m/W. For our fiber, A = $7.85x10^{-11}$ m^2 and L=2.5 m and hence the SRS threshold value is ~5 kW. The peak power of the amplified anomalous pulses is ~4.4 kW. Hence by further increase in the average output power, pulse energy will increase but, the enhancement in the peak power will cause the SRS generation and pose limit on output energy and stability of pulse train.

Figure 5.12 shows the pulse shapes after the power amplifier stage at highest value of pump power at 80 kHz. There is no distortion in the pulse shape or the temporal duration of the pulses after amplification which signifies absence of saturation effect in the amplified pulse but further amplification is limited by the SRS generation.

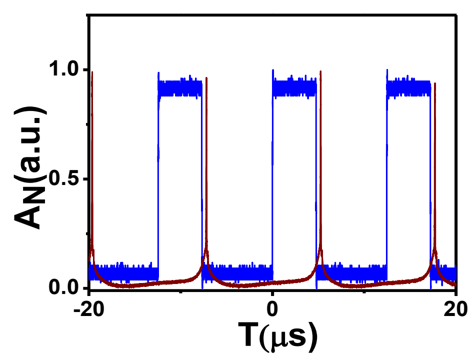

(a)

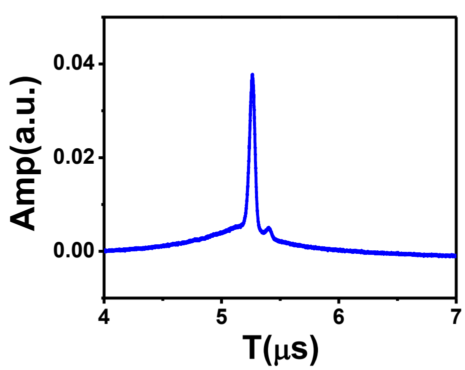

(b)

Fig. 5.12: *(a) Amplified pulse train of anomalous pulses at ~19 W of signal power at repetition rate of 80 kHz. (b) Single amplified anomalous pulse with the pulse duration of ~55 ns.*

Figure 5.13 shows the recorded spectrum of the signal after the oscillator and the power amplifier stage. In the oscillator stage (figure 5.12(a)), the peak is at 1064 nm with FWHM bandwidth of 0.2 nm. Figure 5.12(b) shows the spectrum of the signal at ~19 W of signal power in which ASE is 25 dB down from the peak of the signal and hence the contribution of ASE can be ignored. SRS signal is not observed even at the highest value of the signal power, which is in accordance with our calculation.

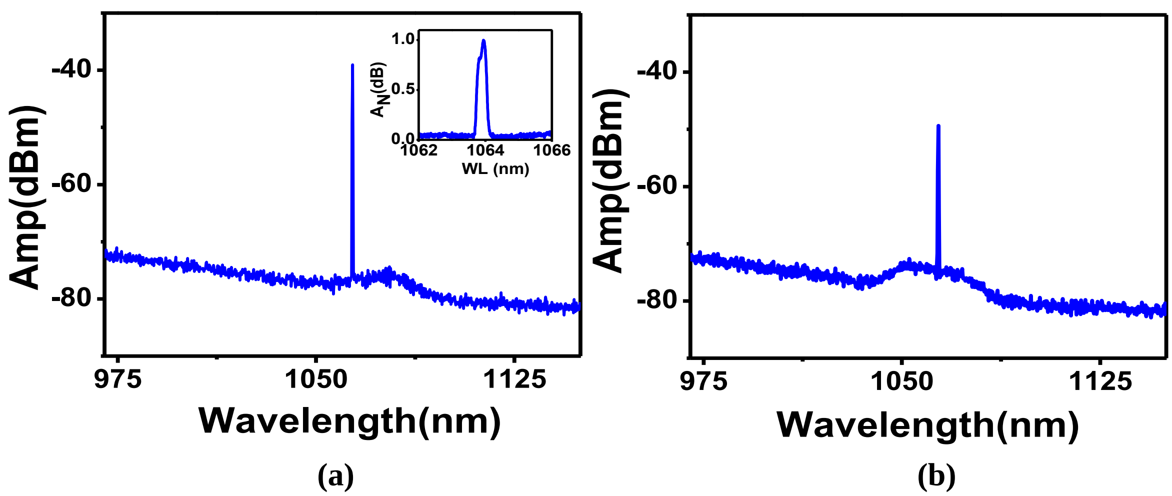

Fig. 5.13: *Spectrum of the signal (a) after oscillator at signal power of 12 mW, and (b) after the power amplifier stage at highest signal power. The signal peak is at 1064 nm with FWHM bandwidth of 0.2 nm.*

5.3.4 Generation and amplification of conventional Q-switched pulses

In this section, we present the development of all-fiber, high average power Yb-doped master oscillator power amplifier seeded by acousto-optic Q-switch fiber laser in conventional Q-switching regime. Laser pulses of duration 600 ns are generated at repetition rate of 80 kHz. Figure 5.14 shows the output average power of the power amplifier as a function of the pump power. The maximum average signal power of 26 W has been achieved with slope efficiency of ~36%. Slope efficiency is low since the input pump power has been taken as the output directly from pigtailed laser diodes. The leakage pump power and the losses in the pump combiner and splice joints has not been taken into account while calculating the slope efficiency. No saturation in the output power was observed even at the highest available input pump power.

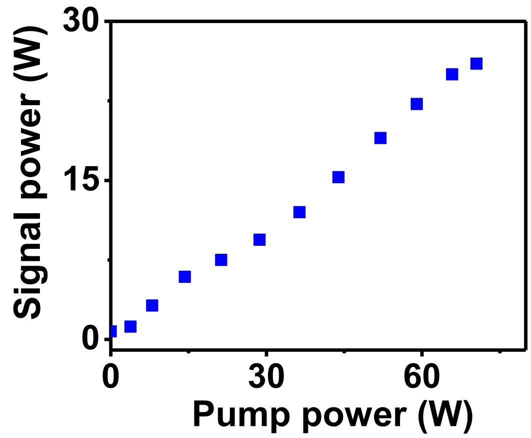

Fig. 5.14: *Output average power of the final amplifier as a function of the input pump power.*

The output power is limited only by the available input pump power. Figure 5.15(a) and (b) show the train of pulses from the power amplifier at 80 kHz of repetition rate and single pulse with pulse duration of ~600 ns, respectively. Pulse energy of ~688 nJ from the oscillator was amplified to ~325 μJ in the final amplifier with the peak power of ~0.5 kW.

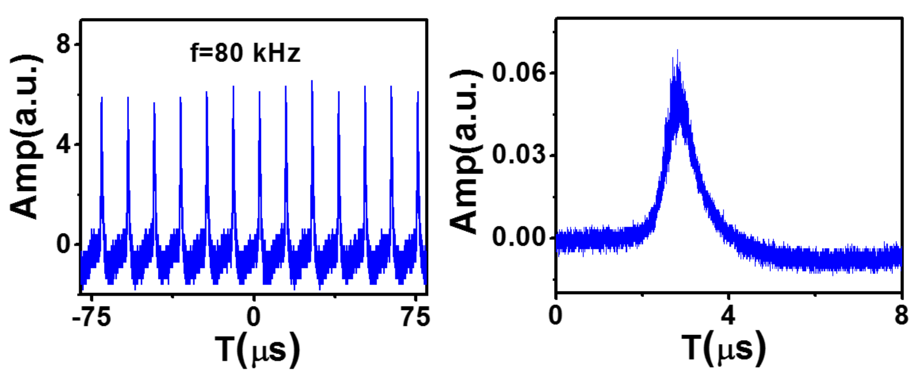

(a) (b)

Fig. 5.15: *(a) Train of pulses from the final amplifier at 80 kHz of repetition rate (T is for time in μs and A is for amplitude in the arbitrary units(a.u.)), and (b) single amplified pulse with ~600 ns pulse duration.*

The calculated saturation energy of 10 μm core diameter YDF is ~55 μJ at 1064 nm and extractable energy can be about ten times the saturation energy. Maximum energy which can be extracted from the fiber is ~550 μJ. Our experimental results are in accordance with the theoretical estimates. These high peak power pulses with near diffraction limited beam quality are suitable for marking application.

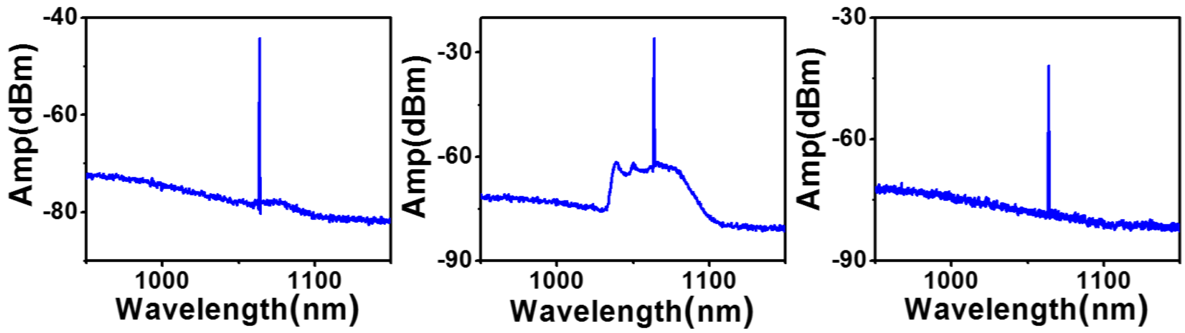

(a) **(b)** **(c)**

Fig. 5.16: *Output spectrum of the (a) Yb-doped Q-switched laser oscillator, (b) pre-amplifier, and (c) final amplifier.*

Figure 5.16(a)-(c) show the output spectrum of the Yb-doped fiber amplifier at different stages of amplification. Figure 5.16(a) shows the spectrum of the laser oscillator at 1064 nm and there is no amplified spontaneous emission (ASE) signal due to the lasing supported by FBG mirrors. Average power of ~55 mW from the oscillator is fed into the pre-amplifier at 1064 nm. Figure 5.16(b) shows the output spectrum from the pre-amplifier at maximum average power of 3.4 W. In the pre-amplifier stage along with the amplified signal at 1064 nm, ASE signal from the YDF also appears due to the low strength of the signal from the oscillator. To reduce the ASE signal in the pre-amplifier stage, output average power from this stage is kept at ~700 mW.

Reduction in the average power from the pre-amplifier reduces the comparative ASE component. In the final amplifier stage, ASE signal nearly disappears at the highest average power of 26 W, and is more than ~40 dB down from the peak of the 1064 nm. As no saturation of signal was recorded, further enhancement of average power is possible.

5.4 Conclusion

In summary, stable sub-cavity round-trip time pulses have been generated in all-fiber Ytterbium-doped Q-switched fiber laser by controlling the modulation window ON-time of acousto-optic modulator (AOM). In different experimental configurations, short pulses of duration in the range of 50-80 ns have been generated in cavity with round-trip time of ~130 ns, when modulation window ON-time of AOM was equal to or shorter than the pulse build-up time of the normal AO Q-switched pulses. The anomalous pulses have sharp trailing edge as compared to the normal AO Q-switched pulses. The anomalous pulses with average power of 12 mW at 80 kHz repetition rate from the AO Q-switched oscillator with pulse duration in the range of 50-55 ns have been amplified to the average power level of ~19 W in the two stage amplifier with single mode output with pulse energy and peak power of 240 µJ and 4.4 kW, respectively. Normal pulses from the oscillator with the repetition rate of 80 kHz, pulse duration of 600 ns and pulse energy of ~688 nJ have also been amplified in single mode Yb-doped all-fiber amplifier to 325 µJ of pulse energy and 0.5 kW of peak power with 26 W of average power. Initial laser marking on metal surfaces have been tried with the developed Yb-doped fiber amplifier and further optimization is underway.

Chapter 6

Amplified Spontaneous Emission and amplification in Yb-doped fiber

6.1 Introduction

Broadband and high power superfluorescent sources have applications as low coherence temporal sources in the areas of medical imaging through optical coherence tomography (OCT), optical coherence radar, rotation sensing and spectroscopy [128-130]. Generally, broadband light sources are obtained from modelocked solid-state lasers like Ti:Al_2O_3 laser [131] and semiconductor superluminescent diodes [132]. Although, modelocked solid-state lasers provide a bandwidth of ~400 nm via supercontinum generation, and output power of tens of mW, but they are bulky and expensive for most of the applications. The other commonly used light source for OCT systems is the superluminescent diodes [128]. It has a bandwidth of about ~80 nm and a few milli-watt output power having a near-Gaussian spectral shape. But, superluminescent diodes are available in the wavelength band of 800 nm range where the scattering losses in the retina becomes significant [128]. Also, low power available from superluminescent diodes is insufficient for other OCT applications like detecting defects. For biological OCT application, the spectral window between 1000 nm -1100 nm has an advantage over 800 nm band because of low absorption and less dispersion in water and hence it allows deeper penetration in retina and other biological tissues [133]. The requirement for achieving high resolution in OCT is a large bandwidth source since the axial image resolution Δz is given by $[2\ln(2)/\pi]\ (\lambda_0^2/\Delta\lambda)]$ where $\Delta\lambda$ is the bandwidth and λ_0 is the central wavelength of the light source [133]. The important factor for OCT is the spectral shape of the output signal, it is desirable to have a smooth spectrum with a near Gaussian spectral profile for low noise in OCT image analysis. Most of the above requirements are met by, low cost optically pumped amplified spontaneous emission (ASE) based Yb-doped fiber sources, and they have emerged as a potential candidate to generate high output power with broad-bandwidth in the 1 μm wavelength range [134, 135]. Large linewidth in Yb-doped fiber source is due to broad fluorescence emission band from ~1010 nm to ~1170 nm [12]. Thus it will be interesting to study the ASE generation in single mode double clad fibers. There are various reports in ASE generation in the amplifier configuration in which power beyond 1 kW has been achieved [19] using large mode area (LMA) fibers having same spectral characteristics in preamplifier and amplifier stage. In all the reported works high power have been achieved in LMA fibers in which the numerical aperture (NA) of the core is less than the typical NA of pure single mode fibers, so feedback suppression and high output ASE power from LMA gain fibers is comparatively easier than in single mode gain fibers. To the best of our knowledge there are no reports of ASE amplification in single mode double clad fibers using fibers with different output spectral characteristics.

In this work, one of the objective of achieving broad ASE FWHM linewidth and ASE of few watts in single mode fibers. Further preliminary experiments were carried out in large mode area fiber to obtain higher ASE power with large linewidth. We have carried out experiments with different pump configuration, fiber length in single mode double clad Yb-doped fibers which is paramount for generating stable, high power and broadband signal output. In single mode fiber with core clad diameter of 10/400 μm, maximum bandwidth of 42 nm have been achieved with 20 mW of signal power. This bandwidth was extended to 75 nm with 32 mW of signal power in the double end pumping configuration with the same type of fiber by using shorter length of the fiber, to avoid the re-absorption effect. This value of signal power is sufficient for OCT applications. The study was extended in amplifier configuration using single mode fibers with different spectral characteristics in the seed part and in the amplifier part. We obtained ASE FWHM linewidth of

~36 nm with 4 W of power. We also carried out our studies with large mode area fibers, in which we obtained 41.8 nm FWHM linewidth with ASE power of 15 W. The study will help in designing low cost source that is useful in OCT measurements.

6.2 Experimental setup

6.2.1 Single end pumping and double end pumping configuration

A schematic of the experimental setup for the study of ASE generation in the single and double-end pumping configuration is shown in Fig. 6.1(a) and 6.1(b), respectively.

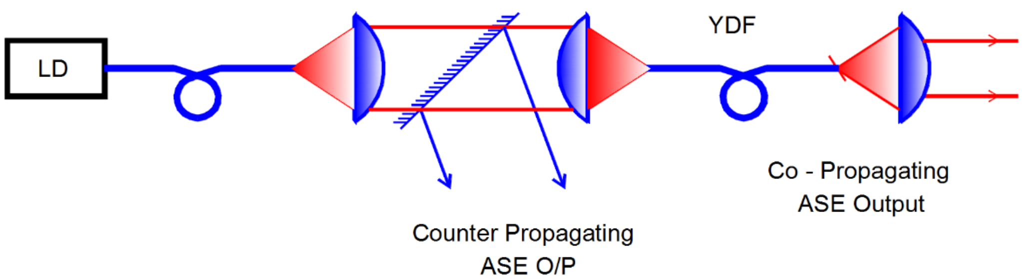

(a)

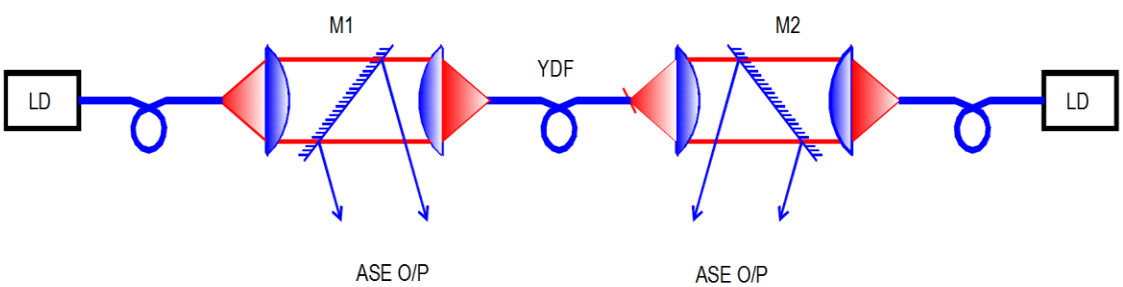

(b)

Fig.6.1: *Experimental setup for Yb-doped fiber superflourescent source in (a) single end pumping configuration and (b) double end pumping configuration.*

It consists of a Yb-doped double clad fiber as a gain medium and pump diode. Yb-doped fibers with different length, core and clad diameter have been used for the study of ASE generation which are tabulated in the Table 6.1

Table 6.1: *List of the Yb-doped fibers used in the experiment*

S.No.	Core /Clad diameter	Pump absorption @975 nm	Lengths used
1.	5/125 μm	1.25 dB/m	9 m
2.	10/130 μm	4.5 dB/m	2.5 m
3.	10/400 μm	0.8 dB/m	4.5 m, 18 m
4.	20/400 μm	1.25 dB/m	5.4 m, 9 m, 13 m

The studies have been performed in single end and double end pumping configuration. In the single end pumping configuration, gain medium is pumped from one end of the fiber and in the double end pumping configuration, gain fiber is pumped from both of its ends. To pump Yb-doped fiber, 20 W and 45 W fiber coupled laser diodes at wavelength of 975 nm with pigtailed core diameter of 200 μm and NA of 0.22 were used as pump sources. The fiber pigtailed diode laser output is collimated and focused using plano-convex lenses to image the pump fiber end on the doped fiber end for the good coupling efficiency. Gain fibers have been angled at 10° to preclude parasitic laser oscillation due to unwanted feedback from fiber end facets which may start the laser oscillations and reduce the laser linewidth. The ASE output is taken from the pump fiber end called as the counter propagating direction as the pump and signal both travel in the opposite direction and when the pump and the signal both travel in the same direction and ASE signal is taken from the other end of the pump direction then it is called as the co-propagating direction as shown in figure 6.1(a). Figure 6.1(b) shows the double end pumping configuration and the concept of co-propagating and counter-propagating doesn't exist. The signal is taken using a dichroic mirrors M1 and M2 having a high transmission at 975 nm and high reflection in a broadband from 1030-1140 nm placed between the two lenses used for pump beam coupling.

6.2.2 Amplifier configuration

The schematic of ASE Yb-doped fiber source in the amplifier configuration is shown in Fig. 6.2 respectively. Two types of Yb-doped double clad fibers (YDF-1 and YDF-2) were used as a gain medium in the seed and amplifier stage. In the seed stage, Yb-doped fiber with the core/clad diameter of 10/130 µm with clad pump absorption of 4.5 dB/m at 975 nm and in the amplifier stage Yb-doped fiber with the core/clad diameter of 5/125 µm with clad pump absorption of 1.25 dB/m at 975 nm has been used. The lengths of Yb-doped fibers in seed and in amplifier stages are 2.5 m and 9 m respectively. Fiber coupled laser diodes of 20 W at wavelengths 975 nm were used as pump sources in the seed and amplifier stage. The fiber pigtailed diode lasers (LD) output was coupled to the inner clad of the gain fiber with the suitable combination of collimating (L1 & L4) and focusing lenses (L2 & L3). Both ends of the doped fibers were angle cleaved to suppress the feedback from ends. Both the stages are separated by fiber optic isolator (ISO) so that the backward signal from the amplifier stage doesn’t affect the seed signal.

Fig. 6.2: *Experimental setup of the ASE generation in the amplifier configuration.YDF1 represents*

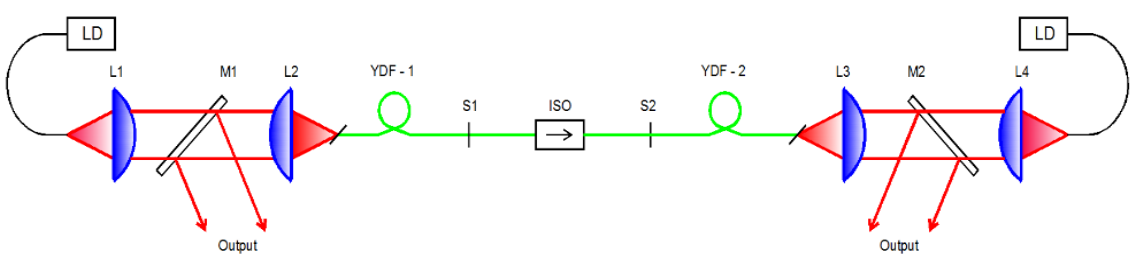

seed fiber and YDF2 represents amplifier fiber. Oscillator and Amplifier are separated by fiber optic isolator (ISO). S1and S2 are splice joints.

For the ASE study from the single stage, ASE signal is taken after isolator and to study the

ASE output in the amplifier, the ASE output is taken from the pump fiber end in the amplifier stage using a dichroic mirror (M2) having a high transmission at 975 nm and high reflection in a broadband from 1030-1140 nm placed between the two lenses used for pump beam coupling. S1 and S2 represents the two splice joints. ASE output power and spectrum were recorded using a digital power meter and a 0.06 nm resolution optical spectrum analyzer respectively.

6.3 Results & Discussion

6.3.1 Results of Yb-doped single mode double clad fibers

6.3.1.1 Single end pumping configuration

For the study of ASE generation in the single end pumping configuration 18 m length of the Yb-doped fibers with core/clad diameter of 10/400 μm with ~14 dB of 975 nm pump absorption have been used in both the co-propagating and counter-propagating direction. In this study the input end of the fiber is kept perpendicular for the better coupling of the pump light into the doped fiber and the output end is angled. Fig. 6.3 shows the ASE spectrum in the counter propagating direction and co-propagating direction for 18 m fiber which is pumped by 975 nm pump laser diode at different values of launched pump power. The output signal spectral characterstics shows uneven shape with high modulations. In the counter propagating direction, maximum FWHM linewidth of 42 nm with 20 mW of ASE power has been obtained at pump power of 2.6 W,which is equal to the maximum FWHM linewidth reported by L. Kong et. al. [136]. Fig. 6.3 (a) shows that with the increase in pump power from 2.6 W to 4.6 W the FWHM linewidth of the output signal in counter propagating direction decreases significantly from 42 nm to 26 nm and the peak wavelength has a considerable shift from 1083 nm to 1056 nm. Fig. 6.3(b) shows in the same pump power range the FWHM linewidth of the output signal in the co-propagating direction decreases slightly from 21 nm to 20 nm, peak wavelength also slightly changes from 1088 to 1087 nm. As seen from Fig.

6.3(a), the increase in pump power level causes lower wavelength ASE generation in the counter propagating direction and the shift in the peak wavelength is considerable. On the contrary in the co-propagating direction there is longer wavelength generation and the peak wavelength shifts marginally towards lower values. This observation can be explained with the help of figure 1.3(a) in chapter 1. Emission in the longer wavelength region 1050 to 1140 nm is due to the atomic transitions from 'e' to 'c' and 'd' and emission in the lower wavelength region i.e. from 1030 nm to 1050 nm range is due to the atomic transitions from 'e' to 'b'.

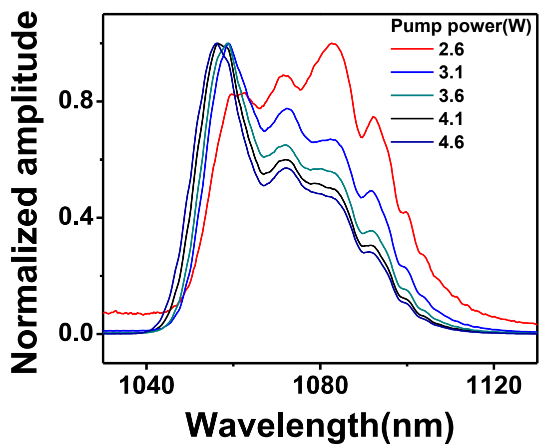

(a)

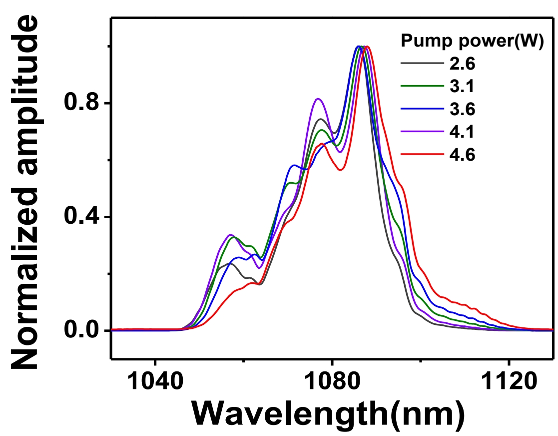

(b)

Fig. 6.3: *ASE spectrum of 18 m Yb-doped fiber in (a) counter-propagating direction and (b)in co-propagating direction at different values of the pump power.*

As level ‘b’ is close to the ground level, at room temperature it is thermally populated with 6% of the ground level population and hence the absorption from level ‘b’ is higher. Since, the spectrum in the counter propagating direction is generated by the portion of the fiber where the population inversion is high and there is no scope of the absorption of the signal, so the emission is predominant at lower wavelengths where the gain is also high. In the co-propagating direction, population inversion decreases exponetially along length of fiber, absorption of lower wavelength region is more pronunced along the length of the fiber and hence it leads to emission at longer wavelengths. With increase in the pump power, population inversion increases and the number of atoms present in the level ‘b’ will decrease which will shift the peak walength towards the lower values.

Fig. 6.4 shows the ASE signal power as a function of the launched pump power. The maximum ASE signal power in the counter propagating direction is 230 mW and in the co-propagating direction is about 190 mW. It is observed that the signal power in the counter propagating direction is slightly higher than the co-propagating direction. The slope efficiency for the total ASE signal power is 18.7%. As the pump power was furher increased, parasitic lasing started to occur. The plausible reason may be that the fiber towards the pump end has higher population inversion as compared to the other end, ground-state absorption of the co-propagating ASE beam will be much more compared to counter-propagating ASE beam, which results in higher counter-propagating ASE power as compared to co-propagating ASE power. It can be observed that the ASE power is less than 1 W. Hence to enhance the ASE power, the studies were done in the double end pumping configuration in two length of the same type of fiber and both ends of the doped fibers were angled.

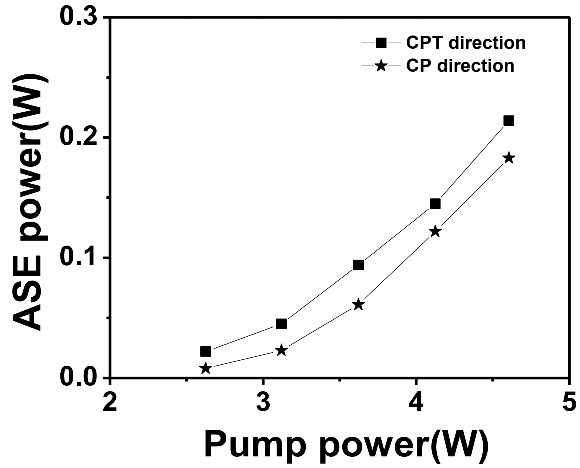

Fig. 6.4: ASE output power from 18 m fiber in the co-propagating and counter-propagating direction.

6.3.1.2 Double end pumping Configuration

Experiments were performed with two lengths of the doped fiber, 4.5 m and 18 m in double end pumping configuration using 975 nm as the pump wavelength with pump absorption of ~4 dB and 14 dB respectively. Both ends of the fiber were angled to avoid the feedback of the signal from the ends which can cause lasing.

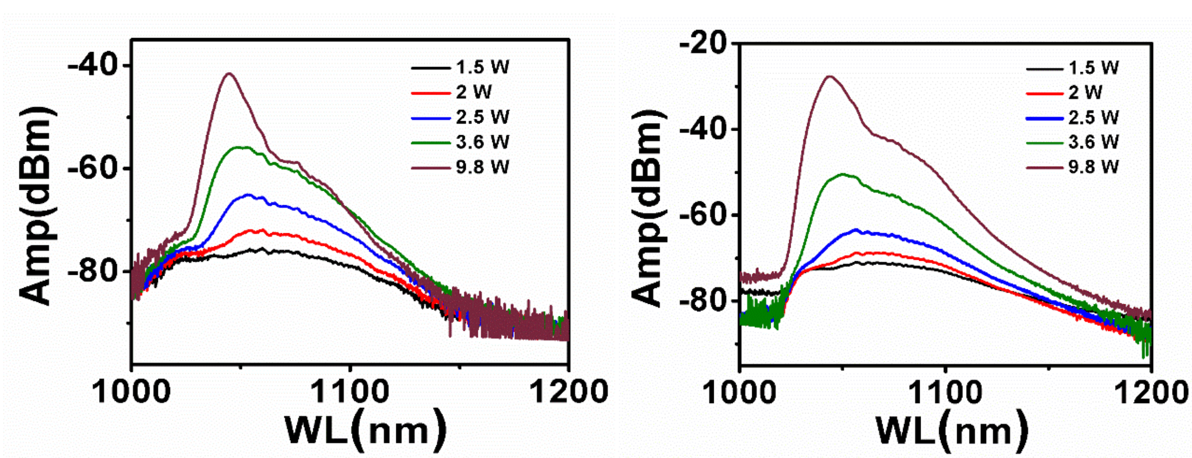

(a) **(b)**

Fig. 6.5: Output ASE spectrum from 4.5 m length of YDF in double end pumping configuration. (a) Spectrum from M1 side and (b) shows the spectrum from M2 side.

Figure 6.5 shows the ASE spectrum in the short length of 4.5 m of the Yb-doped fiber from M1 and M2 side of the experimental setup with low pump absorption. The ASE FWHM linewidth at the pump power of 1.5 W is ~75 nm with the ASE signal power of 32 mW. This is very promising result as the FWHM linewidth of ~75 nm and the ASE power is sufficient for OCT applications for the biological samples [137]. This value decreases to 50 nm with the ASE signal power of 45 mW at pump power of 2 W. At the M1 side, the output signal shifts from the peak wavelength of 1060 nm to 1044.7 nm as the pump power increased from 1.5 W to 9.8 W. At the highest value of the pump power of 9.8 W before lasing, the ASE signal power is 1.4 W but the FWHM linewidth of ASE signal reduced to ~9.3 nm. Similar trend of in the spectrum and output power was observed from M2 side.

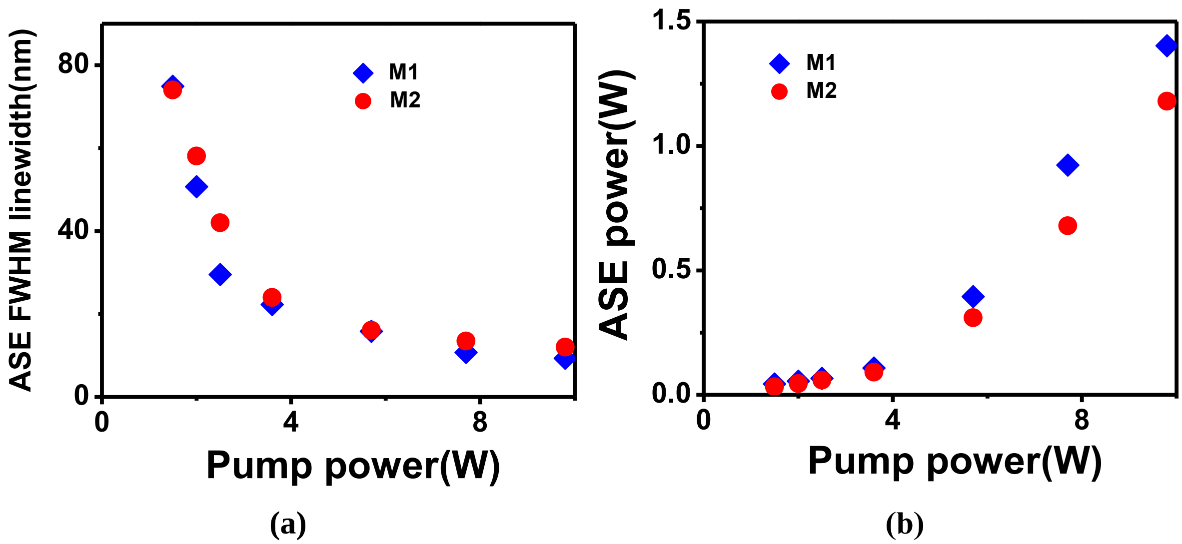

Fig. 6.6: *Spectral linewidth and ASE power as a function of input pump power for 4.5 m length of Yb-doped fiber.*

Figures 6.6 (a) and (b) shows the ASE power and the ASE FWHM linewidth of the spectrum from both the sides of 4.5 m length of the fiber. Due to the uniform pumping in case of the short length of the fiber, the spectrum from both the ends show same behaviour. When the ASE signal is less than 100 mW the ASE linewidth is very broad, but at higher values of the ASE signal

ASE linewidth is short. Since, in the short length of the fiber, the reabsorption effect is very less, so the ASE linewidth obtained is very large at low pump power.

The ASE studies were performed in long length fiber i.e. 18 m long in double end pumping configuration. Figure 6.7 and 6.8 shows the ASE spectrum from both ends of the Yb-doped fiber. Figure 6.7(a) shows the spectrum from M1 side of the fiber the linewidth decreases from 28.4 nm to 14.5 nm and the peak wavelength shifts from 1060 nm to 1051 nm and when the pump power is increased from 3.7 W to 23.6 W. At the highest value of the pump power before lasing, the ASE peak shifts from 1051 nm to 1077 nm. In this case the maximum linewidth of 28 nm is achieved but the ASE power is small i.e. 120 mW. The ASE power increases to 5 W at higher pump power but with reduction of linewidth to ~11 nm. Spectrum from M2 side also shows a similar behavior. In the spectrum from M1 and M2 side dip is observed at 1064 nm. It may be noted that this particular length of the fiber both the lower wavelength and higher wavelength signal are generated and there is a dip at the center of the spectrum at about 1064 nm. The ASE spectral linewidth can be enhanced by preventing a dip in the spectrum.

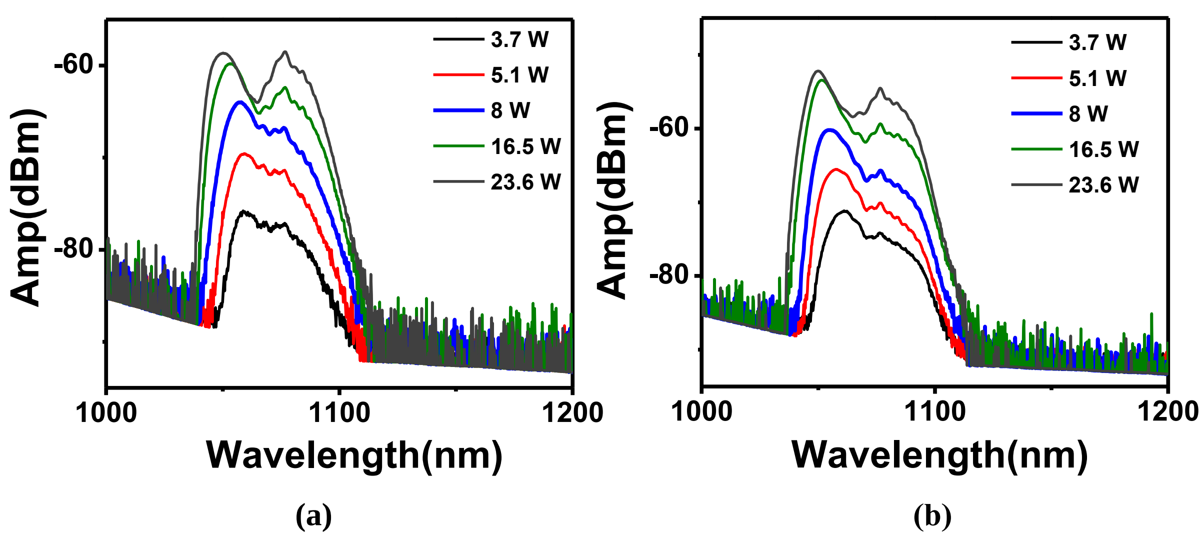

Fig. 6.7: *ASE spectrum from 18 m length of Yb-doped fiber in double end pumping configuration. (a) Spectrum from M1 side and (b) shows the spectrum from M2 side.*

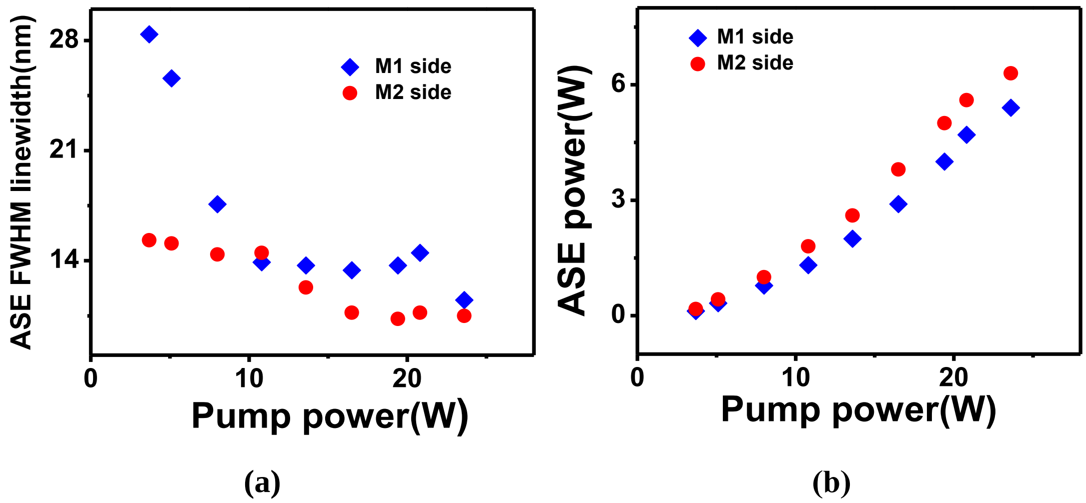

Fig. 6.8: *(a) Spectral bandwidth and (b) ASE power as a function of pump power from both ends of the doped fiber of length 18 m.*

From the single mode double clad fiber, the ASE FWHM linewidth of more than 30 nm was not obtained with ASE power of more than 1W. To achieve higher ASE power studies were conducted in amplifier configuration using single mode double clad fibers with different ASE spectral characteristics.

6.3.1.3 ASE amplification in single mode double clad Yb-doped fiber

Figure 6.2 show the experimental setup for ASE generation and amplification. Figure 6.9 shows the experimental results of the Yb-doped fiber with core/ clad diameter of 10/130 μm fiber in the seed and in the amplifier configuration. The fiber has absorption coefficient of 4.5 dB/m at 975 nm. Without amplifier stage, the ASE spectrum FWHM linewidth is ~23 nm with the peak wavelength at 1038 nm at pump power of 1 W with an ASE power of 100 mW. Further increase in the pump power causes lasing and narrowed the spectrum. To enhance the ASE linewidth and power, ASE signal was amplified in the same type of fiber. Figure 6.9 (b) shows the amplified ASE spectrum in the amplifier fiber of 2.5 m length. The

ASE signal power increased from 100 mW of seed signal with 23 nm linewidth to 14 W of ASE power with linewidth of 17 nm.

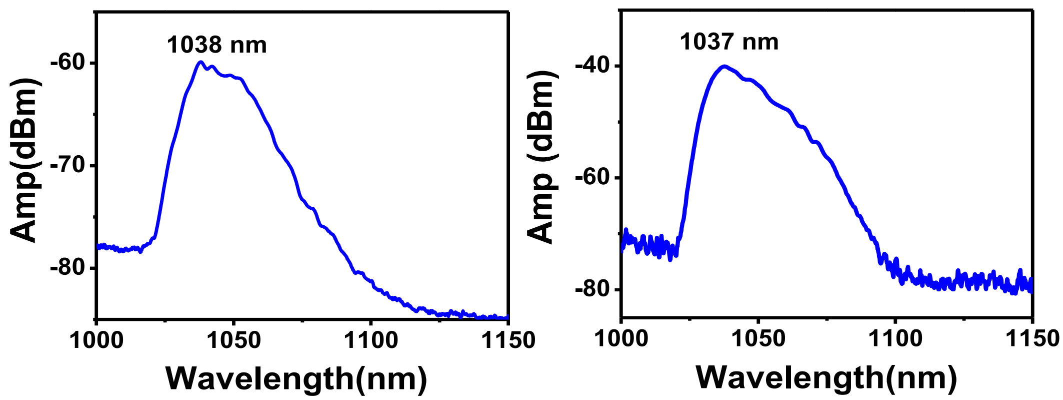

(a) (b)

Fig. 6.9: *(a) ASE spectrum of Yb-doped fiber with core/clad diameter of 10/130 µm from the co-propagating direction, (b) ASE spectrum from the amplifier configuration in which the same fiber was used in the amplifier.*

There is substantial increase in the output ASE power but the FWHM linewidth of ASE decreased from 23 nm to 17 nm at peak wavelength of 1037 nm. However, initially at low value of pump power the ASE linewidth was broad, and ASE power of ~5 W was recorded without any reduction in input ASE linewidth of 23 nm. From figure 6.9 it can be observed that when the same fiber was used as an amplifier and for seed signal then the ASE peak wavelength from amplifier shifted marginally towards lower wavelength at 1037 nm. This is expected since gain peak is towards the lower wavelength.

To enhance the total ASE linewidth, a different fiber in amplifier is used which has ASE peak at longer wavelength, such that combination of ASE spectrum from seed and amplifier would increase the total ASE linewidth. For the amplifier, Yb-doped fiber of core/clad diameter of 5/130 and 9 m length was selected. As the length of the fiber is long it gives ASE peak at the higher wavelength side of 1070 nm range. With the combination of seed fiber of core/clad diameter of 10/130 µm and 5/130 µm in amplifier, the linewidth of the ASE seed source was enhanced from 23 nm to the value of ~36 nm and the power has also increased. Maximum ASE linewidth of 36.2 nm was obtained with an ASE power of 4.2 W at pump power of ~8 W (Fig. 6.10 (a)). Beyond this lasing started. To avoid lasing, seed ASE signal was increased slightly, linewidth of 33.6 nm with output ASE power of 7.14 W was achieved (as shown in figure 6.10(b)).

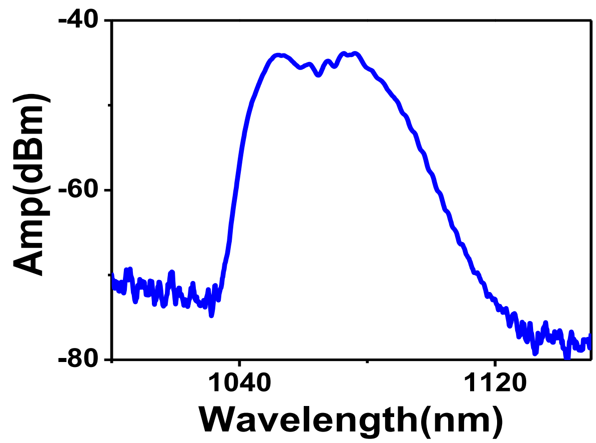

Fig. 6.10: *ASE output of the spectrum when YDF1 is used as a seed fiber and YDF2 is used as an amplifier fiber.*

The two different fibers due to their different lengths and pump absorption have different peak emission and the output spectrum. The net output ASE spectrum can be inferred as the result of the convolution of the two spectrum from the seed and amplifier Yb-doped fiber. The seed fiber has an ASE peak at lower wavelength and the longer fiber used in the amplifier possess ASE peak at higher wavelength. When the seed signal with ASE peak at lower wavelength side ~1040 nm from YDF1 is injected inside the amplifier fiber, it will get amplified, but in the amplifier fiber maximum gain is at ~1077 nm and has a lower gain around 1041 nm. Thus, both the signals at lower wavelength and higher wavelength are amplified and ASE linewidth with broader spectrum and higher power is generated.

6.3.2 ASE generation from large mode area fiber

For high power ASE generation with broad FWHM linewidth, large mode area fibers are favorable due to their large core diameter. Hence studies were carried out in the large mode area fiber with core/clad diameter of 20/400 µm. Three lengths of 5.4 m, 9 m and 13 m of the same fiber with total pump absorption of ~7 dB, ~11 dB and ~16 dB respectively at 975 nm were pumped in the single end pumping configuration.

Figure 6.11 shows the ASE spectrum from the counter-propagating direction of 5.4 m Yb-doped large mode area fiber at different values of the pump power. As the pump power is increased from 8 W to 29.3 W the peak wavelength shifts from 1046 nm to 1041 nm and the ASE linewidth first decreases from 17 nm to ~10 nm and then increases to ~16 nm. Increase in the linewidth with pump power may be attributed to the smaller length of the fiber which precludes the reabsorption effect along the length of the fiber. In the single mode fiber it was observed that with increase in the pump power the bandwidth decreased. Figure 6.12 shows the ASE power as a function of the input pump power. Maximum signal power of 4.3 W is obtained from the counter-propagating end of the fiber at 29.3 W of the pump power. The slope efficiency in this case is ~20% due to the low absorbed pump power in the fiber.

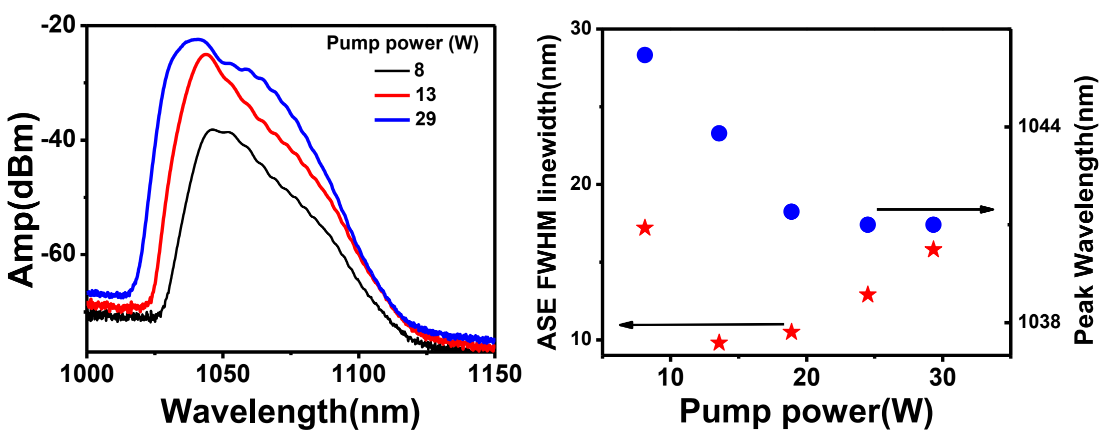

(a) (b)

Fig.6.11: *(a) Spectrum from 5.4 m of the fiber from the counter-propagating direction at different values of the pump power. (b) FWHM linewidth and peak wavelength of the spectrum as a function of pump power.*

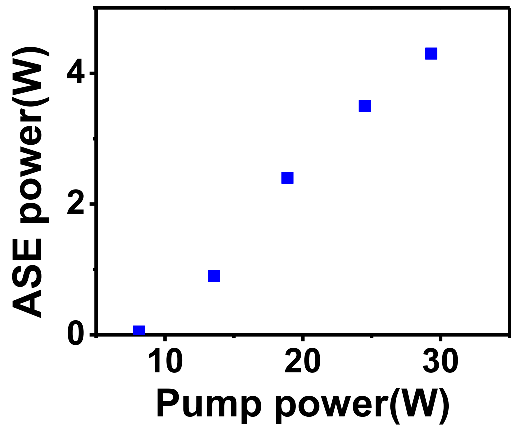

__Fig. 6.12:__ ASE power as a function of the input pump power of 5.4 m LMA Yb-doped fiber with the slope efficiency of ~20%.

Figure 6.13 shows the ASE spectrum from the co-propagating direction of 9 m of Yb-doped fiber at different values of the pump power. As the pump power is increased from 5.5 W to 16.2 W the peak wavelength shifts from 1055.5 nm to 1043 nm and the bandwidth initially decreases from 17.9 nm to 12.4 nm and then increases respectively.

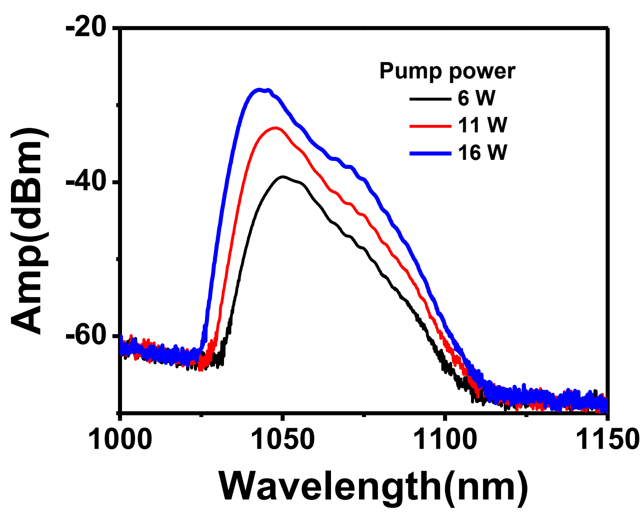

__Fig. 6.13:__ Output ASE spectrum of the 9.5 m of the YDF from the co-propagating direction of the doped fiber.

Maximum output ASE power of 5.2 W was obtained from the output end of the fiber at

16.2 W of the pump power. Further increase in the pump power causes lasing and significantly reduces the linewidth of the spectrum. Figure 6.14 shows the output power with the variation of the input pump power. The slope efficiency in this case is ~40%.

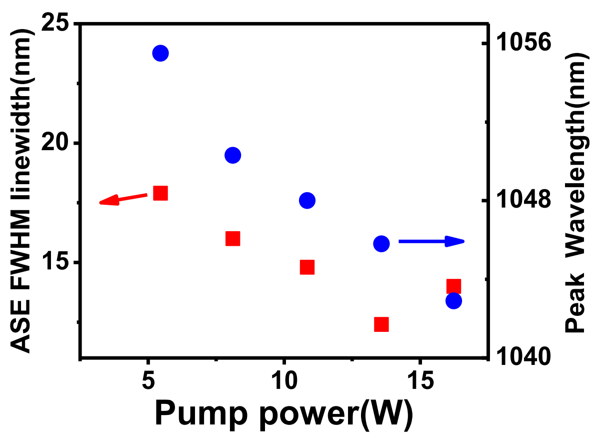

(a)

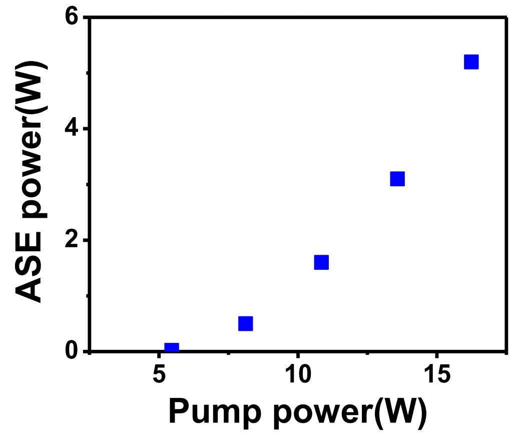

(b)

Fig. 6.14: *(a) FWHM bandwidth and peak wavelength variation with pump power, (b) Variation of output ASE power as a function pump power in 9.5 m length of the fiber.*

ASE was studied in 13 m length of the same fiber. The ASE FWHM linewidth of the spectrum and the ASE power was considerably large in this case compared to the 5.4 m and 9.5 m length of fiber. Here it was observed that maximum bandwidth of 41.8 nm was obtained with the ASE power of 15.34 W in the counter-propagating direction. Figure 6.15(a) shows the evolution of the spectrum at different values of the pump power. At low pump power the linewidth is low and initially the peak shifts to lower wavelength region. With increase in the pump power, higher wavelengths are also generated causing the broadening of the ASE spectrum. At the highest pump power ASE FWHM linewidth of 41.8 nm was recorded (Fig. 6.15(b)). As the Ytterbium doped fiber is three level system, so the length plays very important role in the generation of ASE and the broad linewidth. Figure 6.16 shows the variation of output power as a function of the input pump power.

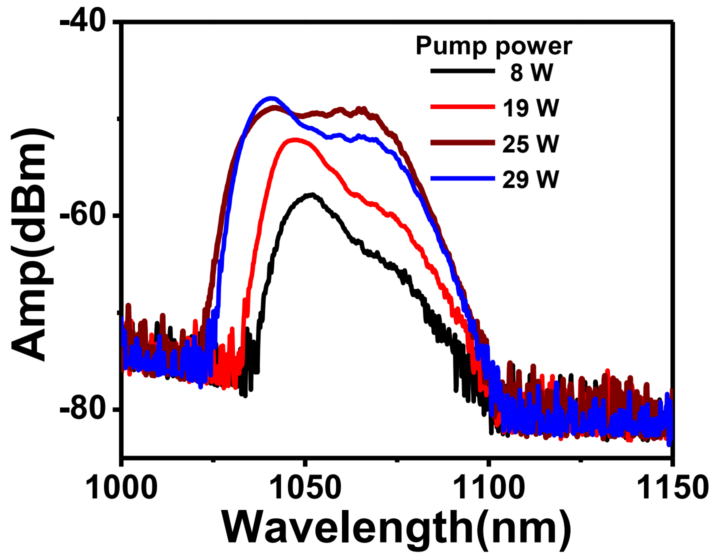

(a)

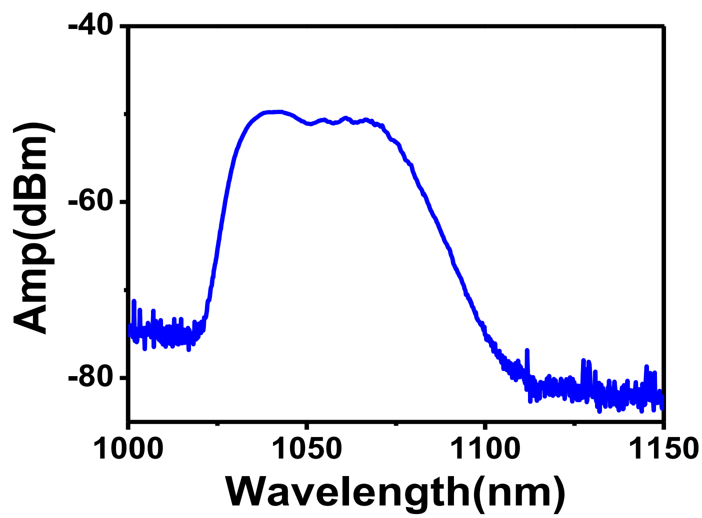

(b)

Fig. 6.15: *(a) Evolution of ASE spectrum in 13 m Yb-doped fiber in the co-propagating direction with pump power, (b) Maximum bandwidth of ASE spectrum at 15 W of signal power with ~42 nm bandwidth.*

At the highest pump power of ~29 W the bandwidth is maximum and the ASE power is more than

15 W. The slope efficiency is ~72% which is highest among all, the fiber studied in the chapter. This may be due to the efficient pump absorption by the gain medium along the length of the fiber. Experiments were also done with 20 m length of the same fiber with total pump absorption of 25 dB. It was obserbved that the ASE FWHM linewidth obtained was ~ 20 nm. The results indicates that there may be an optimum length for broadband ASE generation in Yb-doped fibers.

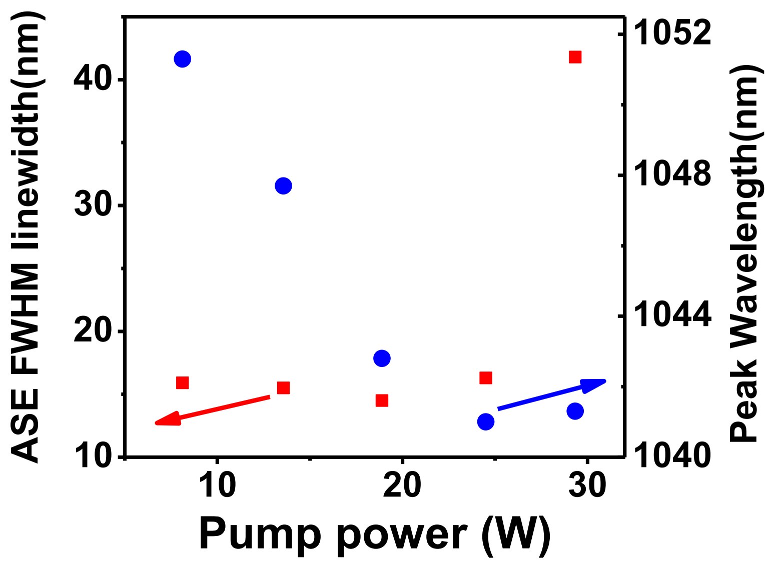

Fig. 6.16: *ASE FWHM linewidth and peak wavelength shift with variation in the pump power.*

The preliminary experimental results on broadband ASE generation has been presented in this chapter. Efforts are being carried out to simulate the ASE broadband generation.

6.4 Conclusion

We have carried out experiments with different pump configuration, fiber length in single mode double clad Yb-doped fibers which is paramount for generating stable, high power and broadband signal output. In single mode fiber with core clad diameter of 10/400 μm, ASE linewidth of 42 nm have been achieved with 20 mW of ASE power. In double end pumping configuration this bandwidth was extended to 75 nm with 32 mW of signal power with the same fiber by using short length of the Yb-doped fiber, to avoid the re-absorption effect. This value of ASE power is sufficient for optical coherence tomography applications in biological samples. The study was extended in amplifier configuration using single mode fibers with different spectral characteristics in the seed part and in the amplifier part and obtained ASE FWHM linewidth of ~36 nm with 4 W of ASE power. We also carried out preliminary studies with large mode area fibers, in which we obtained 41.8 nm ASE FWHM linewidth with ASE power of 15 W. The study will help in designing low cost ASE source that is useful in optical coherence tomography measurements.

Chapter 7

Summary and future Scope

7.1 Summary of the thesis

In this thesis work, detailed study of Ytterbium doped fiber lasers and amplifiers operating in continuous wave and pulsed regime has been carried out. In CW pumping, Yb-doped fiber lasers suffer from detrimental self-pulsing effects which may damage the optical components. We have presented the experimental and analytical study of self-pulsing dynamics in Yb-doped photonic crystal fiber laser in single-end and double-end pumping configurations. It has been found that the intensity of self-pulses is considerably higher in the single-end pumping configuration as compared to that for double-end pumping configuration. Experimental study shows that occurrence of self-pulses is due to the initial relaxation oscillations and re-absorption and there is no role of nonlinear phenomena in the generation of self-pulses. The rate equation analysis shows that the non- uniformity in single pass distribution of upper level population along the fiber length is responsible for re-absorption leading to saturable absorber action and hence self-pulsing. These studies will be helpful to mitigate the effects of self-pulsing to develop high power CW Yb-doped fiber laser for various applications.

In passively Q-switched fiber laser, we have obtained linearly polarized passively Q-switched output from Yb-doped PCF laser using Cr^{4+}: YAG crystal as a saturable absorber in single-end pumping configuration. An average power of 9.4 W with a pulse width of 63 ns and a pulse repetition rate of 60 kHz has been achieved. Output pulses are polarized with polarization extinction ratio of 10.5 dB. The PQS operation of Yb-doped fiber laser in a special T-type double-end pumping configuration has been studied. In this configuration, average output power of 41.6 W has been achieved, which is the maximum average output power in PQS Yb-doped fiber laser oscillator reported so far in the literature. It was possible to achieve such a high value of average output power by means of low-loss end caps spliced at both the ends of the doped fiber. The effect of saturable absorber on random self-pulsing dynamics and on the spectral behavior of the output signal near the threshold for Q-switching has also been investigated. Studies on output pulse characteristics with different linear transmission of saturable absorbers has also been performed. Our results show that with lower values of the initial transmission of the passive Q-switch crystal, output pulse energy increases and pulse-to-pulse stability also improves. Detailed studies were also performed to observe the spectral evolution of PQS Yb-doped fiber laser as a function of pump power as well as the dependence of output spectral characteristics on the length of the gain medium. This studies can be extended to generate optical parametric studies to produce new wavelengths.

The linewidth of active as well as passive Q-switched fiber lasers is broad, however for many applications narrow linewidth pulses are required. Narrow linewidth and tunable operation of an AO Q-switched Yb-doped fiber laser using an acousto optic modulator and multimode interference filter in the linear bulk resonator and all-fiber ring resonator has been demonstrated. In the linear resonator, the spectral bandwidth of the Q-switched signal decreased by two orders of magnitude from a value of 11 nm to less than 0.1 nm by the insertion of the multimode interference filter in the cavity. Spectral tunability of more than 16 nm in the range of 1057 nm to 1073 nm has also been achieved by the combination of the multimode interference filter and a standard polarization controller. Decrease in the pulse duration with a decrease in the spectral bandwidth of the output signal from ~305 ns to ~240 ns was also recorded. In the case of the all-fiber ring resonator with the multimode interference filter, the spectral bandwidth of the output Q-switched signal was decreased from 17 to less than 0.1 nm. A spectral tunability of more than 12 nm in the range of 1038 nm to 1050 nm was achieved by a multimode interference filter and a standard polarization controller. The pulse duration was reduced from ∼200 ns to ∼185 ns. The average output power in the linear resonator with the multimode interference filter is ∼500 mW, which is much higher than the average power obtained in the all-fiber AO Q-switched ring resonator with the multimode interference filter, in which the power is ∼10 mW. However, the tunability range in both the configurations are comparable. Due to the all-fiber nature, the ring cavity resonator with a narrow line-width and tunable operation can be potentially used as an oscillator for further amplification of output power in the master oscillator power amplifier configuration. This work can be further utilized for developing a system for remote sensing applications.

With the use of acousto-optic Q-switching, stable short pulse generation has been made possible by decreasing the ON-time of the modulation signal of AO Q-switch. Short pulses (anomalous pulses) of duration in the range of 50-55 ns have been achieved in all-fiber experimental configurations with the cavity round-trip time of ~130 ns, when modulation window "ON-time" of AOM was equal to or shorter than the pulse build-up time of the normal Q-switched pulses. In the case of normal AO Q-switching, pulses of duration more than 1.3 μs with an average power of 30 mW and pulse energy of 0.38 μJ at 80 kHz of repetition rate were obtained at 2 W of pump power. At the same value of the pump power, the anomalous pulses of ~55 ns with an average power of 12 mW were generated, which are ~24 times shorter than pulses obtained with conventional Q-switching process (normal pulses). These studies were carried out in four different experimental configurations. The anomalous pulses from the AO Q-switched oscillator with ~55 ns pulse duration have been amplified with output power of ~19 W and pulse energy and peak power of 240 µJ and 4.4 kW respectively in all fiber configuration. As the peak power is very high, it has a bright prospects for material processing applications.

Yb-doped fibers have very broad emission bandwidth, which favours broadband amplified spontaneous emission (ASE) generation and hence these are useful as superfluorescent sources for many applications. We have carried out experiments to study the effect of pump configuration, fiber length, fiber core diameter on ASE generation in Yb-doped fibers which is paramount for generating stable, high power and broadband signal output. It has been observed in Yb-doped fibers that generated ASE spectrum depends on the length of the fiber. In single mode fiber with core clad diameter of 10/400 µm, maximum bandwidth of ~42 nm have been achieved with 20 mW of signal power in long length of the Yb-doped fibers This bandwidth was extended to 75 nm with 32 mW of signal power in the double end pumping configuration with the same type of fiber by using shorter length, to avoid the re-absorption effect. Further, to enhance ASE power, an amplifier configuration using single mode double clad Yb-doped fibers with different spectral characteristics in the seed part and in the amplifier part were used to obtain FWHM linewidth of ~36 nm with 4 W of ASE power. We also carried out our studies with large mode area fibers, in which 41.8 nm FWHM linewidth with ASE power of 15 W was obtained. These studies will help in designing low cost broadband ASE source useful for optical coherence tomography measurement.

1.2 Scope for the future work

There are ample of future scope in the study of self-pulsing analysis in Yb-doped fiber laser. The Yb-doped fiber laser has absorption peak at 975 nm and 915 nm. In this thesis self-pulsing has been studied only at 975 nm. The absorption in any given Yb-doped fiber is much higher at 975 nm as compared to 915 nm. It would be important to study the self-pulse generation in Yb-doped fiber with 915 nm as pump source. Further, time domain rate equation analysis can be done to understand the dynamics of the self-pulsing in Yb-doped fiber laser, as these pulses have very high peak power and are random in nature. In future, techniques can be established to control these random pulses which may be converted into well behaved stable pulses with or without using saturable absorber or Q-switch.

In passive Q-switching of Yb-doped fiber laser using Cr^{4+}: YAG crystal as a saturable absorber we obtained very high average power of more than 40 W. In future, it can be used to generate new wavelengths by using Optical Parametric Oscillators.

The linewidth of active Q-switched fiber laser was reduced from ~17 nm to less than ~0.1 nm by incorporating multi-mode interference filter in all fiber Q-switched ring resonator. Spectral tunability achieved was from 1038 nm to 1050 nm. The average power obtained is ~10 mW which can be further amplified to higher power levels by master oscillator amplifier configuration and can be used for LIDAR and sensing applications. Efforts can be made to further reduce the linewidth by changing the parameters of MMI filter.

Anomalous pulses of duration less than the cavity round trip time were generated using AO Q-switching by decreasing the ON-time of the modulation signal of the AO Q-switch. Generation of these pulses have been explained analytically. There is future scope, to understand the generation of these pulses theoretically by time-domain rate equation analysis. The temporal dependence of anomalous pulses on fall time of AO Q-switch, cavity configuration and pump power can be further explored. The output pulse energy can be further enhanced by incorporating large mode area fibers in the amplifier configuration.

ASE generation have been studied extensively and the studies can be utilized for developing superflourescent source. The CW superfluorescent source shows absence of self-pulsing as compared to conventional CW fiber laser. Thus the recent research on generation of kW CW power level use superfluorescent seed source. In the same scheme narrow-linewidth ASE seed source can be developed for further amplification to kW level.

REFERENCES

Chapter 1

[1] T. H. Maiman, "Stimulated optical radiation in ruby", Nature, 187, 493–494 (1960).

[2] W. T. Silfvast, "Laser Fundamentals", Cambridge University Press (2004).

[3] A. K. Ghatak, "Lasers: Theory and Applications", New York, Plenum Press (1981).

[4] A. E. Siegman, "Lasers" Mill Valley, CA, USA: Univ. Science, (1986).

[5] E. Snitzer, "Proposed fiber cavities for optical masers", J. Appl. Phys., 32, 36–39 (1961).

[6] C. J. Koester and E. Snitzer, "Amplification in a fiber laser", Appl. Opt., 3, 1182–1186 (1964).

[7] D. J. Richardson, J. Nilsson, and W. A. Clarkson, "High power fiber lasers: Current status and future perspectives", J. Opt. Soc. Amer. B, 27, B63–B92 (2010).

[8] E. Snitzer, H. Po, F. Hakimi, R. Tumminelli, and B. C. McCollum, " Double-clad offset core Nd fiber laser ", in Proc. Optical Fiber Sensors, Paper PD5(1988).

[9] Y. Jeong, J. K. Sahu, D. N. Payne, and J. Nilsson, " Ytterbium-doped large-core fiber laser with 1.36 kW continuous-wave output power ", Opt. Express 12, 6088–6092 (2004).

[10] M. O'Connor, V. Gapontsev, V. Fomin, M. Abramov, A. Ferin, " Power scaling of SM fiber lasers toward 10 kW ", Conference on Lasers and Electro-optics, Paper CThA3 (2009).

[11] www.ipgphotonics.com

[12] H. M. Pask, R. J. Carman, D. C. Hanna, A. C. Tropper, C. J., MacKechnie, P. R. Barber, and J. M. Dawes, "Ytterbium doped silica fiber lasers—versatile sources for the 1–1.2 μm region " , IEEE J. Sel. Top. Quantum Electron. , 1(1), 1–13 (1995).

[13] A. V. Kir'yanov, Y. O. Barmenkov and I. V. Garcia, "2.05 μm holmium-doped all-fiber laser diode-pumped at 1.125 μm", Laser Physics, 27(8) (2017).

[14] F. Jansen, F. Stutzki, Cesar Jauregui, J. Limpert, and A. Tünnermann, "High-power very large mode-area thulium-doped fiber laser ", Optics Letters, 37(21), 4546-4548 (2012).

[15] A.Ghatak and K.Thyagarajan, “Introduction to Fiber Optics”, Cambridge University Press India Pvt. Ltd., Reprinted (2011).

[16] J.C. Knight, “Photonic crystal fibers”, Nature, 424, 847–51(2003).

[17] P. Russell, “Photonic crystal fibers”, Science, 299, 358–62 (2003).

[18] J. Limpert, T. Schreiber, S. Nolte, H. Zellmer, T. Tünnermann, R. Iliew, “ High- power air-clad large-mode-area photonic crystal fiber laser”, Optics Express, 11, 818–23 (2003).

[19] J. Xu, L. Huang, J. Leng, H. Xiao, S. Guo, P. Zhou, and J. Chen , “1.01 kW superfluorescent source in all-fiberized MOPA configuration”, Optics Express, 23(5), 5485 (2015).

[20] O. Schmidt, J. Rothhardt, F. Röser, S. Linke, T. Schreiber, K. Rademaker, J. Limpert, S. Ermeneux, P. Yvernault, F. Salin, and A. Tünnermann, “Millijoule pulse energy Q-switched short-length fiber laser”, Opt. Lett. 32, 1551-1553 (2010).

[21] E. B. Petersen, W. Shi, D. T. Nguyen, Z. Yao, J. Zong, A. Chavez- Pirson, and N. Peyghambarian , “Enhanced terahertz source based on external cavity difference-frequency generation using monolithic single-frequency pulsed fiber lasers”, Opt. Lett. 35, 2170–2172 (2010).

[22] W. Koechner, “Solid-State Laser Engineering”, Springer, fifth edition (1999).

[23] D. Brown and H. J. Hoffman, “Thermal, Stress, and Thermo-Optic Effects in High Average Power Double-Clad Silica Fiber Lasers”, IEEE J. Sel. Top. Quantum Electron. 2 207-217 (2001).

[24] J. W. Dawson, M. J. Messerly, R. J. Beach, M. Y. Shverdin, E. Stappaerts, A. K. Sridharan, P. H. Pax, J. E. Heebner, C. W. Siders and C.P.J. Barty, “Analysis of the scalability of diffraction-limited fiber lasers and amplifiers to high average power”, Optics Express,16 (17), 13240 (2008).

[25] A. A. Said, T. Xia, A. Dogarlu, D. J. Hagan, M. J. Soileau, E. W. V. Stryland, and M. Mohebi, “Measurement of the optical damage threshold in fused quartz” , Appl. Opt. 36, 3374-3376 (1995).

[26] G.P. Agrawal, “Nonlinear Fiber Optics”, Academic press, fourth Edition (2008).

[27] R. H. Stolen, E. P. Ippen, and A. R. Tynes, “Raman oscillation in glass optical waveguide”, Appl. Phys. Lett. 20, 62-64 (1972).

[28] R. G. Smith, “Optical power handling capacity of low loss optical fibers as determined by stimulated Raman and Brillouin scattering” , Appl. Opt. 11, 2489-2494 (1972).

[29] R. Kashyap, and K. J. Blow, “Observation of catastrophic self-propelled self-focusing in optical fibers”, Electronics Letters, 24, 47-49 (1988).

[30] D.D. Davis, S.C. Mettler and D.J. DiGiovanni, “Experimental data on the fiber fuse”, Proc. SPIE, 2714, 202-210 (1996).

[31] R.M. Wood, “Laser induced damage thresholds and laser safety levels. Do the units of measurement matter? ” Opt. Laser Tech., 29(8), 517-522 (1997).

[32] T.J. Driscoll et al, “Explaining the optical fuse”, Opt. Lett., 16(13), 1046-1048 (1991).

[33] Y. Shuto et al, “Evaluation of high temperature absorption coefficients of optical fibers”, IEEE Photo. Tech., 16(4), 1008-1010 (2004).

[34] J. Wang, S. Gray, D. Walton and L. Zenteno, “Fiber fuse in high power optical fiber”, Proc. of SPIE Vol. 7134 71342E. (2008).

Chapter 2

[35] Y. W. Tzeng, Y. Y. Lin, C. H. Huang, J.M. Liu, H.C. Chui, H.L. Liu, J. M. Stone, J. C. Knight, and S.W. Chu, “Broadband tunable optical parametric amplification from a single 50 MHz ultrafast fiber laser” , Optics Express, 17(09), 7304-7309 (2009).

[36] W.J. Wadsworth, J.C. Knight, W.H. Reeves, P.S. Russell, J. Arriaga , “Yb^{3+} doped photonic crystal fiber laser”, Electronics Letters, 36, 1452–1456 (2000).

[37] Y. Jeong, J. Nilsson, J. K. Sahu, D. B. S. Soh, C. Alegria, P. Dupriez, C. A. Codemard, and D. N. Payne, R. Horley, L. M. B. Hickey, L. Wanzcyk, C. E. Chryssou, J. A. Alvarez-Chavez, and P. W. Turner, "Single-frequency, single-mode, plane-polarized ytterbium-doped fiber master oscillator power amplifier source with 264 W of output power", Opt. Lett. 30, 459-464 (2005).

[38] O. Schmidt, J. Rothhardt, T. Eidam, F. Röser, J. Limpert, A. Tünnermann, K.P. Hansen, C. Jakobsen, J. Broeng, "Single-polarization ultra-large-mode-area Yb-doped photonic crystal fiber", Optics Express, 16(09), 3918-3923 (2008).

[39] D. A. V. Kliner, J. P. Koplow, R. L. Farrow, P. E. Schrader, S. W. Moore, T. A. Reichardt, A. A. Hoops, T. J. Kulp, K. M. Armstrong, R. L. Sommers, P. Schultz, L. Goldberg, and J. Fève, "Fiber-Based Laser Systems for Spectroscopic Trace-Gas Detection", in Laser Applications to Chemical, Security and Environmental Analysis, OSA Technical Digest (CD) paper LTuA3 (2008).

[40] N. P. Barnes, B. M. Walsh, D. J. Reichle, and R. J. DeYong, "Tm: fiber lasers for remote sensing", Opt. Mater. 31(7), 1061–1064 (2009).

[41] X. Feng, Y.Liu, S. Fu, S. Yuan and X. Dong "Switchable dual-wavelength ytterbium-doped fiber laser based on a few-mode fiber grating", IEEE Photon. Technol. Lett., 16, 762-764 (2004).

[42] S. Fu, L. Si, Z. Guo, S. Yuan, Y. Zhao and X. Dong, "Switchable multiwavelength ytterbium-doped double-clad fiber laser based on a multimode fiber grating", Applied Optics, 46, 3579-3582 (2007).

[43] L. Pan, I. Utkin and R. Fedosejeves, "Two-wavelength ytterbium-doped fiber laser with sustained relaxation oscillation", Applied Optics, 48, 5484-5489, (2009).

[44] N. S. Shahabuddina, M.A. Ismail, M.C. Paul, S.S.A. Damanhuri, S.W. Harun, H. Ahmad, M. Pal and S.K. Bhadra , "Multi-wavelength ytterbium doped fiber laser based on longitudinal mode interference", Laser Physics, 22, 252-255 (2012).

[45] E. Lacot, F. Stoeckel, M. Chenevier, "Dynamics of an erbium-doped fiber laser", Physical Review A, 49, 3997–4008(1994).

[46] P. Glas, M. Naumann, A. Schirrmacher, L. Daweritz, R. Hey, "Self pulsing versus self-locking in a cw pumped neodymium doped double clad fiber laser", Optics Communications, 161,345–58 (1999).

[47] F. Brunet, Y. Taillon, P. Galarneau, S. LaRochelle , "A simple model describing both self-mode locking and sustained self-pulsing in ytterbium-doped ring fiber lasers", Journal of Light-wave Technology, 23, 2131–2138 (2005).

[48] S.D. Jackson, "Direct evidence for laser reabsorption as initial cause for self- pulsing in three-level fiber lasers", Electronics Letters, 38, 1640–1642 (2002).

[49] D. Marcuse, "Pulsing behavior of a three-level laser with saturable absorber, "IEEE Journal of Quantum Electronics, 29, 2390–2396 (1993).

[50] L. Luo, Chu PL, "Suppression of self-pulsing in an erbium-doped fiber laser", Optics Letters, 22, 1174–1176 (1997).

[51] W.H. Loh, J.P. de Sandro, "Suppression of self-pulsing behavior in erbium-doped fiber lasers with resonant pumping: experimental results", Optics Letters, 21, 1475–1477 (1996).

[52] W Guan, J.R. Marciante , "Complete elimination of self-pulsations in dual-clad ytterbium-doped fiber lasers at all pumping levels", Optics Letters, 34, 815–817 (2009).

[53] H. Chen, G. Zhu, N.K. Dutta, K. Dreyer, "Suppression of self-pulsing behavior in erbium-doped fiber lasers with a semiconductor optical amplifier", Applied Optics, 41, 3511–3516 (2002).

[54] B.N. Upadhyaya, U. Chakravarty, A. Kuruvilla, A.K. Nath, M.R. Shenoy, K. Thyagarajan, "Effect of steady-state conditions on self-pulsing characteristics of Yb-doped cw fiber lasers", Optics Communications, 281,146–153(2008).

[55] M. Sabaeian, H. Nadgaran, M. De Sario, L. Mescia, F. Prudenzano, "Thermal effects on double clad octagonal Yb: glass fiber laser", Optical Materials, 31, 1300-1310 (2009).

[56] P. Li, C. Zhu, S. Zou, H. Zhao, D. Jiang, G. Li and M. Chen, "Theoretical and experimental investigation of thermal effects in a high power Yb^{3+} doped double clad fiber laser", Optics & laser Technology, 40, 360-366 (2008).

[57] Y. Wong, C.Q. Xu and H. Po, " Analysis of Raman and Thermal effects in kilowatt fiber lasers" Optics Communications, 242, 487-495 (2004).

[58] U. Chakravarty, A. Kuruvilla, B.N. Upadhyaya, S.M. Oak, "Realization of 43W of single-mode linearly polarized Yb-doped photonic crystal fiber laser", Presented at the International conference on Speciality Glass & Optical Fiber, (2011).

[59] U. Chakravarty, A. Kuruvilla , H. Harikrishnan, B.N. Upadhyaya, K.S. Bindra, S.M. Oak, "Study on self-pulsing dynamics in Yb-doped photonic crystal fiber laser", Optics & Laser technology, 51, 82-89 (2013).

[60] I. Kelson and A.A. Hardy, "Strongly pumped fiber lasers", IEEE Journal of Quantum Electronics, 34, 1570–1577 (1998).

[61] X. Limin, Y. Ping, G. Mali, W. Wenlou, and O. Pan, "An approximate analytic solution of strongly pumped Yb-doped double-clad fiber lasers without neglecting the scattering loss", Optics Communications, 230, 401–410 (2004).

[62] B.N. Upadhyaya , U. Chakravarty, A. Kuruvilla, S.M. Oak , M.R. Shenoy and K. Thyagarajan, " Self- pulsing characteristics of a high-power single transverse mode Yb-doped CW fiber laser", Optics Communications, 283, 2206-2213 (2010).

[63] T. Schreiber, F. Röser, O. Schmidt, J. Limpert, R. Iliew and F. Lederer, "Stress induced single polarization single transverse mode photonic crystal fiber with low nonlinearity", Optics Express, 13, 7622–7630 (2005).

[64] F. Shenggui, F. Xinhuan, S. Libin, G. Zhancheng, J. Xiujie, Z. Ying, "Self-pulsing dynamics of high power Yb-doped fiber lasers", Microwave and Optical Technology Letters, 48, 2282–2285(2006).

[65] C. C. Cutler, "Why does linear phase shift cause modelocking?", IEEE Journal of Quantum Electronics, 28, 282–288 (1992).

[66] S. K. Turitsyn, S.A. babin, A.E. El-Taher, P. Harper, D.V. Churkin, V. Karalekas and E.V. Podivilov, "Random distributed feedback fibre laser", Nature Photonics 4, 231-235 (2010).

Chapter 3

[67] L. Pan, I. Utkin, and R. Fedosejeves, "Passively Q-switched ytterbium-doped double-clad fiber laser with a Cr^{4+}: YAG saturable absorber", IEEE Photon. Lett. 19, 1979 -1981, (2007).

[68] L. Pan, I. Utkin, R. Lan, Y. Godwal, and R. Fedosejevs, "High peak power sub nanosecond passively Q-switched ytterbium-doped fiber laser", Opt. Lett. 35, 895-897 (2010).

[69] M. Laroche, H. Gilles, S. Girard, N. Passilly, and K. Ait-Ameur, "Nanosecond pulse generation in a passively Q-switched Yb-doped fiber laser by Cr^{4+}: YAG saturable absorber", IEEE Photon. Technol. Lett., 18, 764-766 (2006).

[70] J. Y. Huang, H. C. Liang, K. W. Su, and Y. F. Chen, "High power passively Q-switched ytterbium fiber laser with Cr^{4+}: YAG as a saturable absorber", Opt. Express 15, 473- 479 (2007).

[71] W. Z. Zhuang, W. C. Huang, Y. P. Huang, K. W. Su, and Y. F. Chen, "Passively Q-switched photonic crystal fiber laser and intracavity optical parametric oscillator", Opt. Express, 18, 8969-8975 (2010).

[72] U. Chakravarty, A. Kuruvilla, R. Singh, B. N. Upadhyaya, K. S. Bindra, and S. M. Oak, "Linearly polarized intracavity passive Q-switched Yb-doped photonic crystal fibre laser" , Pramana, 82, 379-383 (2014).

[73] W. Z. Zhuang, W. C. Huang, P. Y. Chiang, K. W. Su, K. F. Huang, and Y. F. Chen, "Millijoule-level Yb-doped photonic crystal fiber laser passively Q-switched with AlGaInAs quantum wells", Opt. Express 18, 27910-27915 (2010).

[74] J. Y. Huang, W. Z. Zhuang, W. C. Huang, K. W. Su, C. Hu, K. F. Huang, and Y. F. Chen, "Comparative studies for Cr^{4+}:YAG crystal and AlGaInAs semiconductor used as a saturable absorber in Q-switched Yb-doped fiber lasers", Opt. Express 17, 20800 20805 (2009).

[75] J. Y. Huang, W. Z. Zhuang, W. C. Huang, K. W. Su, K. F. Huang, and Y. F. Chen, "Hybrid Q-switched Yb-doped fiber laser", Opt. Express 19, 9364-9370 (2011).

[76] J. Y. Huang, W. C. Huang, W. Z. Zhuang, K. W. Su, Y. F. Chen, and K. F. Huang, "High-pulse energy, passively Q-switched Yb-doped fiber laser with AlGaInAs quantum wells as a saturable absorber", Opt. Lett. 34, 2360-2362 (2009).

[77] Y. Lu and X. Gu, "All-fiber passively Q-switched fiber laser with a Sm-doped fiber saturable absorber", Opt. Express 21, 1997-2002(2013).

[78] Y. Lu and X. Gu, "Kilowatt peak power pulses from a passively Q-switched Yb-doped fiber laser with a smaller-core Yb-doped fiber as a saturable absorber", IEEE Photon. J. 6(3) 1501207 (2014).

[79] G. Das, Z. J. Chaboyer, J. E. Navratil, and R. A. Drainville, "Passively Q-switched Yb- and Sm-doped fiber laser at 1064 nm", Opt. Commun. 334, 258-264 (2015).

[80] D. Jin, R. Sun, H. Shi, J. Liu, and P. Wang, "Stable passively Q-switched and gain-switched Yb-doped all-fiber laser based on a dual-cavity with fiber Bragg gratings," Opt. Express 21, 26027-26033 (2013).

[81] J. Liu, S. Wu, Q.-H. Yang, and P. Wang, "Stable nanosecond pulse generation from a graphene-based passively Q-switched Yb-doped fiber laser," Opt. Lett. 36, 4008-4010 (2011).

[82] J. Zhaoa, Y. Wang, P. Yana, S. Ruana, Y. Tsang, G. Zhang, and H. Li, "An ytterbium-doped fiber laser with dark and Q-switched pulse generation using graphene-oxide as saturable absorber", Opt. Express, 312, 227-232 (2014).

[83] Z. Luo, Y. Huang, J. Weng, H. Cheng, Z. Lin, B. Xu, Z. Cai, and H. Xu, "1.06 Q-switched ytterbium-doped fiber laser using few-layer topological insulator Bi_2Se_3 as a saturable absorber", Opt. Express 21, 29516-29522 (2013).

[84] L. Pan, I. Utkin, and R. Fedosejevs, "Two-wavelength passively Q-switched ytterbium doped fiber laser", Opt. Express 16, 11858 (2008).

[85] L. Pan, I. Utkin, and R. Fedosejevs, "Experiment and numerical modeling of high-power passively Q-switched ytterbium-doped double- clad fiber lasers", IEEE J. Quantum Electron. 46, 68-75 (2010).

[86] J. Limpert, S. Hofer, A. Liem, H. Zellmer, A. Tunnermann, S. Knoke, and H. Voelckel, "100-W average-power, high-energy nanosecond fiber amplifier", Appl. Phys. B, 75, 477-479 (2002).

[87] Y. F. Chen, Y. P. Lan, and H. L. Chang, "Analytical model for design criteria of passively Q-switched lasers", IEEE J. Quantum Electron., 37, 462-468 (2001).

[88] J. J. Degnan, "Theory of optimally coupled Q-switched laser", IEEE J. Quantum Electron. 25, 214-220 (1989).

[89] J. J. Degnan, "Optimization of passively Q-switched Lasers", IEEE J. Quantum Electron. 31, 1890-1901 (1995).

[90] V.Gapontsev, D. Gapontsev, N. Platonov, O. Shkurkhin, V. Fomin, A. Mashkin, M. Abramov, and S. Ferin, "2 kW CW ytterbium fiber laser with record diffraction limited

brightness”, in Proceedings of the Conference on Lasers and Electro-Optics Europe (IEEE, 2005).

[91] M. Zurn, J. Voigt, E. Brinkmeyer, and R. Ulrich, “Line narrowing and spectral hole burning in single-mode Nd^{3+} fiber lasers”, Opt. Lett. 12, 316-317 (1987).

Chapter 4

[92] S. Adachi and Y. Koyamada, “Analysis and design of Q-switched erbium-doped fiber lasers and their application to OTDR”, J. Lightwave Technol. 20, 1506–1511 (2002).

[93] R. J. De Young and N. P. Barnes, “Profiling atmospheric water vapor using a fiber laser lidar system”, Appl. Opt. 49, 562–567 (2010).

[94] Q. Huang, T. Yu, Y. Zheng, J. Zu, and W. Chen, “2.4-W narrow linewidth Q-switched Tm^{3+}-doped double-clad fiber laser”, IEEE Photon. J. 5, 1500406-1500412 (2013).

[95] Y.X. Fan, F.Y. Lu, S.L. Hu, K.C. Lu, H.J. Wang, and Z.Y. Dong, “Tunable high-peak-power, high-energy hybrid Q-switched double-clad fiber laser” , Opt. Lett. 29, 724–726 (2004).

[96] C. Cuadrado-Laborde, P. Pérez-Millán, M. V. Andrés, A. Díez, J. L. Cruz, and Y. O. Barmenkov, “Transform-limited pulses generated by an actively Q-switched distributed fiber laser”, Opt. Lett. 33, 2590–2592 (2008).

[97]. R. J. Williams, N. Jovanovic, G. D. Marshall, and M. J. Withford, “All optical, actively Q-switched fiber laser”, Opt. Express 18, 7714–7723 (2010).

[98] F.W. Sheua and J.J. Kang, “All-fiber actively Q-switched fiber laser tuned by a pair of temperature controlled fiber Bragg gratings”, Opt. Commun. 278, 132–137 (2007).

[99] R. Z. W. Shi, E. Petersen, A. Chavez-Pirson, M. Stephen, and N. Peyghambarian, “Transform-limited, injection seeded, Q-switched, ring cavity fiber laser” , J. Lightwave Technol. 30, 1492–1498 (2012).

[100] D. Popa, Z. Sun, T. Hasan, F. Torrisi, F. Wang, and A. C. Ferrari, “Graphene Q-switched, tunable fiber laser”, Appl. Phys. Lett. 98, 073106 (2011).

[101] H. Ahmad, M. R. K. Soltanian, L. Narimani, I. S. Amiri, A. Khodaei, and S. W. Harun, "Tunable S-Band Q-switched fiber laser using Bi_2Se_3 as the saturable absorber," IEEE Photon. J., 7, 1502508 (2015).

[102] R. Selvas, I. Torres-Gomez, A. Martinez-Rios, J. A. Alvarez-Chavez, D. A. May-Arrioja, P. LiKamWa, A. Mehta, and E. G. Johnson, "Wavelength tuning of fiber lasers using multimode interference effects" , Opt. Express 13, 9439–9445 (2005).

[103] G. Anzueto-Sánchez, A. Martínez-Ríos, D. A. May-Arrioja, and I. Torres-Gómez, "Enhanced tuning mechanism in fibre laser based on multimode interference effects" , Electron. Lett., 42, 1337–1339 (2006).

[104] P. K. Mukhopadhyay, P. K. Gupta, A. Singh, S. K. Sharma, K. S. Bindra, and S. M. Oak, "Note: Broadly tunable all-fiber ytterbium laser with 0.05 nm spectral width based on multimode interference filter" , Rev. Sci. Instrum., 85, 056101-056104 (2014).

[105] J. E. Antonio-Lopez, J. J. Sanchez-Mondragon, P. LiKamWa, and D. A. May-Arrioja, "Wide range optofluidically tunable multimode interference fiber laser," Laser Phys., 24, 085108 (2014).

[106] S. Fu, Q. Sheng, X. Zhu, W. Shi, J. Yao, R. A. Norwood, and N. Peyghambarian, "All-fiber passively Q-switched fiber laser based on the multimode interference effect", in Conference on Lasers and Electro-optics pp. STh4L.2 , (2015).

[107] T. Walbaum and C. Fallnich, "Multimode interference filter for tuning of a mode-locked all-fiber erbium laser", Opt. Lett., 36, 2459–2461 (2011).

[108] S. M. Azooz, A. A. Jasimb, B. A. Hamida, H. Ahmad, S. W. Harun, A. Halder, M. C. Paul, S. Das, M. Pal, and S. K. Bhadra, "All-fiber dual- wavelength fiber laser operating at 1950 nm region based on multimode interference effect" , Optoelectron. Adv. Mater., Rapid Commun. 8, 1035–1038 (2014).

[109] N. Li, M. Y. Liu, X. J. Gao, L. Zhang, Z. X. Jia, Y. Feng, Y. Ohishi, G. S. Qin, and W. P. Qin, "All-fiber widely tunable mode-locked thulium- doped laser using a curvature multimode interference filter" , Laser Phys. Lett., 13, 075103 (2016).

[110] P. Zhang, T. Wang, W. Ma, K. Dong, and H. Jiang, "Tunable multi- wavelength Tm-doped fiber laser based on the multimode interference effect", Appl. Opt. 54, 4667–4671 (2015).

[111] H. Yang, M. Yang, P. E. Morrissey, D. Lu, B. W. Pan, L. Zhao, B. Corbett, and F. H. Peters, "Three-coherent-output narrow linewidth and tunable single frequency 1X2 multi-mode-interferometer laser diode" , Opt. Express 24, 5846–5854 (2016).

[112] B. N. Upadhyaya, A. Kumar, U. Chakravarty, S. M. Oak, M. R. Shenoy, and K. Thyagarajan, "Analysis of output pulse characteristics in Q-switched Yb-doped fiber laser" , IEEE J. Quantum Electron., 47, 786–794 (2011).

Chapter 5

[113] Y. Okamoto, R. Kitada, Y. Uno, H. Doi, "Cutting of solid type molded composite materials by Q-switched fiber laser with high- performance nozzle", J. Adv. Mech. Des. Syst. Manuf., 2, 651–660 (2008).

[114] W. Shi, M. Leigh, J. Zong, S. Jiang, "Single-frequency terahertz source pumped by Q-switched fiber lasers based on difference-frequency generation in GaSe crystal", Opt. Lett. 32, 949–951 (2007).

[115] A. Roy, M. Laroche, P. Roy, P. Leproux, J.L. Auguste, "Q-switched Yb-doped non-linear microstructured fiber laser for the emission of broadband spectrum", Opt. Lett., 32 , 3299–3301(2007).

[116] J. Cascante-Vindas, A. Diez, J.L. Cruz and M.V. Andres, "Supercontinuum Q-switched Yb fiber laser using an intracavity microstructured fiber", Opt. Lett., 34, 3628–3630(2009).

[117] A. Galvanauskas, M.Y. Cheng, K. C. Hou and K.H. Liao, “High peak power pulse amplification in large-core Yb-doped fiber amplifier”, IEEE J. Selected Top. Quant. Electron., 13, 559–565(2007).

[118] C. Zheng, H.T. Zhang, W.Y. Cheng, M. Liu, P. Yan, M.L. Gong, “11-mJ pulse energy wideband Yb-doped fiber laser”, Opt. Commun. 285, 3623–3626 (2012).

[119] H.T. Zhang, C. Zheng, P. Yan, M.L. Gong, Q.R. Xiao, Q. Zhao, “13.9-mJ all fiber wide band ytterbium-doped fiber amplifier”, Laser Phys. Lett., 9 ,744–747 (2012).

[120] F. Stutzki, F. Jansen, A. Liem, C. Jauregui, J. Limpert, A. Tünnermann, “26 mJ, 130 W Q-switched fiber laser system with near diffraction limited beam quality”, Opt. Lett. 37 (6) 1073-1075 (2012).

[121] H. Zhang, X. Wang, P. Zhou, Z. Gong, and X. Xu, “6 mJ, high average power, all fiberized Q-switched fiber master oscillator power amplifier with low repetition rate”, Appl. Opt., 51, 6933–6936 (2012).

[122] L. E. Zarate, Y. O. Barmenkov, S. A. Kolpakov, J. L. Cruz, M. V. Andrés, “Smart Q-switching for single-pulse generation in an erbium doped fiber laser”, Opt. Exp. 20 , 4397–4402 (2012).

[123] S. A. Kolpakov, Y. O. Barmenkov, A. V. Kiryanov, A. D. G. Chávez, Jose L. Cruz and M. V. Andrés, “Comparison of asymmetric and symmetric cavity configurations of erbium-doped fiber laser in active Q-switched regime”, J. Opt. Soc. Am. B, 29, 2453–2461 (2012).

[124] Y. X. Fan, F. Y. Lu, S. L. Hu, K. C. Lu, H. J. Wang, X. Y. Dong, J. L. He, H. T. Wang, “Tunable high-peak-power, high-energy hybrid Q- switched double-clad fiber laser”, Opt. Lett., 29, 724–726 (2004).

[125] D. Hua, S. Jianjia, W. Cui, Y. Yan and P. Jiang, “All-fiberized SBS-based high repetition rate sub-nanosecond Yb fiber laser for supercontinuum generation”, Laser Phys. Lett., 11, 125103–125105 (2014).

[126] B.N. Upadhyaya, U. Chakravarty, A. Kuruvilla, K. Thyagarajan, M.R. Shenoy and S.M. Oak, "Mechanisms of generation of multi-peak and mode-locked resembling pulses in Q-switched Yb-doped fiber lasers", Opt. Express, 15, 11576–11588 (2007).

[127] Y. O. Barmenkov, A. V. Kir'yanov, M. V. Andrés, "Experimental study of the nonlinear dynamics of an actively Q-switched ytterbium-doped fiber laser", IEEE J. Quant. Elect., 48, 1484–1493 (2012).

Chapter 6

[128] D. Zhu, M. Shen, H Jiang, M. Li, M. R. Wang,Y. Wang, L. Ge, J. Qu and J. Wang, "Broadband superluminescent diode–based ultrahigh resolution optical coherence tomography for ophthalmic imaging", J. Biomed. Opt. Vol. 16(12), 126006 (2011).

[129] O. Casel, H. Fuchs, M.A. Tremont, R. Wallenstein, " Multi-watt cw broadband light sources for optical coherence radar and coherence tomography based on InGaAs tapered laser amplifiers", Conference on Lasers and Electro-Optics, CLEO (2004).

[130] www.thorlabs.com

[131] X. Ping and J. G. Fujimoto, "Ultrahigh resolution optical coherence tomography with femtosecond Ti: Sapphire laser and photonic crystal fiber", Chinese Science Bull. Vol. 53(13), 1963-1966 (2008).

[132] T. H. Ko, D. C. Adler, and J. G. Fujimoto, "Ultrahigh resolution optical coherence tomography imaging with a broadband superluminescent diode light source", Optics Express 12 (10), 2112-2119 (2004).

[133] A. W. Sainter, T. A. King and M. R. Dickinson, "Effect of target biological tissue and choice of light source on penetration depth and resolution in optical coherence tomography", Journal of Biomedical Optics 9(1), 193–199 (2004).

[134] P. Yan, J. Sun, D. Li, X. Wang, Y. Huang, M. Gong, and Q. Xiao, "933 W Yb-doped fiber ASE amplifier with 50.4 nm bandwidth", Optics Express, 24(17), 19940-19948 (2016).

[135] Q. Xiao, P. Yan, Y. Wang, J. Hao, and M. Gong, “High-power all-fiber superfluorescent source with fused angle-polished side-pumping configuration,” Appl. Opt. 50(8), 1164–1169 (2011).

[136] L. Kong, Q. Lou, J. Zhou, D. Xue, J. Dong, Y. Wei, “ 2W Yb-doped double-clad fiber superfluorescent source with 42 nm 3 dB bandwidth”, Optics & Laser Technology, 37, 597–600 (2005).

[137] M. Bashkansky, M. D. Duncan, L. Goldberg, J. P. Koplow and J. Reintjes, “Characteristics of a Yb-doped superflourescent fiber source for use in optical coherence tomography”,Opt. Express, 3, 305-310 (1998).

SUMMARY

The present thesis focusses on the development and studies of Ytterbium-doped fiber laser. The overall thesis work includes extensive studies on the self-pulsing dynamics in CW, high average power Q-switched pulses, narrow and tunable Q-switched pulses and super-fluorescent Yb-doped fiber source.

In the CW pumping, the output of Yb-doped fiber lasers consists of random pulses called as self-pulsing in fiber lasers. Studies on self-pulsing dynamics in Yb-doped photonic crystal fiber laser in single-end and double-end pumping configurations have been done. It has been found that the intensity of self-pulses is considerably higher in the single-end pumping configuration as compared to that in the double-end pumping configuration. The rate equation analysis shows that the non-uniformity in distribution of upper level population along the fiber length before the steady state is responsible for re-absorption of signal and hence self-pulsing. Multi-wavelength and narrow linewidth polarized operation of Yb-doped photonic crystal fiber (Yb-PCF) laser by using dichroic mirror and fiber Bragg grating is also presented.

Passive Q-switched (PQS) operation of a Yb-doped fiber laser using Cr^{4+}: YAG crystal as a saturable absorber (SA) in a special T-type double-end pumping configuration has been studied. In this configuration, average output power of up to 41.6 W was achieved, which is the highest average output power in PQS Yb-doped fiber laser oscillator reported so far in the literature to the best of our knowledge. The effect of the SA on the random self-pulsing dynamics and on the spectral behavior of the output signal near the threshold for Q-switching has also been investigated.

Conventional Q-switched fiber lasers have broad spectrum. However for many applications, narrow linewidth pulses are required. Narrow linewidth and broadly tunable

output from Yb-doped Q-switched fiber laser using acousto-optic modulator (AOM) and multimode interference filter (MMIF) in the linear bulk cavity and all-fiber ring cavity configurations has been carried out. The spectral bandwidth of the Q-switched signal was reduced from ~17 nm to less than 0.1 nm by incorporating MMIF in all fiber Q-switched resonator.

The pulse width from AO Q-switched Yb-doped fiber lasers is 100s of nanoseconds. Special techniques are used to generate short, sub-cavity round-trip time pulses. We have generated short pulses in all fiber AO Q-switched fiber laser. The pulses are generated at the falling edge of the modulation window ON-time of AOM. The minimum pulse width was ~50-55 ns and independent of the cavity roundtrip time.

Amplified spontaneous emission (ASE) generation in Yb-doped fibers of different length at two pump wavelengths namely 915 nm and 975 nm has been studied. We also studied the ASE generation in fibers of different absorption coefficient. In large mode area fiber, FWHM bandwidth of 41.8 nm was achieved at 15 W of ASE signal. Amplification of ASE signal was carried out in the master oscillator power amplifier configuration using double clad, single mode YDF to increase the pump power and ASE bandwidth.

LIST OF FIGURES

LIST OF TABLES